Diploma Thesis

Optimisation of Al-Mg-Si extrusion-alloys for safety applications in the automotive industry

carried out at LKR Ranshofen in corporation with HAI Braunau for the purpose of obtaining the degree of Master of Science, submitted at TU Wien, Faculty of Technical Chemistry, Institute of Chemical Technologies and Analytics, by

Stefan Culic

Mat.Nr.: 1026119

Supervisor at TU Wien: Ao. Univ.Prof. Dipl.-Ing. Dr. Christian Edtmaier

Supervisor at LKR Ranshofen: Dr. Johannes Österreicher

Supervisor at HAI Braunau: Dr.-Ing. Andreas Schiffl

_____

Signature

Affidavit

I declare in lieu of oath, that I wrote this thesis and performed the associated research myself, using only literature cited in this volume.

Vienna,

Signature

Abstract

Extruded Al-profiles of the Al-Mg-Si alloy group are used for safety-relevant applications in the crumple zone of automobiles. In case of an accident the crumple zone should deform plastically in a concertina-like way and dissipate kinetic energy of the impact. The amount of kinetic energy which can be absorbed depends on the microstructure and geometry of the extruded profiles. High yield strengths and a high ductility of the material are necessary in order to meet the requirements. In order to meet those criteria, a fine grain structure and a well-defined precipitation pattern of Mg-Si phases is necessary. During the production process of the profiles – which consists of casting, homogenization and extrusion – the homogenization step plays a significant role in obtaining the desired microstructure. During homogenization dispersoid-phases can be formed, which are known to inhibit recrystallization during extrusion. Additionally, formed dispersoids can act as nucleation-sites for Mg-Si precipitation during age-hardening treatments post extrusion. In this work the formation of dispersoid-phases during homogenization and their subsequent role as nucleation-sites for Mg-Si precipitation was investigated. The precipitation of the relevant phases was determined by measurement of the electrical conductivity, Differential Scanning Calorimetry measurements, light- and scanning electron microscopy observations. The mechanical properties were investigated by high temperature compression tests. The results of light- and scanning electron microscopy are discussed and correlated with the electrical conductivity, Differential Scanning Calorimetry measurements and high temperature compression tests. For certain homogenization procedures light and scanning electron microscopy showed the formation of small and finely dispersed phases, which indicates the formation of dispersoids. Further experimental results revealed the enhancing and desired effect on Mg-Si precipitation of those phases.

Stranggepresste Al-Profile der Al-Mg-Si Legierungsgruppe finden Anwendung für sicherheits-relevante Bauteile in der Knautschzone von Automobilen. Im Falle einer Kollision, soll die Deformation der Knautschzone die kinetische Energie des Aufpralls dissipieren. Die Größe der kinetischen Energie welche dissipiert werden kann hängt von der Mikrostruktur als auch von der Geometrie der extrudierten Profile ab. Hohe Streckgrenzen und eine hohe Duktilität sind notwendig, um die nötigen Anforderungen zu erreichen. Die geforderten Eigenschaften lassen sich durch ein fein-kristallines Gefüge sowie eine definierte Ausscheidung von Mg-Si Phasen erreichen. Während des Herstellungsprozesses der Pofile – welcher aus den Teilschritten Gießen, Homogenisieren und Strangpressen besteht – spielt die Homogenisierung eine wesentliche Rolle bei der Erreichung der notwendigen Mikrostruktur. Während der Homogenisierung können Dispersoide ausgeschieden werden, welche eine Rekristallisation während des Strangpressens unterbinden können und auch als Nukleations-Stellen für die Ausscheidung von Mg-Si Phasen fungieren können. In dieser Arbeit wurde die Bildung von Dispersoiden und ihre Auswirkung auf die Ausscheidung von Mg-Si Phasen untersucht. Die Ausscheidung der relevanten Phasen wurde mittels Messung der elektrischen Leitfähigkeit, Differential Scanning Calorimetry Messungen sowie Licht- und Rasterelektronenmikroskopie untersucht. Die mechanischen Eigenschaften wurden mittels Hochtemperatur Kompressions-Versuchen festgestellt. Die Ergebnisse der Licht- und Rasterelektronenmikroskopie wurden mit den Ergebnissen der elektrischen Leitfähigkeit, Differential Scanning Calorimetry-Messungen und Kompressions-Versuchen diskutiert und korreliert. Für bestimmte Homogenisierungs-Behandlungen konnte mittels Licht- und Rasterelektronenmikroskopie Aufnahmen die Ausscheidung fein-verteilter Phasen aufgezeigt werden, welche auf die Ausscheidung von Dispersoiden hindeutet. Weitere Ergebnisse aus den experimentellen Untersuchungen konnten den erwünschten und verstärkenden Effekt dieser Phasen auf die Mg-Si Ausscheidung bestätigen.

Index

1 Introduction

At the beginning of the 19th century, scientists/chemists were able to produce minor amounts of Al and alloys thereof. The German chemist Friedrich Wöhler produced Al-powder by reducing $AlCl_3$ with molten Potassium [1]. This principle was later used by Henri Sainte-Claire Deville to produce commercial Al in industrially relevant quantities. The keystone for the modern-day procedure by electrolysis was laid independently by Paul Heroult and Charles Martin Hall. They were able to produce Al by dissolving Al_2O_3 in Kryolith and applying a high electrical current to the solution. Three years later Karl Friedrich Bayer discovered a method to produce high-purity Al_2O_3 [1]. He used Bauxite as raw material and applied a pressure pulp-method to separate Al-Oxygen compounds from the other ingredients of Bauxite (Iron-Oxides, etc.). The Bayer-Process remains up to this day the major process for the production of Al_2O_3. Today's production of Al exceeds 40 Million tons/a.

The Bayer-Process and the Heroult-Hall electrolysis caused a dramatic decrease of the price of Al, which enabled the application in several parts of the world economy and engineering. At the beginning of the 20th century, Al found numerous applications in the automotive industry. Already in 1912, one of the first all-Al bodies for car was presented with the "Typ 8/24" by the company NSU (Figure 1.1) [2].

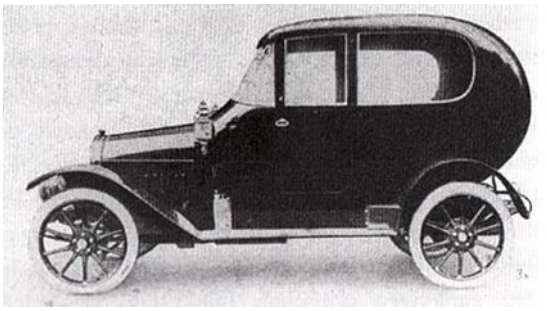

Figure 1.1: Typ8/24 by NSU, full Al body [2].

During the 1950's, the Austrian-born inventor Bela Barenyi introduced numerous design concepts to increase the safety of the car passengers. Sturdy devices/components/materials within the passenger compartment were exchanged by soft materials or stiff materials were covered with softer ones in order to dissipate kinetic energy in the case of an accident when body parts impact these obstacles [3]. Additionally, the idea of the safety steering column was created by Barenyi which significantly decreased the likelihood of a frontal-crash being deadly for the driver. Yet the most revolutionary invention by Barenyi was the concept of the safety passenger cell [3]. Barenyi realized that when the car frame combined a high strength passenger cell and a front and rear crumple zone that the safety of the passengers is highly increased. The high-strength cell – which strongly inhibits any plastic deformation during a collision –protects the passengers from being squeezed during impact, whereas the crumple zones – made of materials which can more readily deform plastically during a collision – absorb high amounts of kinetic energy through plastic deformation. The energy consumed by the deformation of the crumple zones reduces the impact on the passengers and therefore decreases the risk of deadly injuries [3].

Up to this day, the concepts invented by Barenyi remain a major part for the safety standards in the automotive industry.

Al remains a highly used and attractive material for structural automotive body-parts. Due to its lower density of 2.8 g/cm³ – compared to the density of steel of 7.8 g/cm³ – the construction of the first race-cars contained a high percentage of Al parts.

However, the higher price of Al and the lower strength values – and thus higher demand for complex structures compared to steel structures – prevented the large-scale application for mid-prize cars while it was and is used as the major material for higher-prized cars (Figure 1.2)(Figure 1.3) [2].

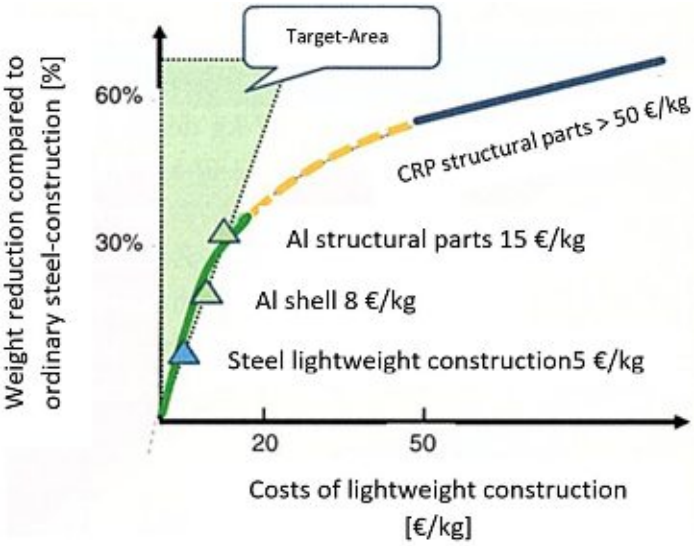

Figure 1.2: weight reduction and prize increase compared to steel [4].

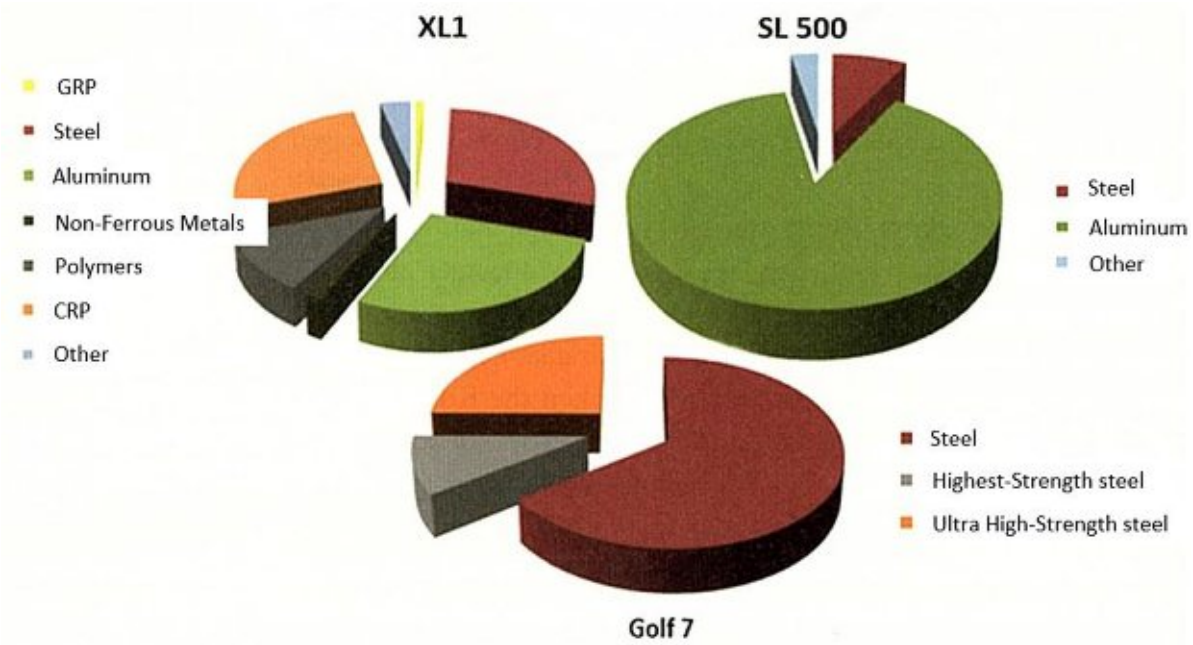

Figure 1.3: Usage of Al for cars in different-prize categories [5].

However, the urgent need for CO_2-Reduction and the therewith stricter regulations by authorities set higher demands for the car producers for constructing cars with lower fuel consumption (Figure 1.4)[6].

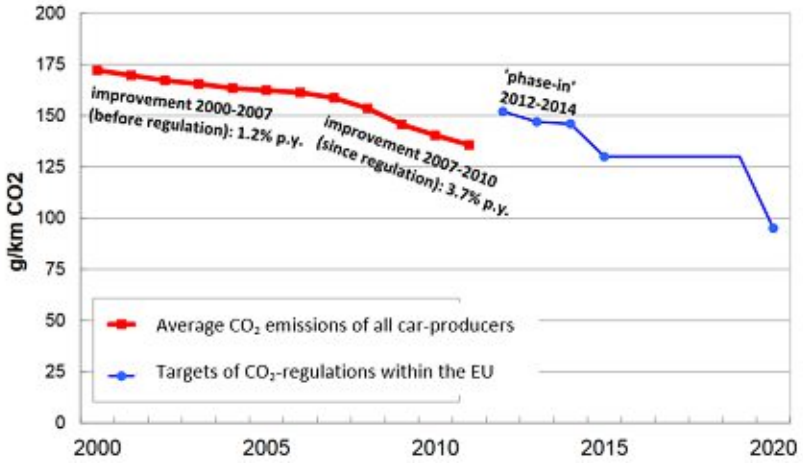

Figure 1.4: EU-CO_2 target goals [6].

One of the options is to design engines which are more fuel efficient, an option which has been carried out intensively during the last couple of years. Additionally, Figure 1.5 shows that weight reduction causes a significant decrease in CO_2 emissions and this can be achieved most efficiently by creating a lighter car body [4].

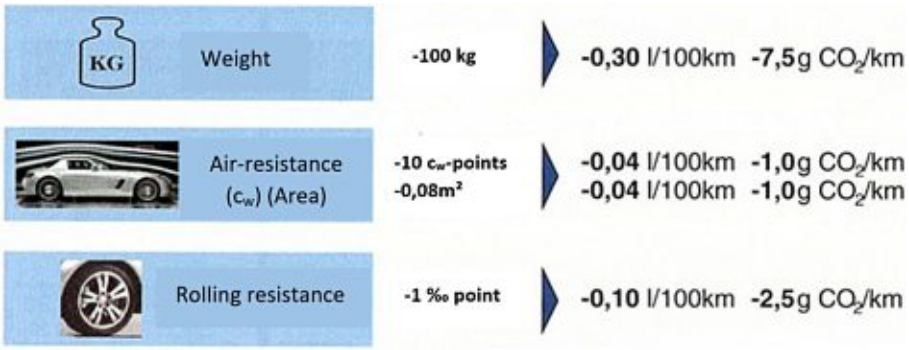

Figure 1.5: Fuel reduction possibilities [4].

It is therefore essential to provide lighter materials at an affordable price for the construction of light-weight car frames. Since composite materials are too expensive for mass production and ordinary steel-alloys are counter-effective for weight-reduction, Al offers an acceptable alternative to meet the demanded criteria (Figure 1.6)[2].

Figure 1.7 shows materials used in the Audi A8 L model [7]. In the front crumple zone, hollow Al profiles are used. In case of an accident, those profiles buckle in a concertina-like way and therefore absorb kinetic energy. Longer profiles would allow higher energy absorption, but the lengths are limited by the desired designs.

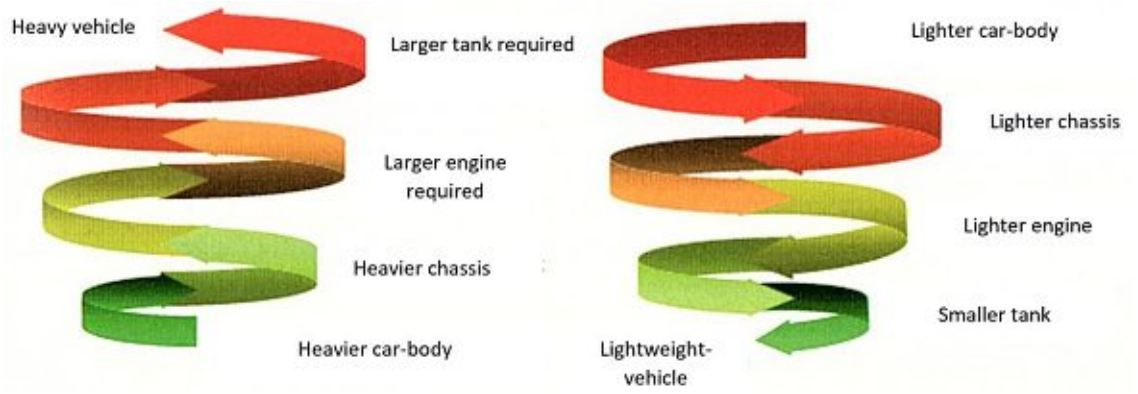

Figure 1.6: Spiral effect for ordinary car bodies (left) and their light-weight counter-parts (right) [2].

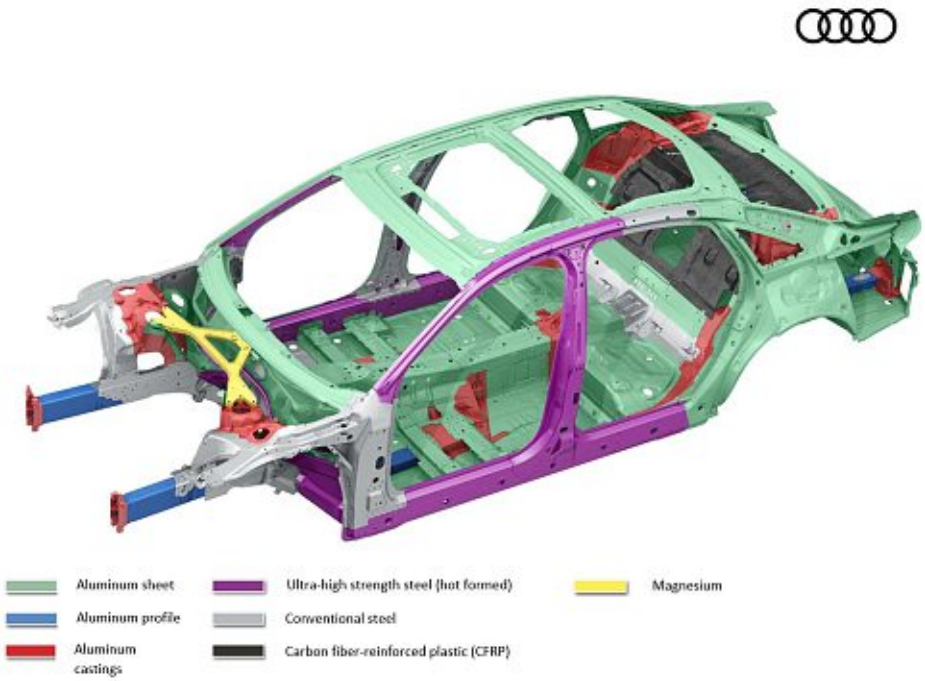

Figure 1.7: Materials used for the Audi A8 L frame [7].

2 Theoretical Part

2.1 "State of the art" production process chain of Al 6xxx extrusion products for the application in the automotive industry and properties thereof

Depending on the containing elements, wrought Al alloys are categorized in seven different groups (Table 1)[2]. Al-alloys which fall into the category of heat-treatable alloys can undergo the process of ageing, which is usually applied at the end of a process chain. This process consists of a heat treatment which causes oversaturated elements to precipitate in a controlled way in order to achieve hardening/stiffening of the material. This effect is called "precipitation hardening effect".

Table 1: Categories of wrought Al-alloys [2]

Series Number	Alloying Element	Alloy Category	Typical content of alloying element [wt-%]
1xxx	Aluminum	Commercially Pure	99.5 % pure Al
2xxx	Copper	Heat-Treatable	3.3 – 6.8 % Cu
3xxx	Manganese	Non Heat-Treatable	0.3 – 1.5 % Mn
4xxx	Silicon	Non Heat-Treatable	1.4 – 13.0 % Si
5xxx	Magnesium	Non Heat-Treatable	0.5 – 6.2 % Mg
6xxx	Magnesium and Silicon	Heat-Treatable	0.25 – 1.2 % Mg, 0.3 – 1.5 % Si
7xxx	Zinc	Heat-Treatable	4.0 % – 8.7 % Zn

Hammerer Aluminum Industries specializes in the casting of Al-alloys and extrusion of profiles thereof. Since this master thesis focuses on the optimization of the extrusion process, only the process steps closely related to extrusion will be discussed in detail.

The process chain of extrusion contains several different steps which are shown in Figure 2.1 [8]. Details of each step will be given in the following chapters.

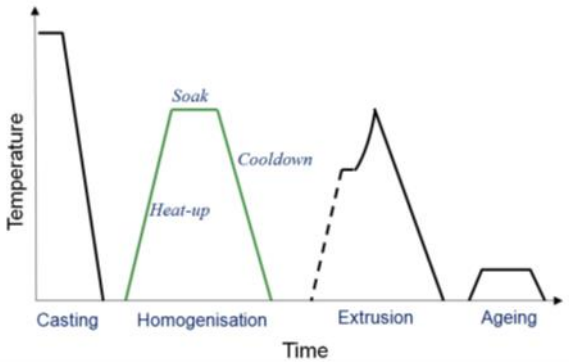

Figure 2.1: Steps of the extrusion process chain [8].

Figure 2.2 show the share of Al extrusion products of the entire Al-market (Figure 2.2) [9]. Since their part of Aluminum products is considerably high, innovation in this sector can cause significant increases in the quality of the extruded products and an increase in productivity.

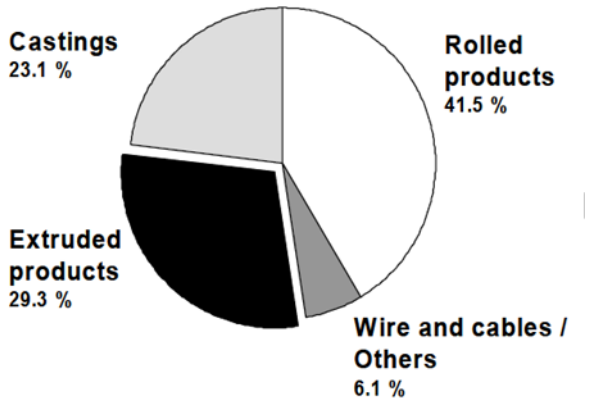

Figure 2.2: Al consumption in Western Europe in 2001 (split on the different product groups)[9].

Figure 2.3 shows that of all extruded Al-groups the 6xxx group is by far the most significant one [9]. They have middle to high strength values, high corrosion resistance, good formability and good extrudability [10]. It is therefore evident that research for this group of alloys causes the biggest impact on productivity of Al extrusion plants. This thesis focuses specifically on 6082-type alloys. During the next chapters details of each part of the process chain of extrusion are discussed.

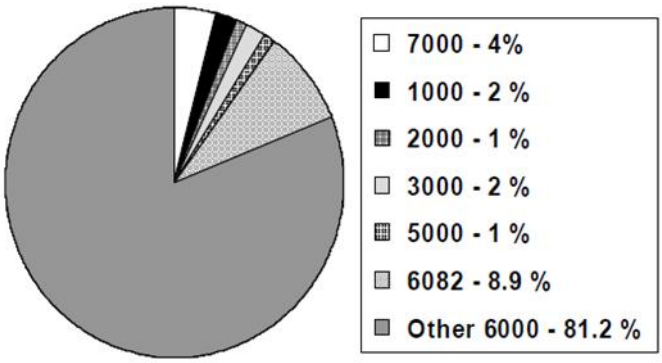

Figure 2.3: Al alloys used for extrusion [9].

2.1.1 Casting

During casting of an alloy, grain refinement can be achieved by adding TiB_2 to the melt. Upon cooling, the melt solidifies/crystallizes and depending on the cooling situation does so in different ways. Since most of the relevant Al alloys solidify in an eutectic reaction, the solidification process happens mostly in the form of dendrites [2]. This way of solidification can be explained by the different velocities of crystal growth in the different crystallographic orientations [11]. The solid/liquid interface is often beyond thermodynamical equilibrium and any inhomogeneity along the interface can cause solidification. Since this process is a random process along the interface, solidification and growth of dendrites occur through the whole solidifying melt, leaving a polycrystalline material with several dendrites in each grain.

2.1.2 Homogenization

If the alloy contains several different elements, their different solubilities cause an inhomogeneous spread along a casted bolt in length and diameter (crystal segregation). Figure 2.4 shows the solubility of various elements in solid Al and Table 2 shows the maximum solubility of industrially relevant elements in Al [2].

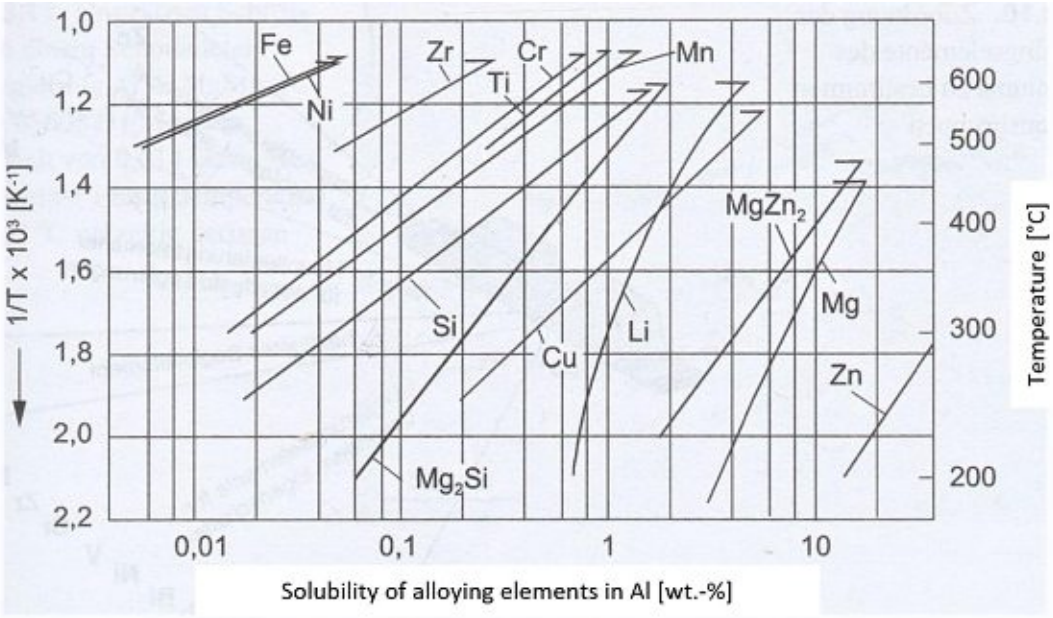

Figure 2.4: Solubility of several elements [x-Axis, wt.-%] in solid Al depending on temperature [y-Axis, °C][2].

Table 2: Maximum solubility of industrially relevant elements in solid Al [wt.-%] [12, 2]

Chromium	0.77
Copper	5.65
Iron	0.052
Lithium	4.0
Magnesium	14.9
Manganese	1.82
Nickel	0.05
Silicon	1.65
Titanium	1.0
Vanadium	0.5
Zinc	82.8
Zirconium	0.28

The segregation can be reduced by homogenization of the bolts. For industrial procedures, the bolts are heated to temperatures between 530-580 °C and held there for several hours.

Figure 2.5 shows the dependence of the diffusion-coefficient on temperature of several alloying-elements [2, 13, 14]. The data for the graphical-plots in Figure 2.5 were obtained by empirical measurements of impurity diffusions and by theoretical calculations using a DFT-approach of the relevant element in an Al matrix.

Impurity diffusion is defined as the diffusion of a solute in a solvent at extremely low concentrations [14]. For the experimental determination of the impurity diffusion, the relevant solute element is added in different quantities to different specimens of high purity Al (99.999 wt % Al)[15]. The maximum concentration of the solute element is approx. 1 wt % [15]. Often Matano's method is then applied in which specimens containing different alloying concentrations are put together and are annealed at a given temperature for a certain time period [16].

The concentration gradient at the interface is frozen by cooling the specimens to room-temperature. After determination of the concentration profile (p.e. through EDX measurements using an electron microprobe) at the interface of the two specimens, Matano's method can be applied, which allows to calculate the diffusion coefficient of the solute element for all concentrations within the concentration range [16]. In order to obtain the diffusion coefficient for impurity diffusion the obtained diffusion-rates/concentration couples are plotted and the graph is extrapolated to very low concentrations of the solute element [14]. Y. Du et al. used such empirical data of a large number of previously published literature and applied the least-squares method to obtain graphs/functions which show the dependence of the impurity diffusion coefficient on temperature (Figure 2.5) [14]. M. Mantina et. al used a different approach [13]. They used a first-principle DFT approach to predict diffusion

coefficients without the need of any empirical data [13]. Combined data from Y. Du's work and M. Mantina's work are shown in Figure 2.5.

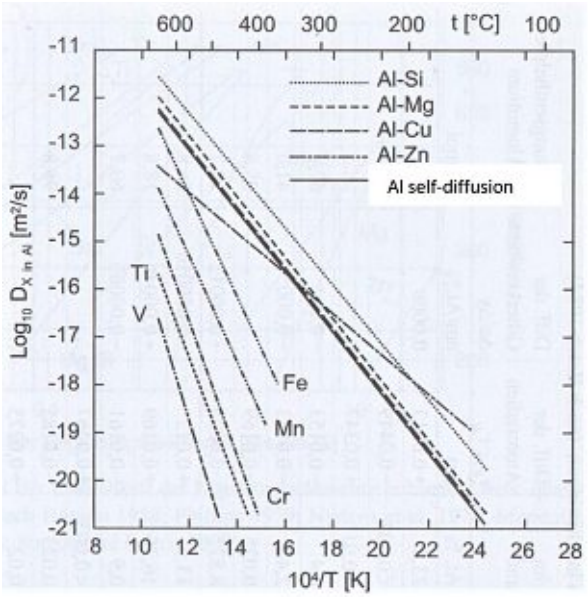

Figure 2.5: Diffusion coefficients of several elements in Al depending on temperature [2, 13, 14].

Changes in element distribution along a grain can be measured by microprobe analysis [8]. Figure 2.6 shows the concentration gradient along a grain/grain boundary of a 6061 alloy before and after homogenization [8, 17].

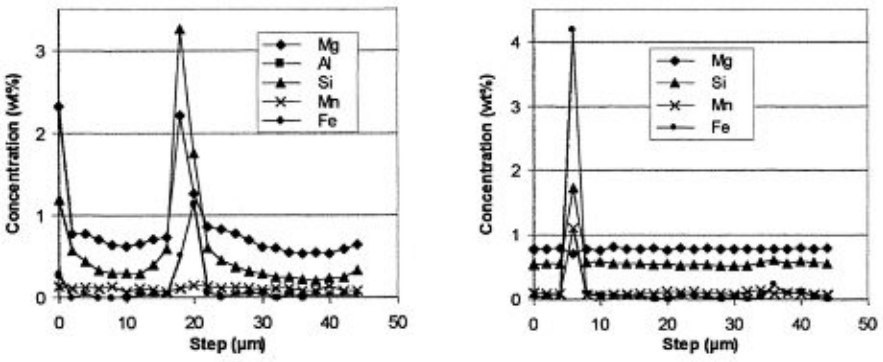

Figure 2.6: Microprobe measurements along a grain boundary illustrate the segregation of elements for an alloy before (left, as cast state) and after homogenization (right, heat treated for 2h at 570°C) of a 6061 alloy [17].

Figure 2.6 shows that the element distribution changes dramatically during homogenization. It is relevant to notice that Mg and Si are enriched towards the grain boundary in the as cast material, whereas the distribution after homogenization shows that Fe has the highest concentration at the grain boundaries. Since the as-cast condition is a highly oversaturated condition, the containing elements can form stable phases during heating up and homogenization, which can later be dissolved again if the solvus temperature of the phases is exceeded.

2.1.2.1 Important aspects about the formation and dissolution of Mg-Si phases during homogenization and heat treatments in general

It has to be mentioned, that during casting the cooling rates are moderately high, but still not high enough as to prevent the formation of Mg-Si-phases at the grain boundaries. Those Mg-Si phases formed during casting are called primary-Mg-Si. Since the diffusion-coefficient of other alloying elements such as Cr and Mn is several magnitudes lower compared to Mg and Si (Figure 2.5), formation of phases containing Cr and Mn during casting can be neglected or are too small to be detected.

Figure 2.7 shows a pseudo-binary phase diagram of Al-Mg_2Si as a vertical section of the ternary Al-Mg-Si phase diagram at a Mg:Si weight ratio of 1.73:1 (which is the according weight-ratio of Mg:Si in Mg_2Si) [2, 18, 19]:

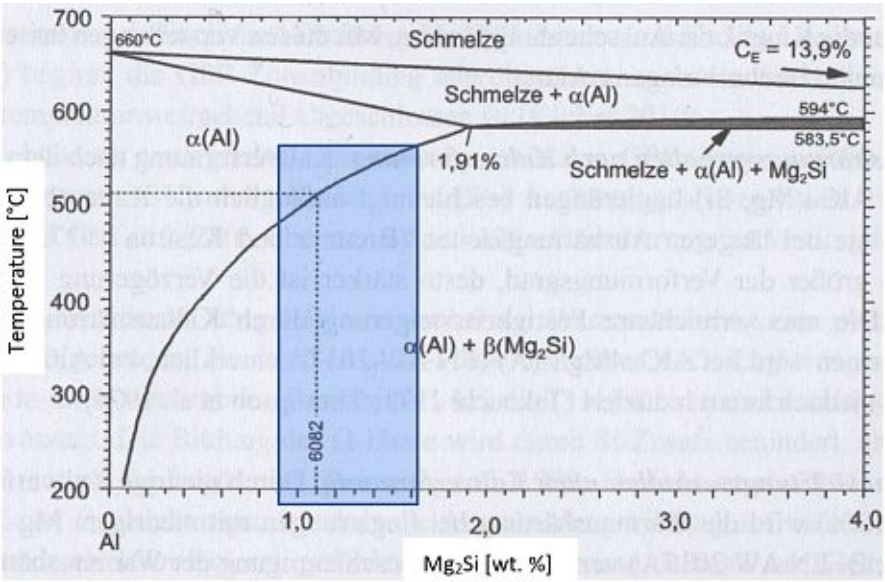

Figure 2.7: Pseudo-binary phase diagram of Al-Mg_2Si, the marked blue area shows the relevant temperature-content region for industrial processes [2, 19].

The blue-area shows the region for industrially relevant Mg_2Si concentrations. If the hold temperature of homogenization schemes or heat treatments is high enough to reach the solvus line, Mg-Si phases will dissolve and form a solid solution with the Al-matrix.

For oversaturated 6xxx-group alloys the first Mg-Si phase which is formed upon heating-up during homogenization (or during artificial aging) are needle-shaped β" precipitates, which are coherent with the Al-matrix along their long-axis and can be seen as a metastable precursor of the equilibrium β-Mg_2Si phase [2]. The precipitation process involves formation of clusters and transition phases for which the existence of vacancies play a major role [2]. The formed clusters of Si and Mg evolve into Guinier-Preston(II) zones, which might act as nucleation sites for β" formation [20–22].

The β" phase is formed at temperatures of 125–200 °C [23]. The composition of this phase in the alloy EN AW-6082 has been reported as Mg_5Si_6 [22, 24]. Between temperatures of 200-250°C the formed β"-needles are substituted by β' (~Mg_9Si_5). It is thought that β' is formed through structural transformation of β". For temperatures above 250 °C, β' transforms to the equilibrium phase of Mg_2Si (β) [25]

The formation processes of Mg-Si phases during heating-up of oversaturated solid solutions of 6xxx alloys can be summarized in the following scheme:

$\alpha_{solid\text{-}solution,\ oversaturated}$ → Si/Mg-cluster/Co-cluster formation during heating up
→ GP(II)-zones (needle-shaped)
→ β'' (semi-coherent along needle-axis, needle-shaped)
→ β' (semi-coherent, rod-shaped)
→ β (plate-like shape, thermodynamical equilibrium phase)

The following scheme shows the precipitation pathway during formation of the stable Q-Phase in Cu-containing Al-Mg-Si alloys [26]:

$$\alpha_{solid\text{-}solution} \rightarrow \text{atomic clusters} \rightarrow \text{GP-Zones} \rightarrow \beta'', Q', L, S, C, QC \rightarrow Q' \rightarrow Q$$

L, S, C, QC = different metastable precursor phases

The sequence is similar to the sequence which occurs during the Mg-Si precipitation process, but the equilibrium phase changes to Q instead of Mg_2Si.

2.1.2.2 Important aspects about the formation of dispersoids during homogenization

Despite reducing segregation during the heat treatment – depending on the containing elements of the alloy – small dispersoids can be formed within the grains due to precipitation mechanisms, as can be seen in Figure 2.8 [8]. Dispersoids are small-sized spherical precipitates within the Al-matrix and can significantly inhibit recrystallization of the alloy during extrusion, due to their Zener-Drag which they impose on grain-boundaries.

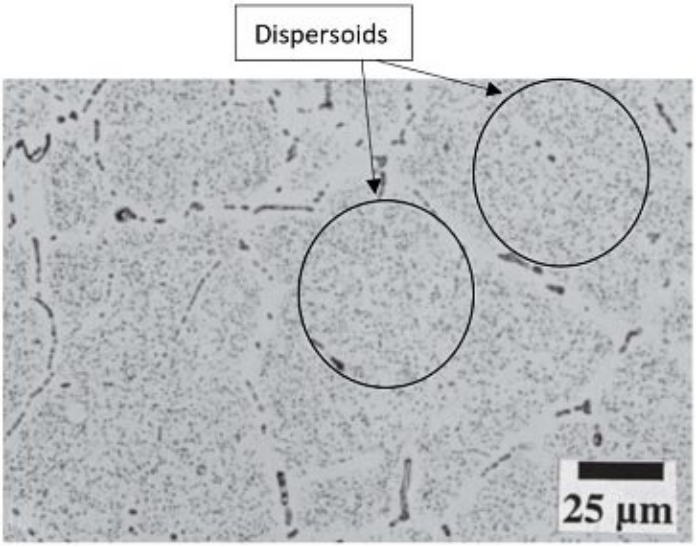

Figure 2.8: Mn containing dispersoids (small black dots, proposed compositions are $Al_{12}(MnFe)_3Si$ and $Al_{15}(MnFe)_3Si_2$ [27]) formed within the grains of an alloy containing 97,69 Al–0.6 Mg–0.95 Si–0.22 Fe–0.54 Mn (figures in wt%) after homogenization at 580°C for 6h [8, 28].

Dispersoids are usually formed when the alloy contains Mn, Cr, Fe and Si. Figure 2.4 shows that for every temperature the solubility of the dispersoid-forming elements is much lower compared to Mg, Si and Mg_2Si. Thus, if Cr and/or Mn are present in an as-cast alloy, upon heating-up of the alloy,

precipitates containing Cr and Mn are formed and remain in the specimen even upon reaching high homogenization temperatures.

It has to be pointed out that the dispersoids are not pure Cr or Mn incoherent-particles within the Al-Matrix, but are rather species which contain additionally Al-Fe-Si-Mg (Table 3) [28–30, 27]. For the formation of dispersoids, properties of those elements have also to be taken into account (diffusion-rates and solubility). Once dispersoids are created the only way to destroy the formed dispersoids is to heat the specimen up until it melts or to exceed the solvus-temperature (if a solvus-temperature exists for the relevant dispersoid phase).

Table 3: properties of dispersoid phases [27]

Alloy Type	Proposed Dispersoid Phases	Formation Temperature	Proposed Nucleation Site	Source
Al + Mg + Si + Fe + Mn	α-$Al_{12}(MnFe)_3Si$, bcc, a=1.26 nm, when Mn:Fe<1.6 at.%, else α-$Al_{15}(MnFe)_3Si_2$, sc, a=1.26 nm	from 400°C	β'- Mg_2Si, via semi coherent 'u-phase' ppte	[2, 7]
Al + Mg + Si + Fe + Mn + Cr	α-Al(MnCrFe)Si	from 400°C	β'- Mg_2Si, via semi coherent 'u-phase' ppte	[2]
Al + Mg + Si + Fe + Cr	α-Al(CrFe)Si, bcc/sc, a=1.26 nm & for Cr > 0.3 wt.% also α'-AlCrSi, fcc, a=1.09 nm	490 – 550°C	β-AlFeSi, via 'u-phase' ppte	[3]

Additionally, dispersoids can undergo Ostwald-ripening when held for several hours at high temperatures.

As can be seen in Figure 2.5 the diffusion coefficient of dispersoid-forming elements is several magnitudes lower than for Mg and Si. Therefore, if precipitation/formation of dispersoids is desired, high temperatures are needed in order to allow significant diffusion of the relevant elements. For Mn-containing dispersoids temperatures of at least 430 °C are required, whereas for Cr-containing dispersoids temperatures of 490 °C are necessary to obtain dispersoids-formation at favorable/decent homogenization durations (Table 3)[27].

Lodgaard and Ryum investigated the formations of Cr and Mn containing dispersoids of 6xxx alloys by electrical conductivity measurements and TEM-investigations [28]. In their work, they presented a theory for nucleation which involves the role of a so-called 'u-phase' which allows for the formation of dispersoids. Figure 2.9 shows the most important aspects [28]. The nucleation of dispersoids occurs during heating-up to homogenization temperature: At a temperature of 100-350°C, the β'-phase (an intermediate Mg-Si-phase of the thermodynamically stable Mg_2Si phase) is formed. During further heating-up the phase changes its composition to the so called 'u-phase' which already contains dispersoid forming elements. Upon further heating-up the diffusion of dispersoid forming relevant elements is increased which causes the formation of thermodynamically stable dispersoids at the u-phase. Further temperature increase causes more dispersoids to be formed at the u-phase whereas the initial β' phase undergoes dissolution processes. At the end of the process, the initial β'-phase is dissolved while the nucleated dispersoids remain or undergo coarsening on further temperature increase.

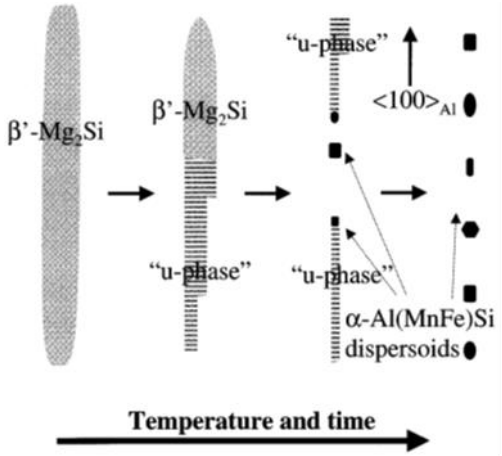

Figure 2.9: Formation of Mn-containing dispersoids involving the role of the 'u-phase' [28].

Österreicher et. al. reported that during cooling-down of the specimen and upon reaching the solvus temperature, TEM-measurements found precipitated Mg-Si phases in the proximity of formed dispersoids, indicating the role of dispersoids as nucleation sites [31]. This same trend/proximity was reported by Rometsch. et. al [32].

In summary, the β'-phases which are formed upon heating-up of as-cast alloys act as nucleation sites for the dispersoid formation. After dissolution of the Mg-Si-phases (during homogenization), the formed dispersoids can in turn act as nucleation sites for Mg-Si-phases (during cooling from homogenization).

Dispersoids can increase the strength of an alloy, for example by the Orowan mechanism [33]. The relative contribution of dispersoids to strength is low for room temperature but makes up for a higher percentage of total strength at higher temperatures. When the alloys are used for hot extrusion, this effect increases the required work pressure for the press [8]. Besides preventing grain growth, additional benefits gained by dispersoids are the increased ductility and fracture toughness of the material [8].

Specifically for extrusion of profiles for car-safety-parts, the inhibition of grain coarsening on the surface of the profile during extrusion is very important [34]. Coarse grains on the surface may cause crack initiation during buckling in case of an accident. Such surface crack-initiation can therefore cause the material to fail at significantly lower forces than expected [35, 34].

Since formed dispersoids have a significant influence on the mechanical properties, a short derivation of the formula for the Zener-Pressure illustrates the major influence of dispersoids on the prevention of grain coarsening.

Figure 2.10 shows a grain boundary interacting with dispersoids/particles [36]. If the assumption is made that all particles are spherical, then the average radius of the particles can be used for calculations. Additional assumptions are that the contact between the grain boundary and the dispersoids is completely random and that the dispersoids themselves are randomly spread within the matrix.

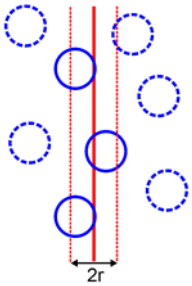

Figure 2.10: Grain boundary interacting with dispersoids/particles [36].

If those criteria are met, the number density can be calculated using Equation (1)[36]:

$$N_{total} = \frac{3 * F_v}{4 * \pi * r^3} \quad (1)$$

N_{total} = number density per unit volume [cm^{-3}]
F_v = Volume fraction of dispersoids
r = average radius of particles [nm]

As can be seen in Figure 2.10, only those particles within one particle radius away from the grain boundary will be able to interact with it, so therefore N_{total} has to be multiplied by a factor of 2*r:

$$N_{interact} = N_{total} * 2r = \frac{3 * F_v}{2 * \pi * r^2} \quad (2)$$

$N_{interact}$ = number density per unit area [cm^{-2}]

If the assumption is made, that all particles exhibit the same maximum force, than the total pressure results to:

$$F_{max} = \pi * r * \gamma \quad (3)$$

γ = surface energy [N/m]

$$P_s = N_{interact} * F_{max} = \frac{3 * F_v * \gamma}{2 * r} \quad (4)$$

P_s = Zener pressure [N/m^2]

It follows from Equation (4) that a high Zener-pressure is achieved by generating a high volume-fraction of dispersoids, which have a small radius.

2.1.2.3 Important aspects about the morphology change of Al-Fe-Si phases during homogenization

All industrially used Al-alloys contain Iron in small quantities, so the formation of Al-Fe-Si phases at the grain boundaries in the 6xxx group has to be considered. During casting, primary plate-like ß-AlFeSi phases are formed (Al_8Fe_2Si, Al_5FeSi, $Al_8FeMg_3Si_6$), which build rather long plates/phases along the grain boundaries [37]. During homogenization those ß-phases are breached-apart into smaller pieces and the edges turn towards round-shaped morphologies which are more favorable since mechanical properties of the extrudate is improved [38].Those Al-Fe-Si phases are called α-Al-Fe-Si.

2.1.3 Extrusion

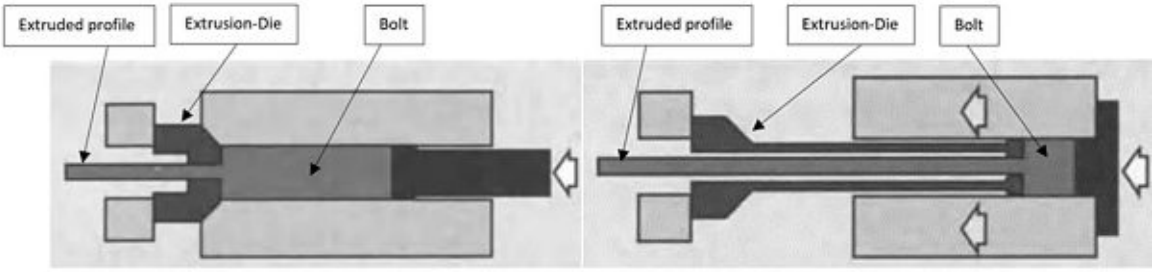

Figure 2.11: comparison direct extrusion (left) and indirect extrusion (right) [39].

Figure 2.11 shows the two different types of extrusion applied in the industry [39]. When direct extrusion is used, the bolt is pressed with pressures of several hundreds of bar against the die and is therefore extruded. For indirect casting, the bolt remains steady while the die is pressed against the bolt. One of the benefits of indirect extrusion is that less pressure is necessary since less friction between the bolt and the wall of the recipient occurs. However, dimensions of the extrudable profiles are limited by the circumference of the recipient. HAI Braunau uses only direct extrusion plants with several MN of force.

Extrudability of a material can be limited by numerous reasons [40]. The extrusion plant itself puts a limit on the extrusion process by the maximum available extrusion pressure, further limits are presented by the desired profiles and therewith necessary tolerances. One of the major extrusion speed limitations is set by the formation of surface defects on the casted profiles.

Since for 6xxx Al-alloys Mg-Si phases play a major role on the extrudability and surface-quality of the profiles, a detailed description thereof should be given.

In the literature, surface defects are categorized as die lines (grooves along the direction of extrusion), pick-ups (small scars in the surface), tearing or hot shortness (surface cracks) and spalling (local thinning of the cross section) [9]. One of the major reasons for those defects are local melting reactions.

For relatively low amounts of Mg and Si (i.e., in 6xxx series alloys), upon slow heating-up of the specimen the Mg_2Si particles can dissolve in the Al-Matrix and the specimen will melt at a relatively high temperature (only a few degrees below the melting point of pure Al, 660°C). However, if the heating-up is not carried out slowly enough, the existing Mg_2Si particles don't have enough time to dissolve and Mg/Si concentration gradients remain. Upon further heating, this will eventually lead to local eutectic melting reactions which will occur at a temperature of 583°C. Therefore, homogenization is carried out below ~585°C. However, local melting can still occur during the extrusion process, when temperature rises due to deformation, causing surface defects [40, 41].

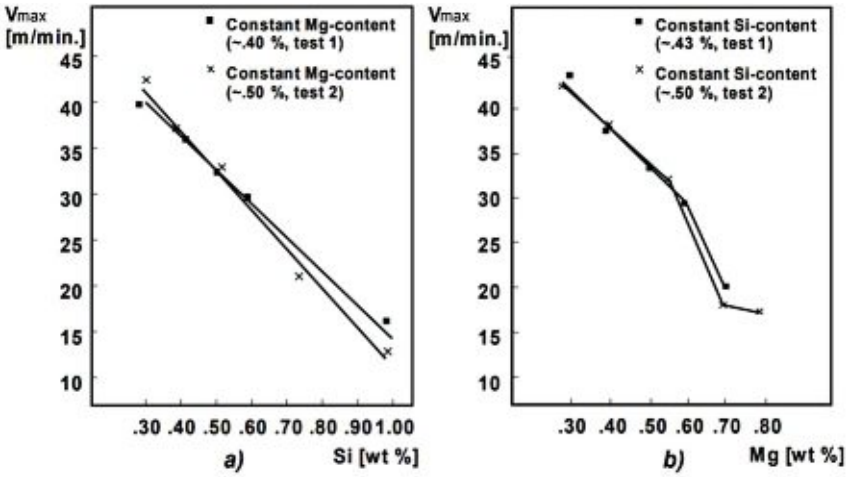

Figure 2.12: Maximum extrusion speed vs. Si content for approx. constant levels of Mg (a) and vs. Mg content for two approx. constant levels of Si (b) [42].

Figure 2.12 shows the effect of Mg and Si on the maximum extrusion speed before tearing occurs [42]. It is clearly visible that both elements significantly lower the extrusion-speed upon increase of their content. For small contents, all of Mg and Si will be in solid solution and thus tearing processes will occur at profile exit temperatures close to the solidus temperature of the alloy. Additionally, both elements have an influence on the deformation resistance. It was shown that the solidus temperature is more sensitive to the Si concentration whereas the deformation resistance is more sensitive to the Mg content [43, 44]. Figure 2.12 b shows that for a Mg-content of approx. 0.55 wt% a kink in the trend-line is caused, which can be attributed to the formation of Mg_2Si and therefore melting at the lower eutectic-temperature.

In order to meet required strength-criteria, the alloy must contain a certain amount of Mg and Si to allow for hardening phases to be precipitated during ageing of the alloy. However, Figure 2.12 shows that no unnecessary excess addition of Mg and Si should occur, since the extrusion process will suffer in productivity by doing so.

Figure 2.13 shows that most 6xxx alloys are on the Si-side of the Mg_2Si line. This can be explained by the fact that previous works have shown that the most effective hardening phases have a Mg:Si ratio which is more closely to be 1:1 compared to the ratio of 2:1 of the equilibrium phase Mg_2Si [21, 45]. In addition, the solubility of Mg_2Si is only slightly influenced by a Si excess, whereas the same Mg excess causes a significant decrease in Mg_2Si solubility [46, 19]. Furthermore, the attainable strength-values are significantly increased by Si excess compared to the same excess of Mg_2Si or Mg [47]. Si therefore increases the volume and/or number density of phases which are responsible for age-hardening, and additionally a Si excess increases the kinetics of cold and warm-hardening which leads to shorter age-hardening periods [2].

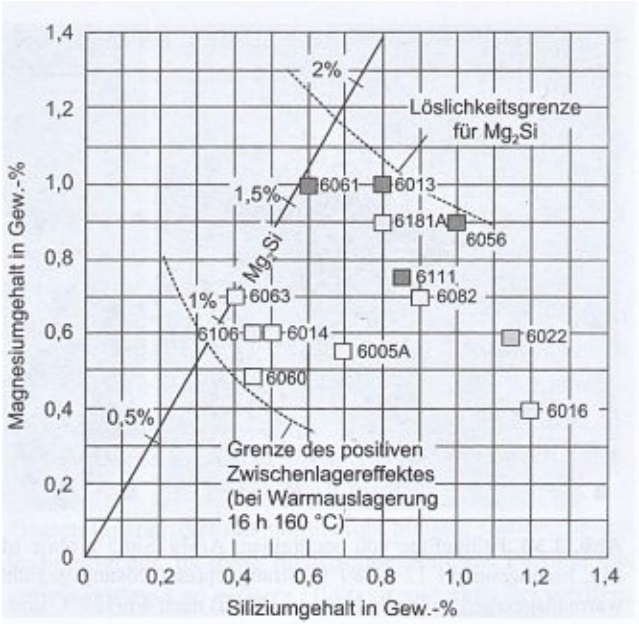

Figure 2.13: Mg [y-Axis, wt-%] and Si [x-Axis, wt-%] content of several 6xxx alloys [2, 48].

The preheating conditions of the billets have a severe impact on the extrusion speed. Figure 2.14 shows the dependence of the extrusion speed on the billet preheating temperature [9][49]. It can be seen that for lower temperatures the available pressure of the press is the limiting factor, since deformation resistance is considerably high for lower temperatures. For higher temperatures the occurrence of surface effects during extrusion sets an upper limit for the billet preheating temperature.

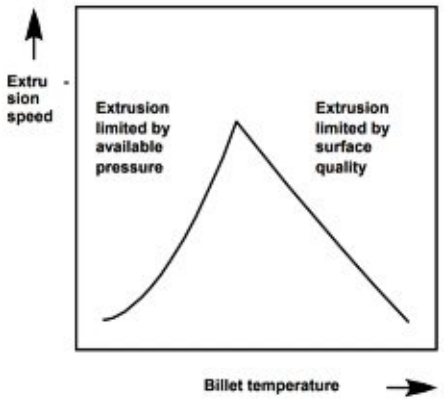

Figure 2.14: Sketch of an extrusion limit diagram [9].

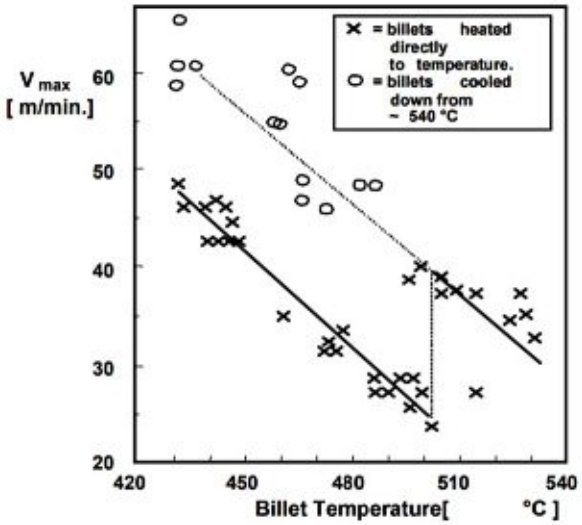

Figure 2.15: Maximum extrusion speed before surface tearing occurs is plotted vs. billet temperature [50].

Figure 2.15 shows the maximum extrusion speed before tearing occurs in dependence on the billet preheat-temperature [50]. Two different approaches were used. In the first one the specimens were directly heated to the according temperature whereas for the second procedure the specimens were preheated to approx. 540 °C and subsequently cooled down to the according temperature. For both procedures, the specimens show a decline of extrusion speed for higher temperatures. This can again be explained by eutectic melting reactions which occur in the material because of heat-generation during extrusion. For higher temperatures, less additional heat can be absorbed so the applicable extrusion speed decreases.

For the directly heated specimens a clear shift in extrusion speed is visible for temperatures of approx. 500°C. This can be explained by the dissolution of coarse Mg_2Si particles. Upon dissolution of those particles the specimen can absorb significantly higher amounts of heat since any melting reaction occurs at the higher solidus reaction compared to the lower eutectic temperature when Mg_2Si particles are present. The same process explains the higher extrusion speeds for lower temperatures for the preheated specimens. Those specimens were cooled fast enough to avoid precipitation of Mg_2Si, again this enabled higher extrusion speeds.

Reiso O. additionally carried out visual inspections of extruded specimens [9]. It was shown that specimens which had a small number of remaining Mg_2Si particles showed good surface-quality whereas specimens which were not heated high enough to enable significant Mg_2Si dissolution showed poor surface quality after extrusion. The hardening phases during age-hardening are the β”-phases. If Mg_2Si phases are existing prior to extrusion, the availability of necessary Mg and Si atoms for β”-formation is reduced, which prevents the alloy from reaching the possible strength requirements.

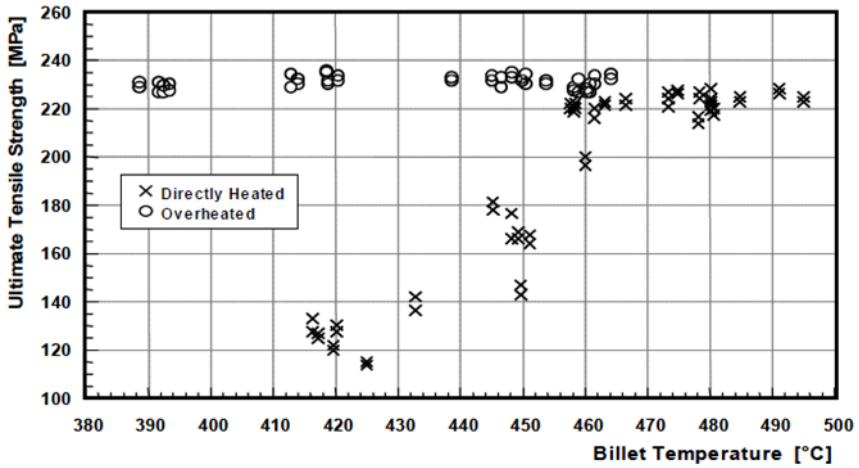

Figure 2.16: Dependence of ultimate tensile strength on billet temperature before extrusion [9].

Figure 2.16 shows the dependence of the ultimate tensile strength after ageing on billet temperature before extrusion [9]. It is clearly visible that specimens which were directly heated to temperatures below 480°C show significantly lower tensile strengths than specimens which were preheated to higher temperatures. Specimens which were overheated and cooled to the relevant temperature reach maximum strengths even for very low temperatures and consistency of the values is additionally very high. This can be explained by full dissolution of primary Mg-Si phases, which increases the value of available Mg and Si atoms during ageing.

Since the major part of this thesis focuses on the homogenization of 6082 alloys, the additional effects of the homogenization practices on extrudability discovered by Reiso O. should be mentioned . In his publication Reiso only focused on the cooling rates for 6060/6063 alloys after homogenization [9]. It was found out, that the characteristic jump in extrusion-speed was shifted to lower temperatures for specimens which were cooled at higher cooling rates. This can be explained by the formation of Mg_2Si particles. For lower cooling rates after homogenization, the precipitated Mg_2Si are considerably large compared to higher cooling rates. Large Mg_2Si particles need more time and higher temperatures in order to keep the diffusion high enough for full dissolution prior to extrusion. Therefore, the characteristic jump/kink in the extrusion-speed diagram is shifted towards higher temperatures. Water quenched specimens show no characteristic jump and show the same trend as the before-mentioned overheated specimens. Here the formation of Mg_2Si particles after homogenization is prevented due to quenching – on condition that the specimens were homogenized at temperatures above the solvus temperature. Upon heating-up of those specimens the precipitation of Mg_2Si was prevented by choosing high enough heating-up rates, which inhibited precipitation of Mg_2Si formation during heating-up.

Interestingly, Reiso found out, that for the tensile strength the water quenched specimens showed a high influence on the billet preheat-temperature [9]. It was expected that in those specimens, all of the available Mg and Si atoms are in solid solution and should therefore lead to the highest tensile strength values, independent of the preheat-temperature. The unexpected trend was explained by the formation of small Al-Fe-Si dispersoids, which act as nucleation sites for Mg-Si phases. It was found that the number density of the dispersoids decreases with higher preheat-temperatures [51].

If the specimen contains a large number of Fe-dispersoids during extrusion, the dispersoids cause significant precipitation of Mg-Si phases during cooling after extrusion. Those precipitates have almost no effect on the hardening of the specimens and are therefore to the disadvantage of the ultimate tensile strength, since necessary Mg-Si-atoms for age-hardening are consumed by those precipitates.

Due to the fact that the number density of the mentioned Fe-dispersoids is lowered for higher preheat-temperatures (Ostwald-ripening), the lower number of dispersoids causes less Mg-Si precipitates to form during cooling after extrusion. This leads to a higher number of available Mg-Si atoms for age hardening and therefore to a higher ultimate tensile strength as shown in Figure 2.17 (right)[9].

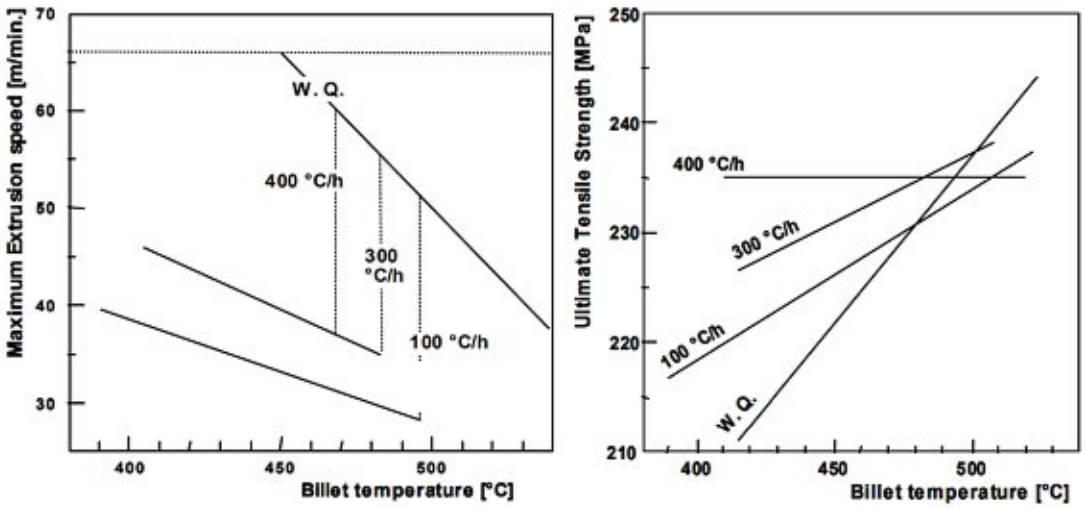

Figure 2.17: Dependence of extrusion speed (left) and ultimate tensile strength (right) on billet preheat-temperature [9].

2.1.4 Ageing

6xxx Al-alloys, for Mg_2Si contents of approx. 1.2%, Mg_2Si phases are dissolved when reaching temperatures above approx. 525°C. When the material is cooled fast enough from temperatures above the solvus temperature, the solute Mg and Si remain oversaturated in solid solution. After extrusion and quenching of the material, a controlled heat treatment can precipitate Mg and Si containing phases in such a way that a significant increase in the hardness/stiffness of the material is obtained. This increase in stiffness of the material due to an additional temperature-treatment is industrially called “ageing”. In the scientific literature the effect itself is called “precipitation hardening effect” and is applicable for 2xxx, 6xxx and 7xxx Al-alloys.

For Al-alloys of the 6xxx group, the extruded profiles have to be cooled-down quickly or even quenched to room-temperature (cooling-rates range from 60°C/min up to 8000°C/min) in order to obtain a highly oversaturated condition, which is the major requirement for natural aging (which occurs at room temperature) and artificial ageing (which is carried out at higher temperatures up to 250 °C)[2, 52].

The applicable cooling rate in the industry depends on the material thickness and the geometry of the extruded products and the available cooling medium (water, air and water/air-combinations) [2]. It is desired to keep the distortion of the profiles due to quenching/cooling-down as low as possible in order to reduce additional stretching-processes to a minimum.

It is assumed that a major requirement for achieving desired material parameters after ageing (high yield & tensile strength and high elongation at break) is the existence of vacancy-solute element-complexes after quenching, which enable volume-diffusion even at room temperature [2, 53].

2.1.4.1 Processes during natural ageing at room temperature

Profiles which have been quenched after extrusion contain at this stage no clusters of solute-elements, the solute-elements are rather spread homogenously in the solid solution [2, 54]. During cooling-down it is assumed that formation of vacancy-solute element-complexes occured, which enable diffusive mobility of the solute elements [2, 55]. The first step during natural ageing is the formation of Si-clusters, and later on Mg-clusters are formed [2, 56]. During the next days at room temperature a dissolution of the Mg-clusters occurs and Mg-enrichment of the existing Si-clusters leads to the formation of Mg/Si co-clusters [2, 55]. Those co-clusters form Guinier-Preston(I) zones. The following scheme summarizes the precipitation processes during natural ageing:

$\alpha_{\text{solid-solution, oversaturated}}$ → Si-cluster formation, followed by Mg-cluster formation
→ Dissolution of Mg-clusters and formation of Mg/Si co-clusters (spherical shape, structure unknow)
→ GP(I) zone formation (structure unknown)

If quenching processes directly after extrusion do not lead to desired mechanical properties after ageing, the extruded profiles can undergoe an additional heat-treatment after extrusion, during which the products are heated above the soluvs-line of the Al-Mg_2Si phase diagram (solution-treatment) and are then subsequently quenched (Water, air or water-air combination). Products which are naturally aged after this procedure are in the industrally "T4-stage" (Solution heat treated and naturally aged to a substantially stable condition) [12].

Figure 2.18 shows the dependence of the stiffness ($R_{p0.2}$ and R_m) and the elongation at fracture (A_5) on the ageing-period of a naturally aged extruded 6082 profile. It is evident, that for this alloy a stable level of the mechanical-parameters is reached after approx. 10 days of natural ageing.

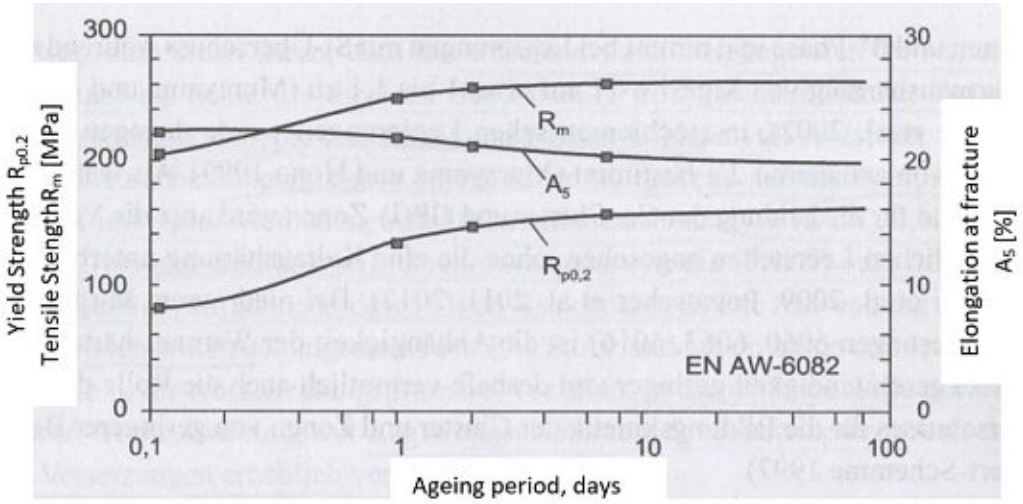

Figure 2.18: Natural ageing of extruded profiles of EN-AW 6082 after solution treatment at 530°C/20 min and subsequent quenching in water [2].

2.1.4.2 Processes during artificial ageing

The ageing procedure for 6xxx alloys can happen at room temperature but is usually accelerated by applying temperatures of 80 – 250 °C, this procedure is called artificial ageing. It has been reported that maximum strength values are achieved for ageing-times of 5-8 hours at temperatures of 160–185 °C [2]. Figure 2.19 shows the dependence of the stiffness ($R_{p0.2}$ and R_m) and the elongation at fracture (A_5) on the ageing-period of an artificially extruded 6082 profile [2].

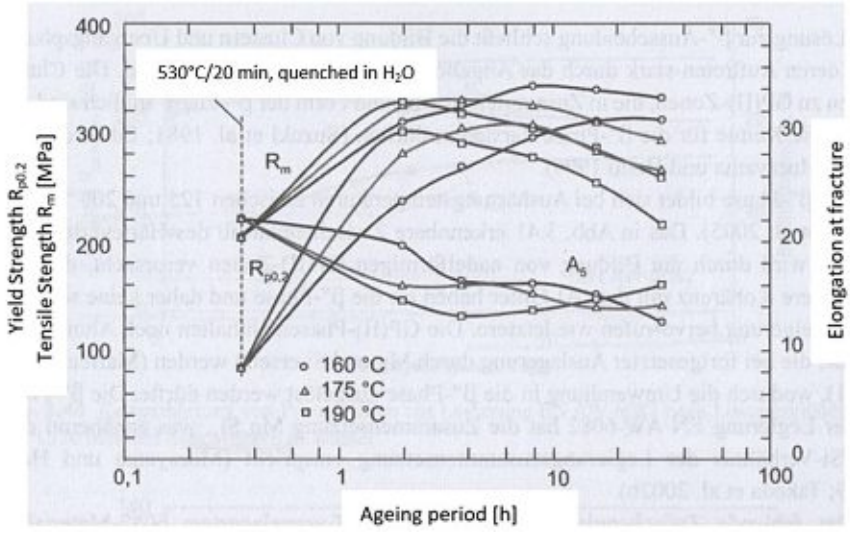

Figure 2.19: Artificial ageing of extruded 6082 profiles after solution-treatment at 530°C/20 min and subsequent water-quenching [2]. Ageing was carried out at three different temperatures T = {160°C, 175°, 190°}[2].

The formation scheme of Mg-Si phases during heating-up of oversaturated 6xxx-group alloys was already mentioned in chapter 2.1.2.1.

It is generally assumed that the hardness of 6xxx-alloys with Si-excess is mainly caused by the β”-phase [2, 57]. Upon over-ageing (when the ageing procedure is carried out to long for a certain temperature) the β”-phase transforms into the β’-phase which causes a decrease in stiffness and hardness of the material. In Figure 2.19 it can be seen that for an ageing temperature of 190°C the strength values reach a maximum after ≈ 2 hours of ageing and decrease upon further ageing of the extruded profiles [2]. It is therefore necessary to determine the right ageing-parameters (temperature and duration of artificial ageing) in order to obtain optimum strength values.

2.1.5 Summary of all processes of the extrusion process-chain of 6xxx Al-alloys

Figure 2.20 gives a summary of all processes which can occur during homogenization of 6082 alloys containing Cr and/or Mn. In this picture a standard homogenization scheme is shown, in which bolts are heated up with a moderate rate (3K/min) and held at high temperatures (between 530°C–580°C) for a duration of several hours (4-5 h) and are then subsequently cooled (in this case approx. 200 K/hour) to room temperature.

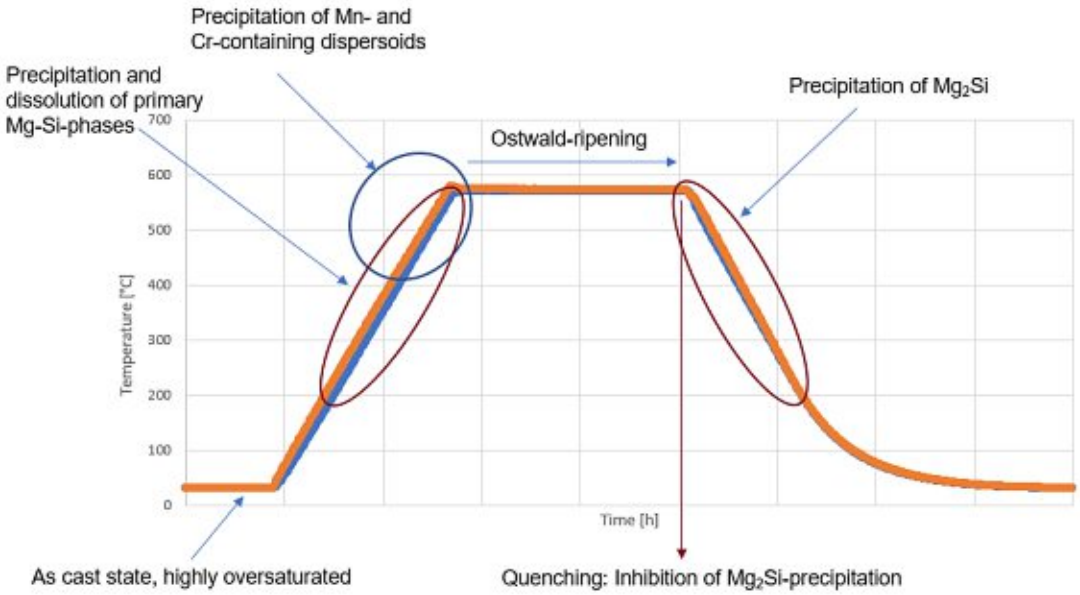

Figure 2.20: Summary of all processes during homogenization.

During heating-up of an alloy oversaturated Mg and Si atoms start to precipitate and form Mg-Si phases (β'', β' and Mg_2Si) in a stepwise manner. However, if the solvus line of Mg_2Si is reached, Mg_2Si forms a solid solution with the Al-matrix (Figure 2.7, blue area). In addition, primary Mg-Si-phases (which were formed during casting), are additionally dissolved upon reaching the solvus-line. If the alloy contains Cr and/or Mn at temperatures above ≈ 400°C (for Mn-dispersoids, formation of Cr-dispersoids requires temperatures of at least ≈ 490°C) dispersoids start to form. When specimens are kept above the mentioned temperatures formed dispersoids can undergoe Ostwald-ripening. For hold-temperatures which are above the solvus-temperature of Mg_2Si, solid solutions of Al and Mg_2Si are formed.

By quenching specimens from above the solvus-temperature in water the precipitation of Mg-Si phases is inhibited whereas when cooling the specimen in the homogenization furnace the precipitation of Mg-Si phases occurs. Those two different procedures can be differentiated by electrical conductivity measurements. Through metallographic observations different patterns of Mg-Si-precipitates can be seen which offer insight on formation of phases/dispersoids which could act as nucleation sites for Mg-Si-phases.

2.2 Detection of precipitation or dissolution of phases by electrical conductivity measurements

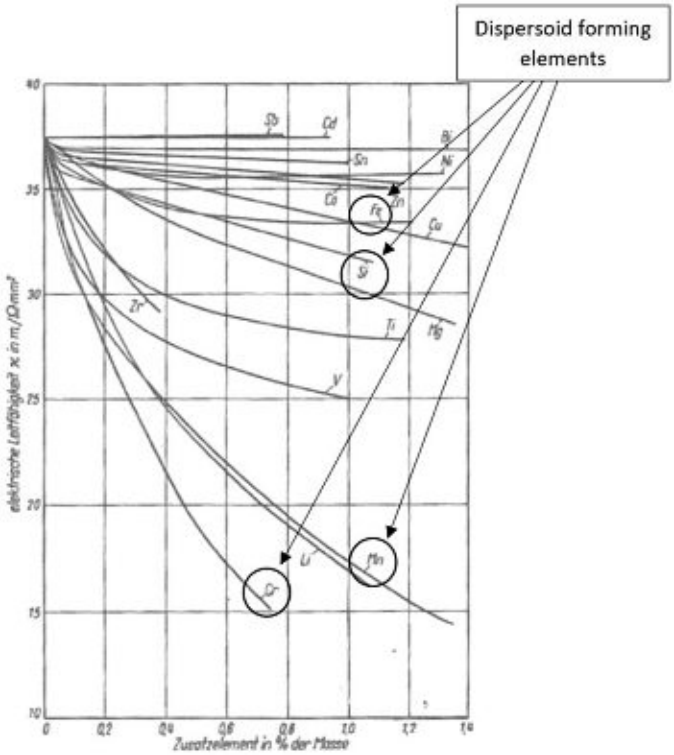

Figure 2.21: Influence on electrical conductivity [y-Axis] of different elements in binary constitution [58].

Elements which are added to metals cause a decrease in electrical conductivity compared to the pure metal, since the necessary formation of electron-waves for electron-transport is disturbed by external elements. An additional change in electrical conductivity can be achieved by whether those elements are in solid solution or present as precipitates. Since foreign atoms in solid solution disturb the formation of electron-waves more than precipitates, the difference between atoms in solid solution or precipitates thereof can be detected by measurements of the electrical conductivity.

First illustrations on the increase in electrical resistance of solid solutions were probably carried out by Norbury [59, 60]. He indicated that the change in electrical resistance was associated with the differences in valence of the solute and solvent metals. In a series of thorough investigations Linde observed an empirical relationship for the resistivity change of alpha solutions in copper, silver and gold [59, 61–63]:

$$\Delta\delta = [\kappa_2 + \kappa_1 * (Z_\beta - Z_\alpha)^2] * A \qquad (5)\ [59]$$

$\Delta\delta$ = increase in resistivity per addition of A
A = atomic pct. of the solute
Z_α = valence of the solvent
Z_β = valence of the solute
κ_1 & κ_2 = solute-constants for the relevant period of the periodic table

A theoretical explanation for the empirical observation of Linde was given by Mott [64, 65, 59]. Mott described the change in electrical conductivity by the fact that the core of the solvent atom carries a charge of $Z_\alpha * e$ (e = elementary charge of a proton) whereas the core of a solute element carries a

charge of Z_β*e, thus an effective scattering charge of $(Z_\beta - Z_\alpha)$*e acts on a conduction electron. Since the intensity of scattering of conductivity electrons is proportional to the square of the scattering charge, a change in conductivity is proportional to $(Z_\beta - Z_\alpha)^2$. (5) therefore implies that solute elements which have a higher horizontal distance in the periodic table of the solvent/host element also cause a higher difference in conductivity than solute elements which are horizontally closer to the host element.

However, only solute elements which are standing to the right of the host metal in the periodic table cause changes in resistivity which are in good agreement with the Norbury-Linde rule (5) [66]. Elements which are standing to the left of the host metal, especially transition elements, cannot be covered by the Norbury-Linde rule [66].

When transition metals are added to an Al matrix, a new energy state, a "virtual" bound state – associated with the unfilled 3-d shell of the transition metal – may form in the vicinity of the transition metal [67]. Speaking in terms of energy, if the "virtual" state lies at energies within the conduction band, an electron from the Fermi-level may temporarily be trapped/bound in the "virtual" state and give rise to a large scattering effect [67]. Calculating the density of states of possible "virtual" states for each of the elements of the transition series leads to a Gaussian density-distribution of virtual-states. Figure 2.22 shows that the peak of the density-distribution is shifted as we go along from Sc to Ni [67, 68]. For a certain element the peak of the distribution-function lies at energies close to the Fermi-Level of the conduction-band of the host metal and causes a significant scattering effect and therefore significant decrease in conductivity [67].

For Al this scattering effect peaks for Cr and Mn and explains the strong influence on resistivity of those two elements as can be seen in Figure 2.21.

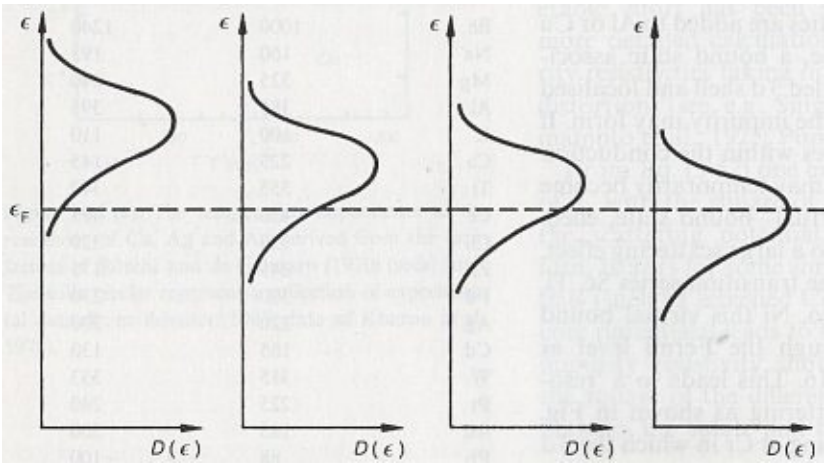

Figure 2.22: Density of states (Gaussian-shape curve)(x-Axis) in dependence on the energy (y-Axis) for the possible "virtual" states created by the addition of a transition element to an Al-matrix. The shift of the curve is schematically shown as we go from Sc to Ni [67, 68].

In the as cast state most of the elements are in supersaturated solution. Upon heat treatments those elements form equilibrium phases. Figure 2.21 shows that the various relevant dispersoid-forming elements partially have a severe influence on the electrical conductivity of the Al-matrix.

Table 4: Average increase in resistivity per wt-% [µΩ * cm] at 20 °C for industrially relevant alloying elements [12]. Values in Table 4 have to be added to the base resistivity of high purity-aluminum of 2.65 µΩ * cm at 20 °C [12].

	In solution	Out of solution (a)	Maximum solubility in solid Al [wt-%]
Chromium	4.00	0.18	0.77
Copper	0.344	0.030	5.65
Iron	2.56	0.058	0.052
Lithium	3.31	0.68	4.0
Magnesium	0.54 (b)	0.22 (b)	14.9
Manganese	2.94	0.34	1.82
Nickel	0.81	0.061	0.05
Silicon	1.02	0.088	1.65
Titanium	2.88	0.12	1.0
Vanadium	3.58	0.28	0.5
Zinc	0.094(c)	0.023(c)	82.8
Zirconium	1.74	0.044	0.28

(a) Limited to about twice the concentration given for the maximum solid solubility, except as noted.
(b) Limited to approximately 10 wt-%. (c) Limited to approximately 20 wt-%.

Table 4 shows the average increase in resistivity for industrially relevant alloying elements in and out of solid solution of Al [12]. When the composition of an alloy is known due to chemical analysis, the values presented in Table 4 allow for the calculation of resistivity/conductivity-values of the assumed as-cast state and post-heat-treatment state of an alloy. The calculated results can be compared to results obtained by experimental measurements of the electrical conductivity.

Therefore, by carrying out electrical conductivity measurements the formation of dispersoids and precipitation of Mg and Si within the Al-Matrix can be detected and a rough quantitative estimation of dissolved/precipitated species can be made by calculations using the literature values of Table 4.

2.3 Problem statement & scope of this master thesis

Since 6082-alloys are of major commercial interest and are used to a large extend in the automotive industry for car safety-parts, optimization of the parameters of the various steps of the process chain of those alloys (Figure 2.1) lead to a higher productivity (higher extrusion speeds) and higher quality of the products (surface quality, high stiffness & high ductility). It has been shown in the past, that the microstructure plays a major role in the ductility-behavior of 6082 alloys, and although the concertina-like behavior of automotive security parts is not yet fully understood, empirical data show that a small average grain size leads to higher ductility of extruded 6082 profiles [34]. Since the ductility of extruded profiles plays a major role for customers of HAI Braunau, small average grain sizes are necessary to meet the demands of HAI's customers. Dispersoids which are formed during the homogenization step of the process chain – can inhibit recrystallization processes during extrusion and lead to a desired fine grain of the product. Since Mg-Si phases can lead to eutectic melting reactions during extrusion – which can cause poor surface quality (cracks, pick-up defects) – the dissolution of those phases during homogenization should be achieved.

This master thesis focusses on the homogenization step of the process chain.

The major goals are:

- The optimal homogenization parameters (time-temperature curves) should be determined in order to obtain a high number density of small and finely distributed dispersoids (a high number density of small dispersoids causes a higher Zener-Drag and therefore inhibits recrystallization more likely).

- The dissolution and precipitation of Mg-Si phases should be investigated. The role of dispersoids as nucleation-sites for formation of Mg-Si phases should be found out.

- Formed dispersoids and the dissolution and precipitation of Mg-Si phases should be analyzed through metallographic observations, SEM investigations, DSC measurements and through electrical conductivity measurements.

- Mechanical properties relevant for the extrusion of the considered 6082 alloys should be found out by carrying out compression tests.

3 Experimental Procedure

3.1 Materials

Five different alloys were produced by horizontal direct chill (DC) casting at the LKR and were used for the practical part of the thesis. Table 5 shows the different alloys used and the standard composition of EN AW-6082 (alloy 6082.30 v was produced by vertical DC-casting and was investigated during previous theses and is listed in Table 5, since comparisons with 6082.30 h investigated in this thesis and 6082.30 v were carried out). The Mg and Si contents of the experimental alloys are within the limits of EN AW-6082 whereas Mn is outside the limit of EN AW-6082. Although the Mn contents are outside the standard limits of EN AW-6082, the alloys are designated as "6082.xx" in this work to be consistent with HAI's nomenclature of experimental alloys.

Table 5: Chemical composition of alloys used [wt-%]

Specimen number	Cu	Mn	Cr	Fe	Si	Mg
6082.29	---	---	---	0.06	0.80	0.68
6082.30 h	---	---	---	0.18	0.77	0.76
6082.30 v				0.292	0.822	0.72
6082.47	---	---	0.19	0.17	0.78	0.76
6082.48	0.18	---	0.18	0.16	0.78	0.76
6082.49	---	0.2	---	0.15	0.76	0.76
EN AW-6082	≤ 0.10	0.4 – 1.0	≤ 0.25	≤ 0.50	0.7 – 1.3	0.6 – 1.2

The alloys were provided as bolts with a diameter of 10" and length of 5m. For this thesis pieces of approximately 30 cm length were cut out of those bolts. Chemical composition of the alloys was determined by optical emission spectrometry measurements (Spectro Spectromaxx 6) which were carried out along the whole diameter of the cut-out pieces. Eleven measurements were made for each specimen, Table 5 shows the average values (error indication was excluded since the values were too small, but are typically in a +/- range of 0.01 % for Mg and Si and 0.001-0.003 % for the remaining alloying elements of Table 5).

Alloys 6082.29 and 6082.30 were chosen in order to investigate the influence of Fe/formation of Fe-containing phases. Alloys 6082.47 and 6082.49 should give an insight into the formation and distribution of Cr or Mn containing dispersoids, respectively. An addition of Cu usually leads to a further strength increase, in order to investigate this expected effect alloy 6082.48 was chosen. For the trials carried out in this thesis, according pieces were cut-out at approximately half-radius of the bolts. Although the measurement of chemical-composition along the diameter showed a low standard-deviation, it is assumed that the segregation of elements should be lowest within this section of the bolts.

In previous theses, el. conductivity measurements were carried out with specimen number 6082.30 v. In this master thesis all specimens were produced by horizontal DC casting. Since differences between horizontal and vertical DC casting cannot be excluded, el. conductivity measurements were carried out for specimen number 6082.30 v for reasons of comparison.

3.2 Homogenization Variations

For the homogenization-processes, five different heat-treatments were used. For all heat-treatments, a heating-rate of 3K/min was used. The furnace was a Carbolite Gero HRF 7/45B furnace with a temperature range of 30-750 °C and the thermo-couples for temperature-measurements were IEC-584-K- thermoelements (NiCr-Ni). The device for the temperature record was a Testo 735. The thermo-couple was placed inside of an Al-dummy, which was of cubic dimension of 2×2×2 cm with a drill hole which ended in the centre of the specimen. This should ensure that the required set-temperatures were also reached within the specimens. In addition, a thermo-couple measured the air-temperature within the furnace. Both thermo-couples only showed minor differences of about 2-3 °C for all homogenization schemes. All homogenization schemes were carried out under air-atmosphere.

For all homogenization schemes, specimens of dimensions 6×2×2 cm were used (each of the specimens was polished after cutting in order to obtain a smooth surface).

For all schemes the following abbreviation will be used:

Hold-temperature[°C]_duration of homogenization[h]_method of cooling[wq or f]

wq =water quenching
f=furnace cooling

For all alloys and homogenization schemes the transformation of β-AlFeSi into α-AlFeSi should be investigated.

Heat-treatment 580_0_wq

For this heat-treatment the specimens were heated up to 580 °C and subsequently quenched in water (Figure 3.1). This heat-treatment should give insight on the duration of dissolution of Mg-Si phases (primary Mg-Si phases which are existent as precipitates in the as-cast state and secondary Mg-Si phases which are precipitated from the supersaturated as-cast state during heating-up). Due to quenching the specimens in water, precipitation of Mg-Si phases is inhibited. Metallographic specimens of this heat-treatment should reveal if the short time-period which the specimens spend above the solvus line of Al-Mg_2Si is enough to allow for complete dissolution of Mg-Si phases.

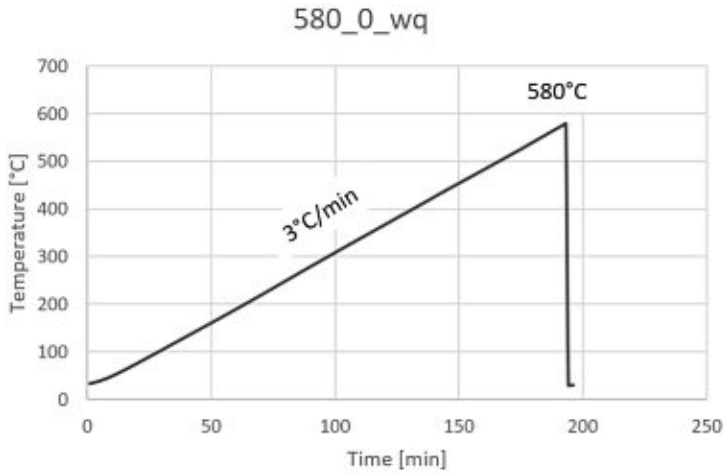

Figure 3.1: Time-Temperature curve of heat-treatment 580_0_wq.

Heat-treatment 580_0_f

For this heat-treatment the specimens were heated up to 580 °C and were then let to cool off to room temperature by turning the furnace off when the Al-dummy reached a temperature of 580 °C (Figure 3.2). Differences compared to 580_0_wq can be attributed to the precipitation of Mg-Si phases after the specimens reach temperatures below the solvus-temperature. Those differences can be detected through metallographic analysis and especially by el. conductivity measurements.

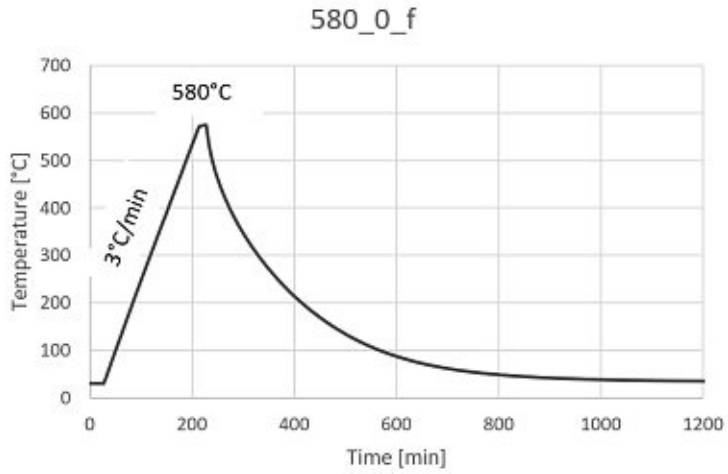

Figure 3.2: Time-Temperature curve of heat-treatment 580_0_f.

Heat-treatment 530_4_wq

In this scheme, the specimens were heated up to 530 °C, held for four hours and then quenched in water (Figure 3.3). The temperature of 530 was applied in order to keep the specimens slightly above the solvus line of Mg_2Si and to reveal if all Mg-Si phases are dissolved after four hours. The duration of four hours is a standard duration period for industrial homogenization schemes. In addition the longer homogenization duration compared to the previous schemes should ensure that dispersoid-forming elements have enough time to form dispersoids of sizes/dimensions which should be detectable by SEM-observations and – if right etching techniques are applied for light-microscope specimens – by light microscope observations.

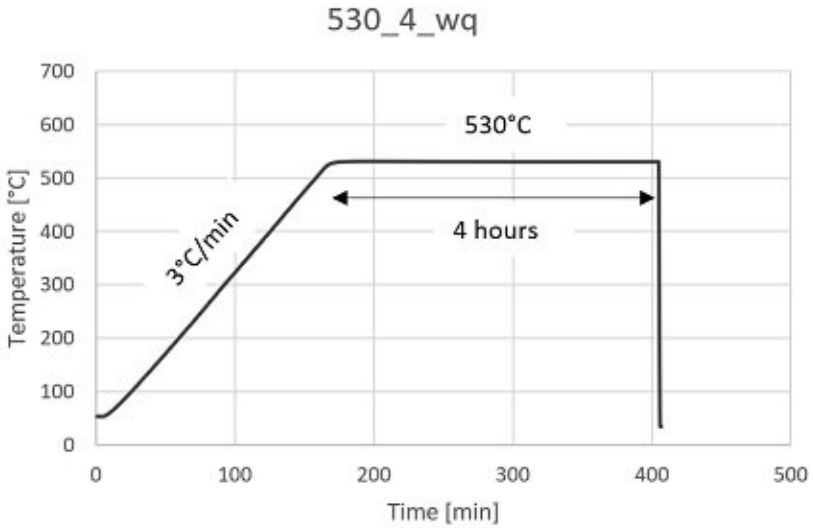

Figure 3.3: Time-Temperature curve of heat-treatment 530_4_wq.

Heat-treatment 580_4_wq

For this heat-treatment, the specimens were heated up to 580 °C, held for four hours and were then quenched in water (Figure 3.4). The differences between this heat-treatment and 580_0_wq in el. conductivity measurements and SEM and light microscope observations should give insight on the formation of dispersoids. A higher number density of dispersoids – or lower number density due to Ostwald-ripening – compared to 580_0_wq could be revealed by SEM observations and light-microscope observations – and the difference in amount of precipitation of dispersoid-forming elements Cr/Mn could by revealed by el. conductivity measurements. In addition the comparison between this heat-treatment and 530_4_wq should reveal if the higher temperature allows for higher-number densities of dispersoids.

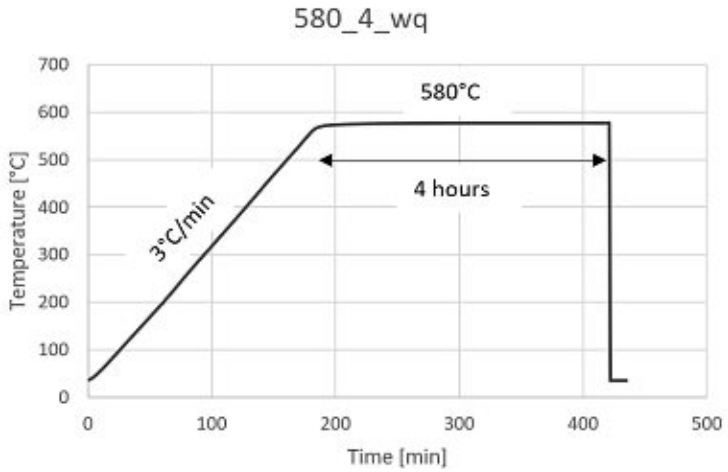

Figure 3.4: Time-Temperature curve of heat-treatment 580_4_wq.

Heat-treatment 580_4_f

Heat-treatment 580_4_f is close to one of the standard heat-treatment procedures in the industry. In this case, the specimens were heated up to 580°C and kept for four hours at this temperature and were then furnace cooled to room temperature by turning the furnace off at the end of the hold-period of four hours (Figure 3.5). Comparison of this heat-treatment and 580_0_f should reveal if more Mg-Si phases precipitate for this heat-treatment (alloys containing dispersoid-forming elements may form dispersoids during the hold-period which might act as nucleation sites for Mg-Si precipitation and therefore allow for more quantitative precipitation of Mg-Si). A higher amount of Mg-Si precipitation compared to 580_0_f could be detected through el. conductivity measurements and dispersoids acting as nucleation sites could be detected through light microscope-observation (different patterns of Mg-Si precipitates reveal if Mg-Si nucleation occurred at a higher number of nucleation sites compared to 580_0_f).

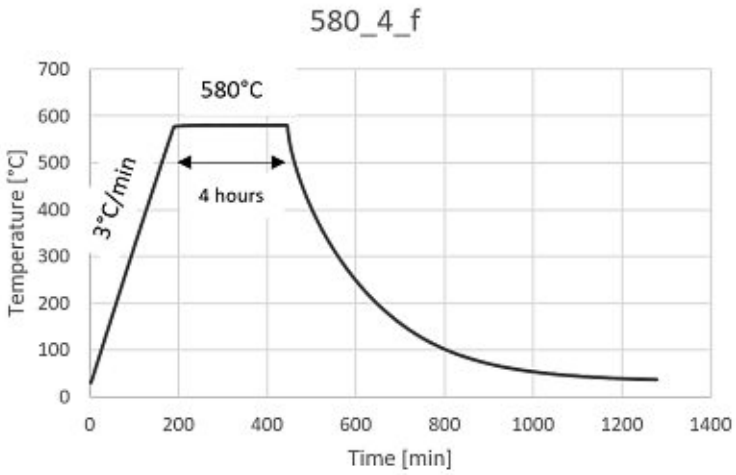

Figure 3.5: Time-Temperature curve of heat-treatment 580_4_f.

3.3 Electrical conductivity measurements

The conductivity measurements show the differences in conductivity before (as-cast) and after homogenization. The different homogenization schemes are ordered depending on their heat input (area under the curves of time-temperature records) towards the specimen.

The device for the conductivity measurements was a SIGMASCOPE®SMP with an integrated ES40 temperature measurement head. The device produces eddy-currents through a coil which is placed on the surface of the specimen [69]. The strengths of the eddy-currents depend on the conductivity of the material. The formed currents produce an electro-magnetic field which is opposed to the initial field of the coil. The opposed electro-magnetic field is detected by a receiver-coil and the conductivity of the material can be determined by the difference of initial and opposed electro-magnetic fields [69].

Since the conductivity is temperature-dependent, the temperature of the specimens was measured with the integrated temperature probe. The probe was placed on the surface of the specimen and held on the surface till the temperature value remained steady, meaning that the probe and specimen-surface had the same temperature. The internal temperature-compensation of the SIGMASCOPE®SMP calculated the conductivity for room temperature [69].

The diameter of the SIGMASCOPE®SMP probe for measuring the el. conductivity and temperature has a diameter of 10 mm. From HAI'S previous experience from el. conductivity measurements with this device it is known, that specimens should have dimensions of at least- 15x15x15 mm in order to avoid negative influence on the formation of Eddy-currents within the specimens during measurement (smaller dimensions cause the measured values to have a high standard-deviation). For this thesis the size of the specimens was chosen to be 6x2x2 cm, and all surfaces of the specimens were grind-polished using SiC#180 grind-paper in order to obtain a smooth surface.

14 conductivity measurements were made for each specimens in the as-cast state and in the homogenized state. The differences in conductivity for those two states are shown in the relevant chapter for each alloy.

3.4 SEM-Observation

For scanning electron microscopy (SEM) measurements, a TESCAN MIRA 3 was used. The TESCAN MIRA 3 has a Schottky field emitter gun as electron source [70]. A four-quadrant solid-state backscattered electron detector and an Everhart-Thornley detector (operated as secondary electron detector) were used.

3.5 Metallographic analysis

For metallographic analysis an Olympus BX51 M incident-light microscope was used, pictures were taken using a Olympus DP 26 digital camera and the microscope-software was Steam Motion.

For metallographic preparations a Struers Tegramin 30 grinding and polishing machine was used. Specimens were embedded in epoxy resin and the following grinding/polishing program was carried out:

Table 6: Grinding/Polishing programm applied for preparation of metallographic specimens

Program-Step	grinding/polishing pad	Lubricant	Time per step [min]
1	SiC #180	water	0:30
2	SiC #360	water	1:30
3	SiC #800	water	2:00
4	SiC #1200	water	2:00
5	SiC #2400	water	2:00
6	SiC #4000	water	4:00
7	Struers MD-Mol polishing pad	Struers DP Lubricant-Blue and Struers DP-P 3 µm water-based diamond suspension	4:00
8	Struers MD-Chem polishing pad	Struers OP-S, colloidal silica suspension	0:40

In order to make the grain-structure of 6xxx alloys visible HAI Braunau carries out electro-polishing using the Barker reagent (200 ml H_2O and 5 ml of 35% Tetrafluoroboric-acid)[71]. For electro-polishing a Struers Lectro-Pol 5 electro-polishing device was used. Using the Barker reagent as etching electrolyte a voltage of 24 V was applied for 90 seconds.

For the determination of the average-grain size light microscopy specimens of the as-cast condition of all alloys were prepared, except for alloy 6082.29 (since alloy 6082.29 is of no industrial relevance). Electro-polishing of specimens using Barker's reagent was applied. The Steam Motion software of the microscope uses an intersection-method to determine the grain size. A line/circle-pattern is drawn by the software (green lines/circles in Figure 3.6). The intersection points of the green lines/circles and grain-boundaries (red circles in the smaller picture of Figure 3.6) are drawn manually using the software.

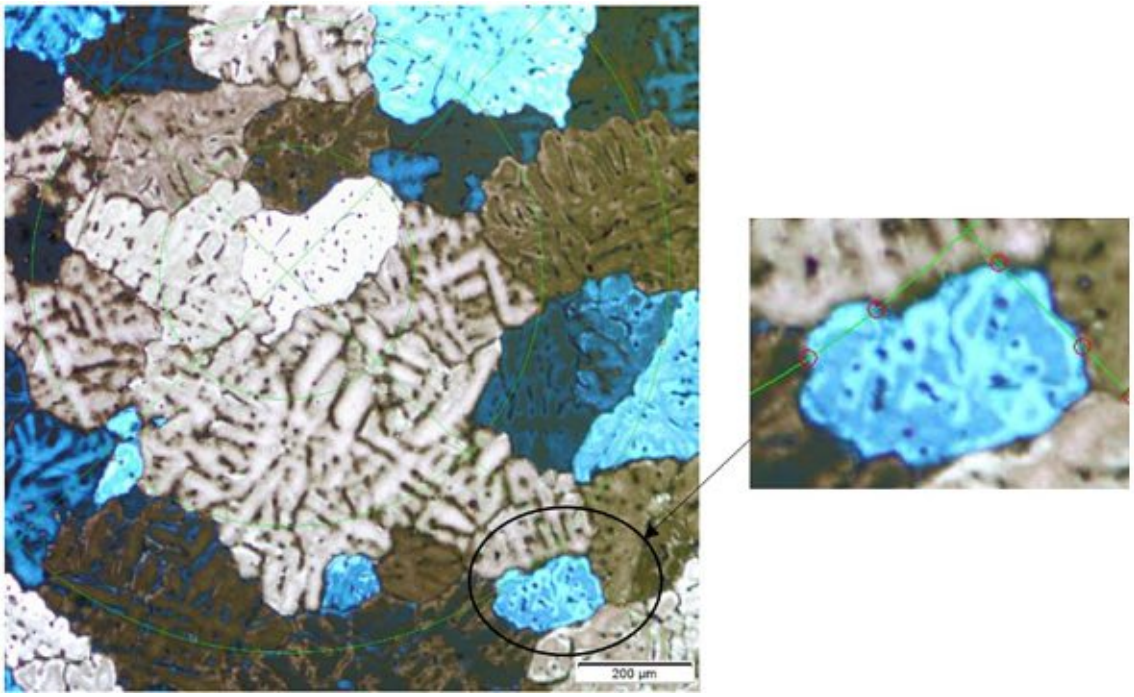

Figure 3.6: Intersection-method for determination of the average grain size, green lines/circles (large picture) are drawn by the Steam Motion software, intersection points of the green lines/circles and grain-boundaries (red dots in the small picture) are determined manually.

Five different micrographs of Barker-etched specimens of each alloy were used for the estimation of the average grain size. The mean grain size of the alloys was determined. The software returns an average grain size number of the five different micrographs. Using the ASTM E 112-113 standard, the average grain-size can be calculated by the following scheme:

ASTM E 112-13 contains a formula for calculating the number density:

$$G = (3.321928 * log_{10} N_A) - 2.954 \quad (6)$$

G = grain size number []
N_A = Grains/Unit Area [no./mm²]

After rearranging Equation (6) for N_A, the number density is obtained:

$$N_A = 10^{\frac{(G+2.954)}{3.321928}} \quad (7)$$

The reciprocal value of N_A gives the average grain area in mm²

In order to make dispersoids visible by light-microscope observation, specimens which were quenched at the end of a homogenization scheme – quenching prevents the precipitation of Mg-Si-phases – were etched for two minutes at 70 °C in 20 wt% sulfuric acid. This etch-method was described by Loodgard and Ryum and offers an easy and quick way to investigate the formation of dispersoids and gives a rough information of their spatial distribution [28]. Since for heat-treatment 580_0_wq no significant formation of dispersoids was expected (due to a lack of isothermal sections), no etching procedures were performed for this homogenization scheme.

3.6 DSC measurements

For DSC measurements a Netzsch DSC 204 F1 differential scanning calorimeter was used. Of each alloy two separate DSC runs of the as-cast state were carried out. The specimens were heated up at 3K/min up to 600 °C. As reference material Al of 99,98 % purity was used. In order to obtain the heat-flux of the formed/dissolved phases of interest (Mg-Si-phases and dispersoids) the measured heat-flux of the reference-material was subtracted from the measured heat-flux of alloys 6082.29-6082.49.

3.7 Dilatometer measurements

Hot compression tests of homogenized specimens (details on which homogenization scheme was applied prior to compression tests are given in chapter “4.14”) were carried out using a deformation and quenching dilatometer DIL805A/D from TA Instruments. The geometry of the specimens was cylindrical with a 5 mm diameter and 10 mm in height. The specimens were heated up with 15 K/s to a deformation temperature T = {450 °C, 480°C, 510°C} and were then deformed at a deformation rate of $\dot{\varphi} = 1.0\ s^{-1}$ up to a strain of 1.0. For each deformation temperature three specimens were deformed.

3.8 ThermoCalc Calculations

In order to determine the thermodynamic phase-composition for the relevant alloys, thermodynamic calculations were carried out using ThermoCalc. The version of the software was “ThermoCalc 2020 a”, the database applied was “Thermo-Calc TCA16”. The obtained data was plotted using “Origin Pro 2015”.

Since the alloys contain several different elements the question occurs, if the solvus line of phases of interest (especially Mg_2Si) is reached for the applied heat-treatments. For this reason a phase-composition diagram was calculated for all specimens using ThermoCalc.

3.9 Statistical analysis of experimental data

Whenever mean-values were used to calculate a new mean-value, the standard-deviation of the result was calculated using Gaussian error propagation [72]:

Table 7: Equations for the determination of the standard-deviation of a calculated mean-value [72]

	Standard-deviation of the calculated mean-value
$\bar{z} = \bar{x} + \bar{y}$	$\Delta z = \sqrt{(\Delta x)^2 + (\Delta y)^2}$
$\bar{z} = \bar{x} - \bar{y}$	
$\bar{z} = C * \bar{x} * \bar{y}$	$\left\lvert\frac{\Delta z}{\bar{z}}\right\rvert = \sqrt{\left\lvert\frac{\Delta x}{\bar{x}}\right\rvert^2 + \left\lvert\frac{\Delta y}{\bar{y}}\right\rvert^2}$
$\bar{z} = C * \frac{\bar{x}}{\bar{y}}$	

$\bar{x}$; $\bar{y}$; $\bar{z}$= Mean values of variables x, y, z
Δx; Δy; Δz = Standard deviation of variables x, y, z
C = constant value

For the characterization of the reference alloy 6082.30 h, el. conductivity measurements were carried out using a SIGMASCOPE®SMP device. In previous theses vertically casted 6082.30 v alloy was investigated, for this alloy el. conductivity measurements were carried out using a SIGMASCOPE® MMS device.

In order to determine differences between vertically and horizontally casted alloys, el. conductivity measurements of equivalent heat-treatments of both alloys were compared. Since two different devices were used for the different alloys (SIGMASCOPE®SMP for horizontally casted 6082.30 and SIGMASCOPE® MMS for vertically casted 6082.30), the question occurs if those devices are equivalent and if separate measurements of those devices can be compared.

A statistical method to determine this was applied [72]:

μ_1 and μ_2 are mean-values of el. conductivity of the same alloy obtained by two different devices (it is assumed, that the measurements underly a Gaussian-distribution). A statistical test should determine, whether or not those two mean-values are equivalent, so two cases are to be tested:

In order to carry this test out, an additional "help"-parameter is calculated:

$$\mu = \mu_1 - \mu_2$$

μ = Difference of the two mean-values μ_1 and μ_2

then, the

$$\text{Zero-Hypothesis } H_0: \mu = 0$$

is tested against the

$$\text{Alternative-Hypothesis } H_1: \mu \neq 0$$

Since the assumption is made, that the measured values underly Gaussian-distribution, the Zero Hypothesis has a lower and upper boundary, which depends on the level of significance. For this test a level of significance of $\alpha = 0.01$ was chosen. Further a test-variable has to be calculated [72]:

$$\hat{t} = \frac{\bar{z}}{\frac{s}{\sqrt{n}}}$$

$\hat{t}$ = Test-Variable
$\bar{z}$ = mean value of μ for a certain number of measurements
s = standard deviation of $\bar{z}$
n = number of measurements

Figure 3.7 shows the upper and lower boundary which are determined by the paramter c for the Zero-Hypothesis (light-grey area, the dark-grey areas show the area of the Alternative-Hypothesis) [72]. The parameter c underlies the student t-distribution and can be taken from tables in the literature (c depends on the number of measurements and the level of significance) [72].

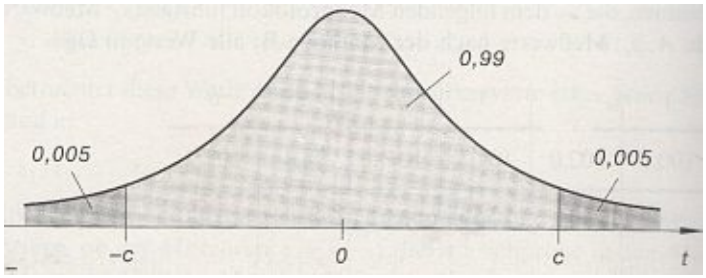

Figure 3.7: Bright-grey area shows the area of the Zero-Hypothesis (which depends on the parameter c, the level of significance in this picture is α = 0.01, which causes the Zero-Hypothesis to have a value of 1- α = 0.99), the dark-grey areas show the Alternative-Hypothesis, in sum both areas of the Alternative-Hypothesis equal to α = 0.01 [72].

If the test-variable t lies within the boundaries of the Zero-Hypothesis, the Zero-Hypothesis can be accepted, otherwise it has to be dismissed and the Alternative-Hypothesis has to be accepted.

If the test reveals that the Zero-Hypothesis is true, the assumption can be made (with a certainty of 1-α), that the two devices are equivalent, if however the test reveals that the Alternative-Hypothesis is true, the assumption that the two devices are equivalent has to be dismissed and measurements carried out with the tested devices on the same specimen cannot be compared.

In order to determine whether or not the Zero-Hypothesis can be accepted, 10 el. conductivity measurements were carried out on four different alloys in the as cast state (6082.30 h, 6082.47, 6082.48, 6082.49 and 6082.50) with both devices. Further, only the results of alloy 6082.30 h are shown since the other alloys delivered the same end-result:

Table 8: Values of el. conductivity (and their differences) obtained with SIGMASCOPE®SMP AND SIGMASCOPE®MMS

Number of measurements	**Values of el. conductivity obtained with SIGMASCOPE®SMP [MS/m]**	**Values of el. conductivity obtained with SIGMASCOPE®MMS [MS/m]**	**Differences in values of el. conductivity between SIGMASCOPE®SMP and SIGMASCOPE®MMS [MS/m]**
1	27.3	27.1	0.2
2	27.5	27.3	0.2
3	27.6	27.5	0.1
4	27.7	27.5	0.2
5	27.8	27.6	0.2
6	27.1	27.1	0
7	27.5	27.2	0.3
8	27.6	27.4	0.2
9	27.8	27.6	0.2
10	27.7	27.6	0.1
Sum of values	275.6	273.9	1.7

Next, the mean value of the differences has to be calculated using the following formula:

$$\bar{z} = \frac{1}{n} * \sum_{1}^{n} z_i$$

$\bar{z}$ = mean value of the differences in el. conducvitivy [MS/m]
n = number of measurements
z_i = difference in el. conductivity of i[th] measurement [MS/m]

$$\bar{z} = \frac{1}{10} * \sum_{1}^{10} z_i = \frac{1}{10} * 1.7 \text{ MS/m} = \underline{0.17 \text{ MS/m}}$$

Then, the standard deviation of $\bar{z}$ has to be calculated:

$$s^2 = \frac{1}{n-1} * \sum_{1}^{n} (z_i - \bar{z})^2$$

s = standard deviation of $\bar{z}$ [MS/m]
n = number of measurements

The differences $(z_i - \bar{z})$ and the squares of those are calculated:

Table 9: Differences in el. conductivity of table 7 and the mean value and the squared-values of those

Number of measurement	$(z_i - \bar{z})$ [MS/m]	$(z_i - \bar{z})^2$ [MS/m]²
1	0.03	0.0009
2	0.03	0.0009
3	-0.07	0.0049
4	0.03	0.0009
5	0.03	0.0009
6	-0.17	0.0289
7	0.13	0.0169
8	0.03	0.0009
9	0.03	0.0009
10	-0.07	0.0049
Sum of values	0	0.061

Then, the standard-deviation can be calculated using:

$s^2 = \underline{0.0068 \text{ [MS/m]}^2}$

$s = \underline{0.082 \text{ [MS/m]}}$

Since all necessary variables are calculated, the test-Parameter $\hat{t}$ can be calculated:

$$\hat{t} = \frac{\bar{z}}{\frac{s}{\sqrt{n}}} = \frac{0.17 \left[\frac{MS}{m}\right]}{\frac{0.082 \left[\frac{MS}{m}\right]}{\sqrt{10}}} = \underline{6.53 \text{ [MS/m]}}$$

The test-parameter $\hat{t}$ has now to be compared with the parameter c. For 10 measurements and a level of confidence of α = 0.01 the value for c obtained from the literature equals to 3.25 [72].

Since the test parameter $\hat{t}$ is outside the area of the Zero-Hypothesis, the Alternative-Hypothesis has to be accepted, which means, that the two devices (SIGMASCOPE®SMP and SIGMASCOPE®MMS) are not equivalent and results obtained by the two devices cannot be compared.

However, since no vertically casted specimens were available during this Master-thesis, the comparison of the eletrical conductivity measurements was still carried out in order to observe if major differences between vertically and horizontally casted specimens could be seen, keeping in mind, that for a statistically relevant comparison electrical conductivity measurements of vertically and horizontally casted specimens should be carried out with the SIGMASCOPE®SMP in the future.

4 Results and discussion

4.1 Characterization of reference material

In previous theses at HAI Braunau vertically casted alloys were investigated. Since all alloys used in this thesis were produced by horizontal direct-chill (DC) casting, the question occurs if horizontally casted alloys and vertically casted alloys can be compared. In order to determine this, el. conductivity measurements were carried out for alloy 6082.30 h. Specimens were heated up to a certain temperature and subsequently quenched in water. The differences in el. conductivity after-quenching and the as-cast state are plotted in Figure 4.1 for a vertically and horizontally casted 6082.30 alloy.

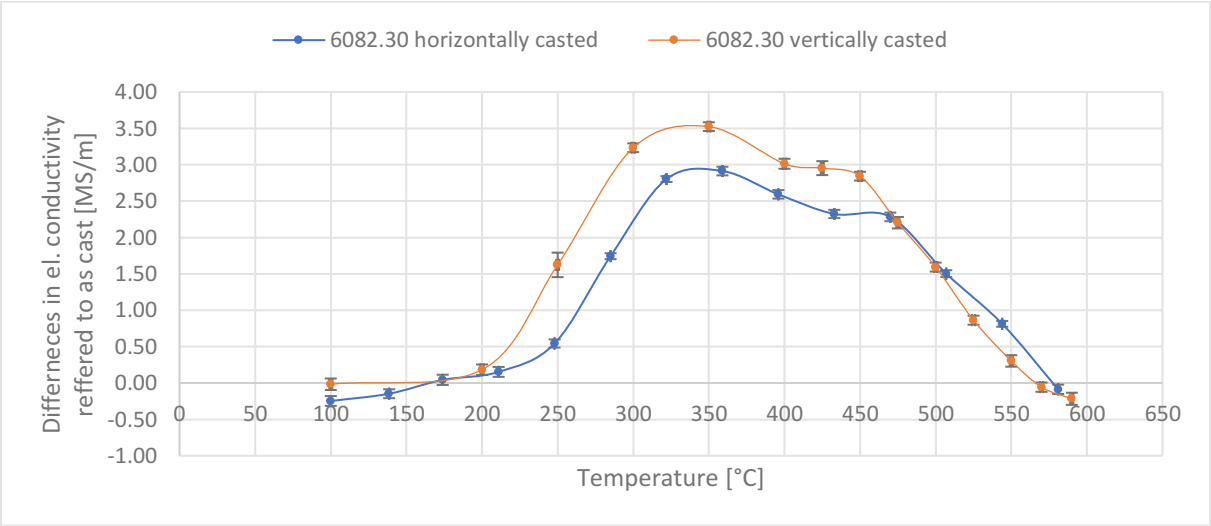

Figure 4.1: Differences in el. conductivity (Δσ) post-heat-treatments (after water-quenching) and as-cast state of horizontally (measured with SIGMASCOPE®SMP) and vertically (measured with SIGMASCOPE®MMS) casted 6082.30 alloys (black bars for each measurement are standard deviations, specimens were heated up to the corresponding temperature and were then subsequently quenched in water and el. conductivity was measure immediately after water-quenching).

Table 10 shows the difference in chemical composition of the two alloys.

Table 10: Chemical composition of horizontally and vertically casted 6082.30 alloys [wt-%]

Specimen number	Fe	Si	Mg
6082.30 h	0.18	0.77	0.76
6082.30 v	0.292	0.822	0.72

ThermoCalc calculations of both alloys were carried out in order to determine the phase-composition at different temperatures (Figure 4.2). The solvus-temperature for Mg_2Si is 525°C, $Al_9Fe_2Si_2$ and Al_8Fe_2Si are expected to represent different stoichiometry of Al-Fe-Si phases. Excess silicon which is not incorporated during Mg_2Si formation shows a solvus-temperature of 430 °C (6082.30 h) and 420 °C (6082.30 v).

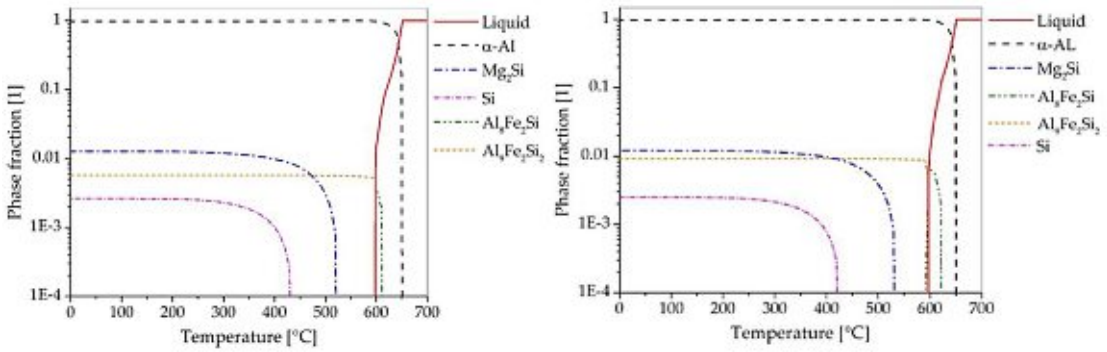

Figure 4.2: ThermoCalc calculations showing the phase-composition of alloys 6082.30 h (left) and 6082.30 v (right) for a temperature range of 0-700°C. The major difference between the two alloys is, that the AlFeSi phases have a higher content for 6082.30 v, since this alloy contains more Fe.

As can be seen in Figure 4.1 the shape of the el. conductivity/temperature curves of the horizontally and vertically DC casted materials match reasonably well. The horizontal shift could be explained due to the higher Fe-content. It is known through HAI's experience of former trials that Al-Fe-Si phases act as nucleation sites for the precipitation of Mg-Si phases. Therefore, the higher Fe content of 6082.30 v could cause the precipitation of more Al-Fe-Si phases – and therefore Mg-Si phases – to occur at lower temperatures. In addition, the vertical shift could also be explained due to the different chemical composition (Table 10). Since alloy 6082.30 v contains more Fe, more Al-Fe-Si phases can be precipitated, which lead to a higher increase in el. conductivity compared to 6082.30 h. Using Table 4 to calculate the difference in el. conductivity, a vertical shift of ≈ 0.2 MS/m can be explained due to the higher Fe content. In addition, it has to be kept in mind, that measurements of the horizontally and vertically casted materials were carried out using two different devices. In the previous chapter it was shown – applying statistical methods – that the two devices are not equivalent. The further shift in electrical conductivity – which can't be explained by the difference in chemical composition of the specimens – could be explained due to the fact that the SIGMASCOPE®SMP (horizontally casted specimens) and SIGMASCOPE® MMP (vertically casted specimens) are not equivalent.

Since no significant differences could be seen between the differently casted materials, it is assumed that horizontally or vertically casted materials should show the same material behavior for different homogenization variations.

4.2 Average grain size

The average grain area showed similar values except for alloy 6082.47, which showed a significantly higher value for the average grain area. In order to receive greater grain areas, elements can be added which enlarge the solidification interval during casting. This can be achieved by adding elements to the molten material which have small diffusion-coefficients in the solid state like Cr (Figure 2.5).

Grain size was calculated according to the ASTM E 112-13 standard and the obtained values are shown in Table 11:

Table 11: grain size-numbers

Specimen number	Average grain size number []	Standard deviation of grain size number +/- []	**Average grain area [mm²]**	Standard deviation of grain area +/- [mm²]
6082.30	2.84	1,42	**0.018**	0.048
6082.47	0.42	0.76	**0.096**	0.076
6082.48	2.51	0.21	**0.023**	0.11
6082.49	2.84	0.30	**0.018**	0.11

4.3 Near-ternary Al-Mg-Si alloy (6082.29)

4.3.1 Microstructure of the as cast state

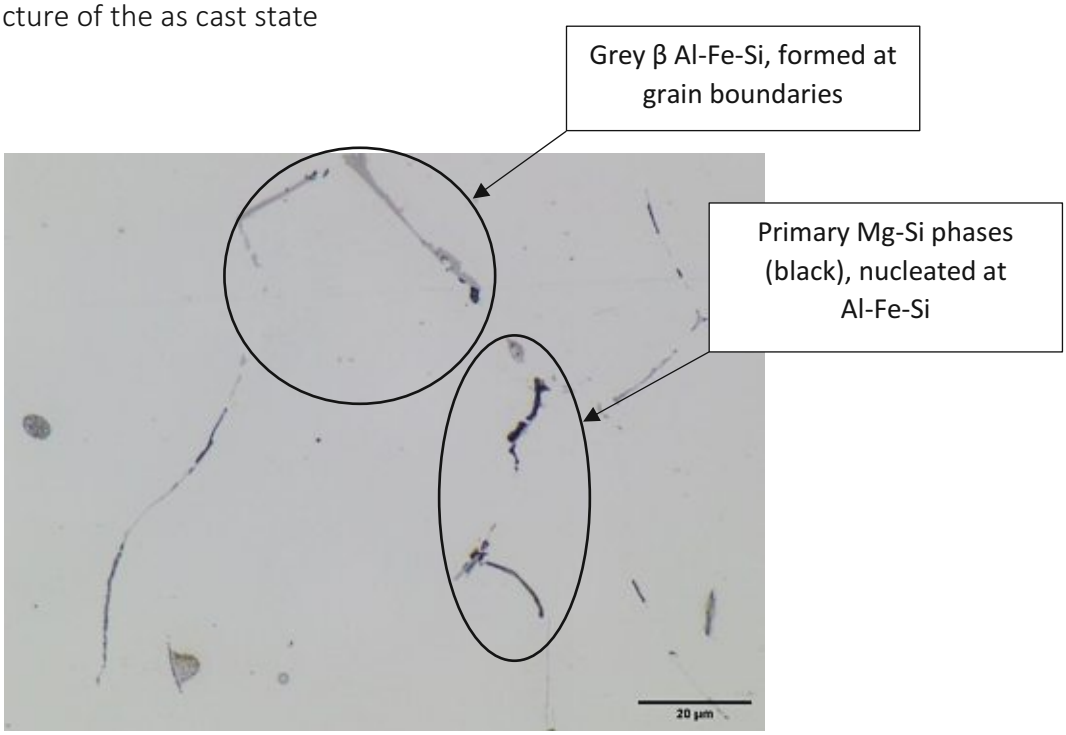

Figure 4.3: as cast condition of alloy 6082.29, grey Al-Fe-Si phases and black primary Mg-Si phases are visible (unetched).

Figure 4.3 shows the as-cast state of alloy 6082.29. Grey β-Al-Fe-Si phases which precipitate at the grain boundaries during casting and primary Mg-Si phases which precipitate on Al-Fe-Si phases also during casting, are both visible.

4.3.2 El. conductivity measurements and metallography

Since Table 4 allows to calculate the electrical conductivity of a specimen in a certain state (as-cast-state or post-heat-treatment state) electrical conductivity of expected phase compositions (alloying elements in solid-solution or in precipitated state) were calculated and compared to the values obtained by measurement.

At the beginning of this chapter the el. conductivity measurements of the as-cast state of alloy 6082.29 should be discussed. For the calculation of the electrical conductivity of the as-cast state of alloy 6082.29 two assumptions were made. For the first calculation, it was assumed that the whole Mg and Si content of the specimen is in supersaturated solid-solution and all of the Fe content is out of solution (since the metallographic observation showed significant Al-Fe-Si precipitation at the grain boundaries). For the second calculation it was assumed that Mg, Si and Fe are out of solid-solution. Those two calculations should give the values of el. conductivity of the as-cast state of two “extreme” cases, setting an upper and lower limit for the el. conductivity. The values of el. conductivity obtained by measurement should give insight which of the two assumed cases explains the as-cast state more likely.

Figure 4.4 shows the obtained results. It is obvious that the first assumption (Fe out of solution, Mg and Si in supersaturated solid solution) describes the as-cast state significantly better than the second assumption. The as-cast state could therefore be better explained by assuming that the major part of

Fe is precipitated as Al-Fe-Si phases at the grain-boundaries during casting, whereas only a minor part of Si and Mg precipitate as primary Mg-Si phases at the Al-Fe-Si phases and the rest of Mg and Si remain in supersaturated-solid-solution.

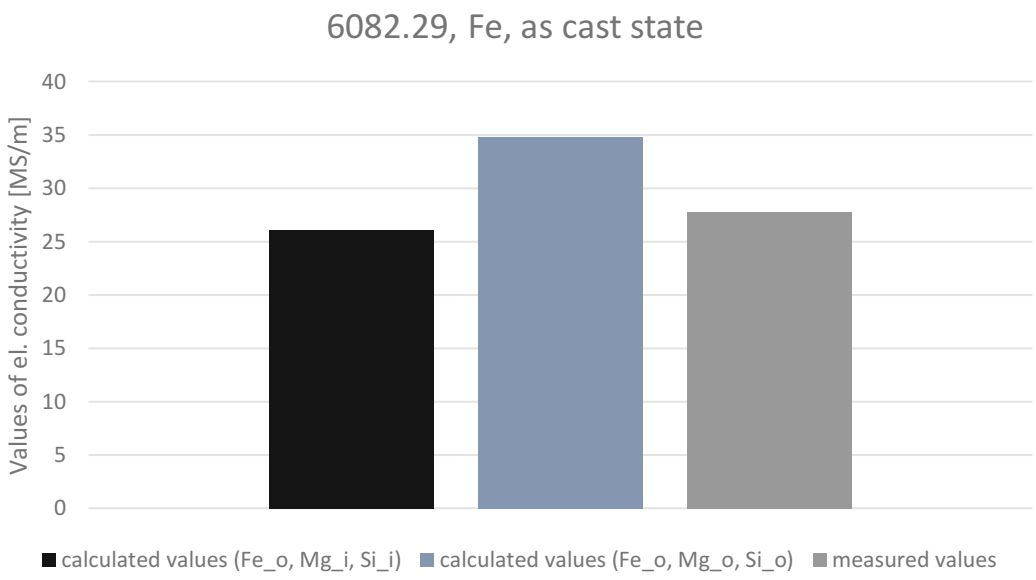

Figure 4.4: Values of el. conductivity of alloys 6082.29 of the as-cast state (bars for standard-deviation of the measured values are excluded since they were too small to be seen in this figure).
Abbreviations:
Element_o = Element out of solution
Element_i = Element in solid solution (super-saturated-solution).

For the applied heat-treatments equivalent calculations of the assumed state of the alloying elements were carried out and compared to the measured-values (the assumed states of the alloying-elements in solid solution or out of solution are shown in Table 12). The assumptions are also made based on calculations carried out using the Thermo-Calc software, keeping in mind that calculations of the phase-composition only show the thermodynamic-stable phases and give no insight on the kinetics of precipitations or dissolution (Figure 4.5). The Al_8Fe_2Si and $Al_9Fe_2Si_2$ phases in Figure 4.5 are assumed to be Al-Fe-Si phases of different stoichiometry. The solvus line for Mg_2Si is reached at a temperature of 525 °C, whereas excess Si which is not incorporated during Mg_2Si formation has a solvus-temperature of 460 °C.

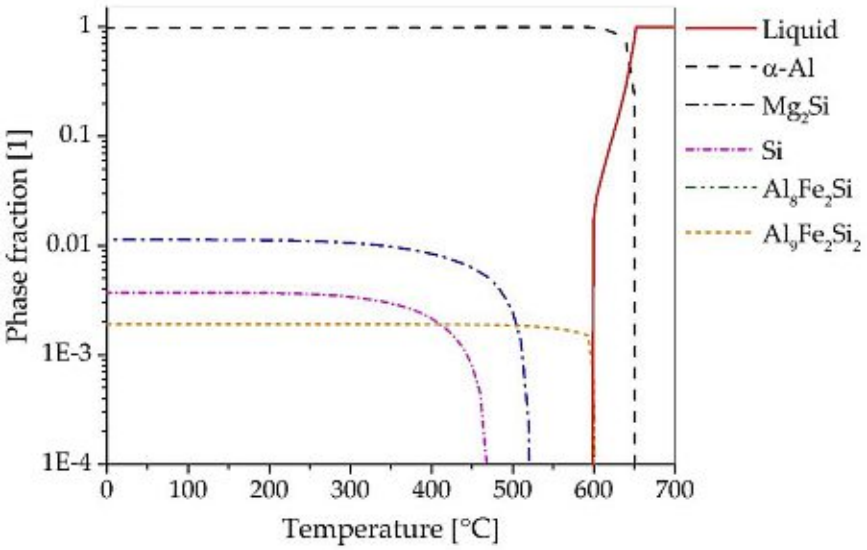

Figure 4.5: Thermo-Calc calculations of the phase-composition depending on temperature for alloy 6082.29.

Table 12: Assumed state of the alloying elements for the calculation of el. conductivity values after corresponding heat-treatments.
Abbreviation:
Element_o = out of solution
Element_i = Element in solid-solution

Heat-treatments	Fe	Si	Mg
580_0_wq	Fe_o	Si_i	Mg_i
580_0_f	Fe_o	Si_o	Mg_o
530_4_wq	Fe_o	Si_i	Mg_i
580_4_wq	Fe_o	Si_i	Mg_i
580_4_f	Fe_o	Si_o	Mg_o

Figure 4.6 shows the difference in el. conductivity of the calculated values and the measured values. In addition, the measured values of the el. conductivity post-heat treatments compared to the measured-values of the as cast state (by subtracting the measured el. conductivity of the as-cast-state from the el. conductivity measured after heat-treatment) are discussed (Figure 4.7). Thorough explanations of the results for each heat-treatment are given in the following sections.

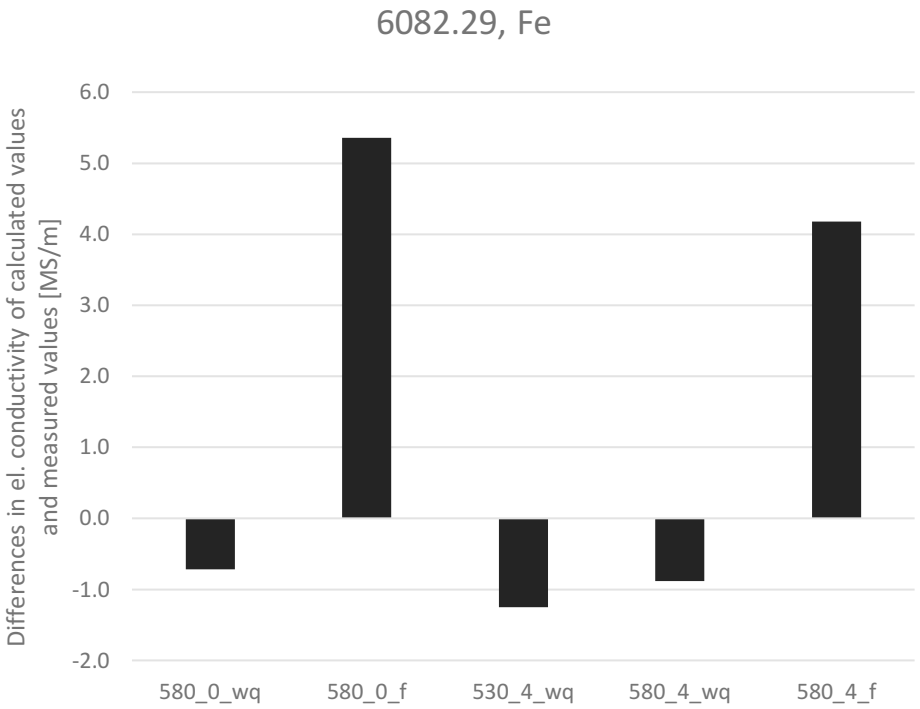

Figure 4.6: Differences in el. conductivity (Δσ) for calculated values (of assumed states of the alloying elements) after heat-treatment and the according measured values post heat-treatment.

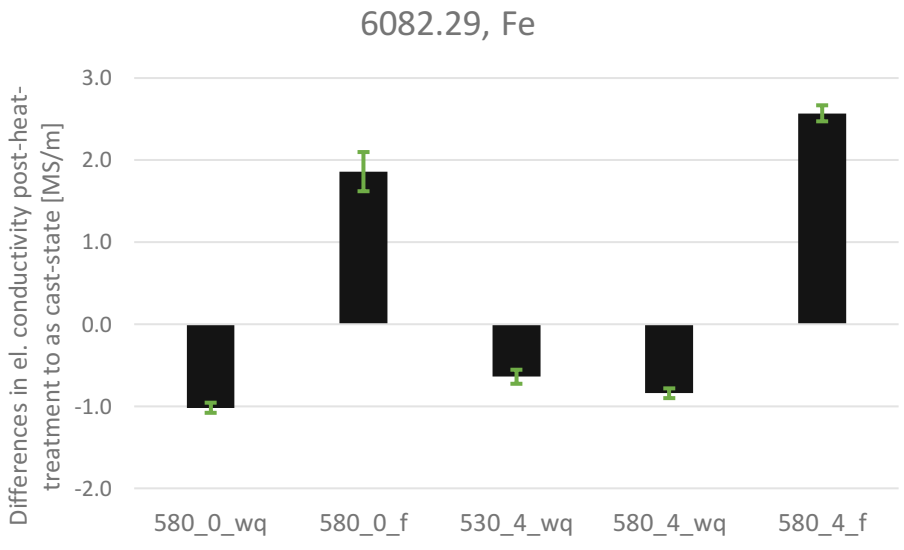

Figure 4.7: Differences in el. conductivity (Δσ) post-heat-treatments and as cast state of the according specimens of alloy 6082.29 (green bars indicate standard-deviations of Δσ and were calculated using Gaussian-error propagation).

Since alloy 6082.29 contains Fe only in small quantities (besides Mg and Si) the differences in the conductivity measurements can mainly be explained by formation/solution of Mg-Si phases in the Al Matrix.

Heat-treatment 580_0_wq

Differences in el. conductivity of the calculated values and measured values (Figure 4.6)

For this heat-treatment it was assumed that Fe is out of solution and both Mg and Si are in solid-solution (in this case the incorporation of Mg and Si in the Al-Fe-Si phases was neglected since only a rough-estimation is desired at this stage). This assumption was made since for this heat-treatment the temperature goes above the solvus-temperature of Mg_2Si (525 °C). Although the specimens remain rather shortly above the solvus-temperature (and therefore complete dissolution of primary Mg_2Si is rather unlikely), these assumptions set a lower-limit for the expected value of el. conductivity for this heat treatment. The negative value of $\Delta\sigma$ in Figure 4.6 for this heat-treatment shows that the measured-value was higher than the calculated value. This observation can be explained, due to the fact, that probably a certain amount of Mg and Si remain as precipitates in the Al-matrix (which precipitate upon heating-up from the super-saturated-state) and do not form a solid-solution with the Al-matrix since time period above the solvus-temperature is too short.

Differences in el. conductivity of the measured-values post heat-treatment and the as-cast state (Figure 4.7)

For 580_0_wq, the decrease in conductivity for the water quenched specimens can be explained by the partial dissolution of primary Mg-Si. Due to the short heat input, probably only a minor part of the primary Mg-Si dissolves before the specimen is quenched (as it was assumed in the previous section). The dissolved amount remains in solid solution because of the quenching process. It is assumed, that during the heating-up, secondary Mg-Si phases (Mg-Si which is in supersaturated solid solution in the as cast alloy) are precipitated in the grains homogenously but are partially dissolved again upon exceeding the solvus temperature. The dissolution of secondary Mg-Si phases should occur rather quickly since it is assumed that they are relatively small in size.

Figure 4.8 shows that the grey Al-Fe-Si phases are mostly free of primary Mg-Si (which would appear as black dots next to Al-Fe-Si-phases). The low Fe content leads to the formation of fewer Al-Fe-Si phases, which leads to less formation of precipitates of primary Mg-Si (since it is know from HAI's previous experience that Al-Fe-Si phases act as nucleation agents/sites for Mg-Si-phases). It would therefore require shorter time-periods in order to dissolve all primary Mg-Si phases for temperatures above the solvus line. It seems that the short time interval of 580_0_wq was enough to dissolve the majority of primary Mg-Si for alloy 6082.29. However, the result obtained in Figure 4.6 shows that a certain amount of Mg and Si probably remains undissolved in the Al-matrix. Since the metallographic observation in Figure 4.8 shows no visible remaining primary Mg-Si phases, it is assumed that the undissolved Mg-Si phases are secondary Mg-Si phases, which are precipitated upon heating-up (from the super-saturated as-cast state) and not complete dissolved after exceeding the solvus temperature.

Nevertheless, the fact that $\Delta\sigma$ for 580_0_wq is higher than for 530_4_wq and 580_4_wq is still unclear. It has to be kept in mind that the specimens represent only a small fraction of the casted bolts and that each specimen may show a slightly different chemical composition. Although the standard deviation for the optical emission spectrometry was very low, the rather small specimens may show differences in chemistry which could lead to unexpected results in conductivity measurements.

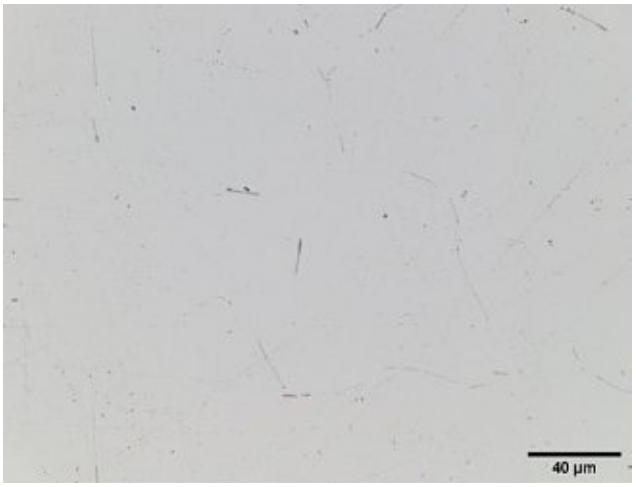

Figure 4.8: 6082.29 after 580_0_wq (unetched).

Heat-treatment 580_0_f

Differences in el. conductivity of the calculated values and measured values (Figure 4.6)

For this heat-treatment the value for Δσ in Figure 4.6 shows a high value. For the calculation it was assumed that this heat-treatment allows dissolved Mg-Si phases to precipitate completely upon cooling-down below temperatures of the solvus-temperature. It was therefore assumed that Fe, Mg and Si are completely out of solid solution. Since the calculated value for this heat-treatment was severely higher than the measured value, it can be assumed that the majority of Mg-Si remains in solid-solution and during cooling-down. When calculating the lower limit for the el. conductivity (Mg and Si both completely in solid-solution) and comparing it with the result of Figure 4.6 a rough estimation can be made, that approximately 2/3 of Mg and Si remain in solid-solution and do not precipitate during cooling-down (this estimation can be made if the lower-limit for el. conductivity is calculated, assuming that all Mg-Si phases remain in solid-solution and comparing the obtained value with the measured value).

Differences in el. conductivity of the measured-values post heat-treatment and the as-cast state (Figure 4.7)

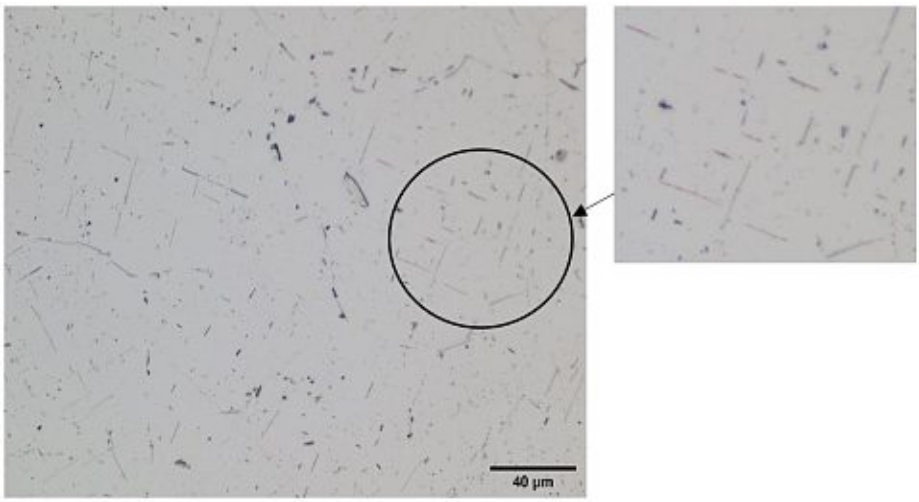

Figure 4.9: 6082.29 after 580_0_f, (unetched) large Mg_2Si-needles are visible (smaller-picture).

For 580_0_f, the high increase for Δσ in Figure 4.7 is explained by the fact that a certain part of Mg-Si is precipitated upon cooling-down. Those Mg-Si phases precipitate during heating-up (as secondary Mg-Si phases from the super-saturated as-cast state; or are present as primary Mg-Si phases in the as-cast state) and dissolve again upon exceeding the solvus-temperature. Therefore, when reaching the solvus line during cooling-down Mg and Si atoms have time at those high temperatures to form phases mentioned in chapter "Ageing". Since the time-period above the solvus-line is approximately twice as long as in 580_0_wq (Figure 3.2), more Mg-Si phases can be dissolved and precipitated during this heat-treatment. Figure 4.9 shows the formation of Mg-Si phases, appearing as long needles in the micrograph.

Heat-treatment 530_4_wq

Differences in el. conductivity of the calculated values and measured values (Figure 4.6)

Figure 4.6 shows Δσ for the el. conductivity of the calculated and measured values. For this heat-treatment the assumption was made, that the temperature of 530 °C (solvus-temperature 525 °C) is enough to enable complete dissolution of Mg-Si phases during the heat-treatment of four hours. This assumption should give a lower limit of the electrical conductivity which could occur if all Mg-Si phases are dissolved (keeping in mind that the set temperature which is only slightly above the solvus-temperature won't probably enable complete dissolution of Mg-Si-phases, however it should give a rough insight on how much of Mg-Si phases is dissolved for this heat-treatment). For Fe complete precipitation is assumed in form of Al-Fe-Si phases (in this case the incorporation of Mg and Si in the Al-Fe-Si phases was neglected since only a rough-estimation is desired at this stage).

The value of Δσ in Figure 4.6 can be explained, due to the fact, that not all Mg-Si phases are dissolved for this heat-treatment. However if the assumption is made that all Mg-Si are in undissolved state (setting an upper limit for the calculated el. conductivity) and compared with the measured-values (which results in a Δσ value of 7.5 MS/m), it is clear that the major part of Mg-Si phases are dissolved and remain in solid-solution upon water-quenching the specimen. It remains unclear why the value of Δσ is higher than for heat-treatment 580_0_wq. The opposite was expected, since the calculated values for the el. conductivity of both heat-treatments are the same, it was expected that the measured value for the el. conductivity for 530_4_wq should be higher since more time for dissolution of the phases is given, however the higher temperature during 580_0_wq may induce significantly stronger diffusion for Mg and Si atoms and therefore the higher temperature might outweigh the longer heating-period of 530_4_wq.

Differences in el. conductivity of the measured-values post heat-treatment and the as-cast state (Figure 4.7)

Figure 4.10 shows a metallographic observation of alloy 6082.29 after homogenization scheme 530_4_wq. Primary Mg_2Si is dissolved during homogenization for temperatures which are above the solvus temperature and the elongated β-Al-Fe-Si phases split into smaller fractions and their edges turn towards round-shaped morphologies. Those changes in morphology for the Al-Fe-Si phases have a positive influence on the ductility of the material [38]. Most of the Al-Fe-Si phases in Figure 4.10 are free of primary Mg_2Si, some Al-Fe-Si phases show black dots, which may be holes by ripped off Al-Fe-Si which occurred during preparation. The decrease in conductivity can be explained by the same effects as in 580_0_wq, nevertheless it remains unclear why Δσ is lower than for 580_0_wq. One explanation (as given in the previous section) could be, that the higher temperature for 580_0_wq

allows for stronger diffusion of Mg-Si phases and this effect outweighs the higher heat-duration for 530_4_wq. It has also be kept in mind, that the temperature of 530_4_wq is only slightly above the solvus-temperature of 525°C and although according to thermodynamics a solid solution of Mg-Si phases should be formed, the process might be kinetically hindered due to diffusion which is too slow for a temperature of 530°C, whereas the higher temperature for 580_0_wq might allow better dissolution of phases (although the time-period above the solvus-temperature is significantly lower). In Figure 4.11 an etched specimen is shown, which shows that no formation of dispersoids is detectable by the method applied.

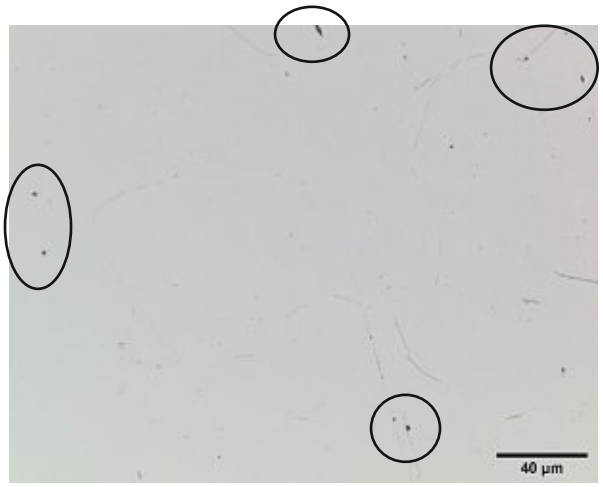

Figure 4.10: 6082.29 after heat-treatment 530_4_wq (unetched), specimen is mostly free of primary Mg-Si, black dots on Al-Fe-Si phases (marked with circles) are rather impurities or Al-Fe-Si phases which are ripped off due to metallographic preparation.

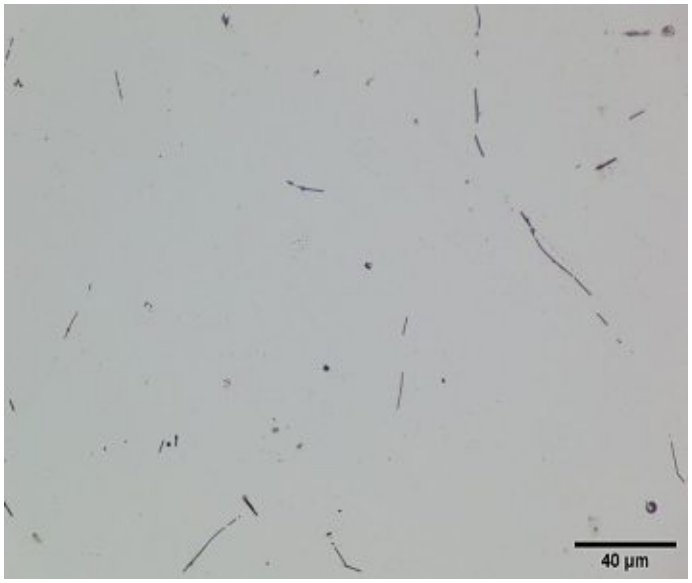

Figure 4.11: Specimen of 6082.29 after heat-treatment 530_4_wq (etched with H_2SO_4).

Heat-treatment 580_4_wq

Differences in el. conductivity of the calculated values and measured values (Figure 4.6)

Figure 4.6 shows Δσ for calculated-measured values of el. conductivity. For the calculation it was assumed that Mg and Si are in solid solution, whereas Fe is precipitated in the form of Al-Fe-Si phases (neglecting the incorporation of Si for Al-Fe-Si formation for simplicity). The negative value of Δσ could be explained due to the fact, that not all Mg-Si phases are completely dissolved for this heat-treatment,

but it remains unclear, why the value of Δσ is smaller than for 580_0_wq. The higher duration for 580_4_wq should allow for higher diffusion and it's expected that a higher amount of Mg-Si phases should form a solid-solution with the Al-matrix (the solvus-temperature is 525 °C) than for 580_0_wq, however, the opposite result was achieved and a reasonable explanation for this result is at this stage missing.

Differences in el. conductivity of the measured-values post heat-treatment and the as-cast state (Figure 4.7)

The conductivity measurements for 580_4_wq in Figure 4.7 shows the same trend as 530_4_wq, the higher decrease can be explained by the higher temperature and therefore stronger diffusion, facilitating dissolution of certain phases like primary Mg_2Si. However, the reason for the slightly lower value of Δσ compared to 580_0_wq remains unclear (see previous section). Metallographic preparations shown in Figure 4.12 show no significant difference compared to 530_4_wq. Even the etched specimen in Figure 4.13 shows no difference compared to Figure 4.11, so no observation of Fe-dispersoid formation could be detected through light-microscope observations.

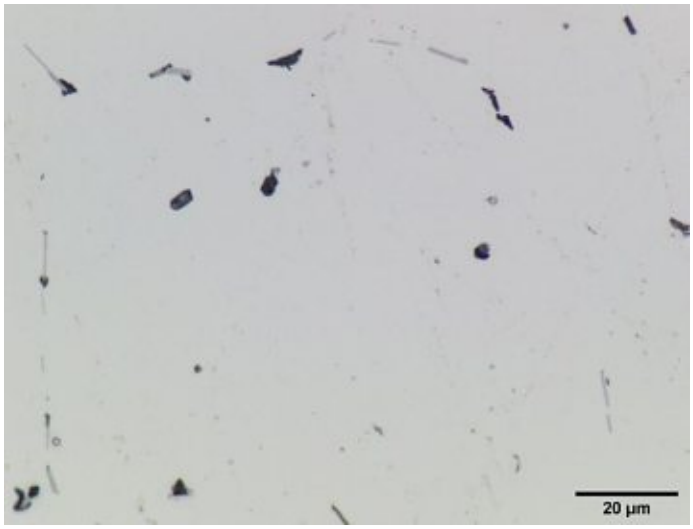

Figure 4.12: Alloy 6082.29 after heat-treatment 580_4_wq, black dots are rather Al-Fe-Si phases – which have been ripped off during metallographic preparation – than primary Mg-Si phases.

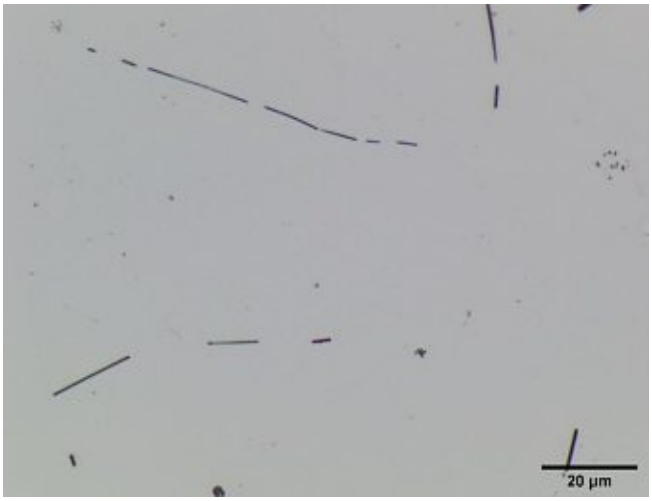

Figure 4.13: Alloy 6082.29 after heat-treatment 580_4_wq (etched with H_2SO_4), no visible formation of Fe-dispersoids could be detected by this method.

Heat-treatment 580_4_f

Differences in el. conductivity of the calculated values and measured values (Figure 4.6)

Figure 4.6 shows Δσ of the el. conductivity of the calculated-measured values for 580_4_f. The value for this heat-treatment is lower compared to 580_0_f. This could be explained due to the fact that more Mg-Si phases are precipitated during cooling-down once the temperature is beneath the solvus temperature of 525 °C. A possible explanation for this event could be the formation of Fe-dispersoids which act as nucleation sites for Mg-Si precipitation and therefore magnify the precipitation. If Fe-dispersoid formation occurs for this alloy, the longer heating-period of 580_4_f compared to 580_0_f should create a significantly higher number of dispersoids. The formation of Fe-dispersoids couldn't be detected through metallographic observations (as shown in the previous section). It is therefore assumed, that if Fe-dispersoids were formed their size is too small to be detected by light-microscope observation.

Differences in el. conductivity of the measured-values post heat-treatment and the as-cast state (Figure 4.7)

The high increase in conductivity for 580_4_f in Figure 4.7 can be explained by the same reason as for 580_0_f. The longer holding-period of four hours for 580_4_f probably allows the major part of primary Mg-Si to dissolve completley, which during cooling-down precipitates also to a large extent.

Since the cooling-down curves for 580_0_f and 580_4_f are basically the same, the question is raised, if Fe-dispersoid formation has occurred for 580_4_f. Fe-dispersoids might have been formed for 580_4_f which act as nucleation sites for Mg-Si phases and therefore allow more Mg-Si to be precipitated during cooling compared to 580_0_f. Figure 4.14 shows that the Mg-Si-needles show a significantly different pattern compared to 580_0_f. The higher number of Mg-Si needles in Figure 4.14 and their shorter length compared to the pattern of the phases in Figure 4.9 would affirm the assumption that Fe-dispersoids were formed.

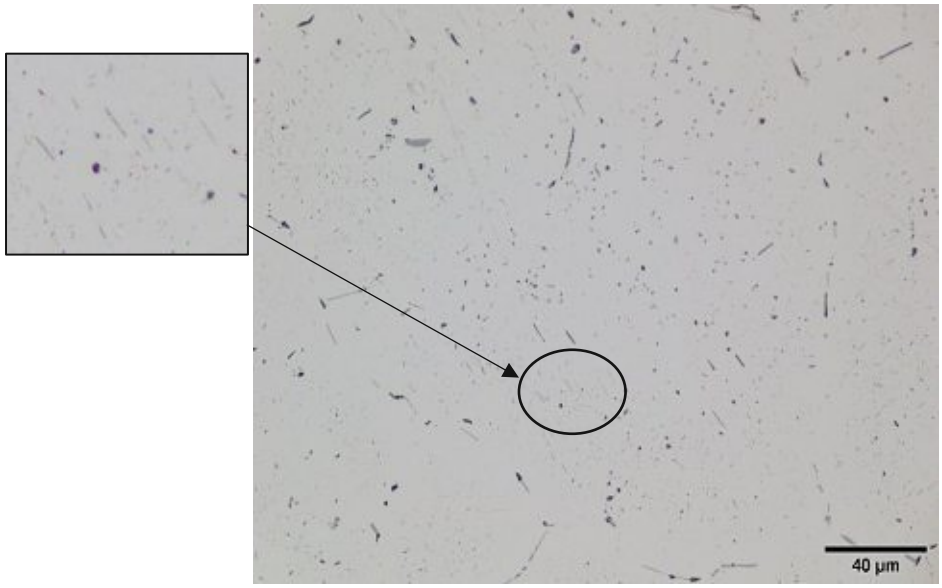

Figure 4.14: 6082.29, after heat-treatment 580_4_f, needle-shaped phases (most likely Mg-Si phases) which are homogenously spread within the grains are visible.

4.3.3 SEM-Observation

Since the observation of dispersoids by light-microscope methods is clearly limited, observation of specimens of 530_4_wq and 580_4_wq were additionally characterized by SEM at the LKR.

Heat-treatment 530_4_wq

Specimens of post heat-treatment 530_4_wq show that no visible Fe-dispersoid formation occurred (Figure 4.15). The low Fe-content might not have allowed for significant Fe-dispersoid formation for alloy 6082.29 so therefore no Fe-dispersoids formation could be observed for this heat-treatment.

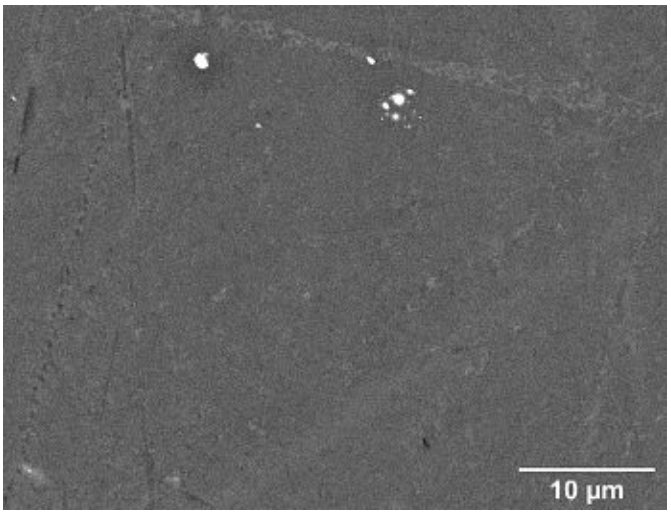

Figure 4.15: 6082.29, SEM-Observation of heat-treatment 530_4_wq (unetched) shows no visible formation of Fe-dispersoids.

Heat-treatment 580_4_wq

Specimens of 580_4_wq show likewise no visible Fe-dispersoid formation (Figure 4.16). Since the precipitation pattern for Mg-Si was considerably different for 580_0_f and 580_4_f, the question is raised that Fe-dispersoids might have formed but are too small in order to be detected by SEM-observation and optical investigation methods. Methods which offer a higher resolution such as transmission electron microscopy (TEM) might give a further insight on Fe-dispersoid formation.

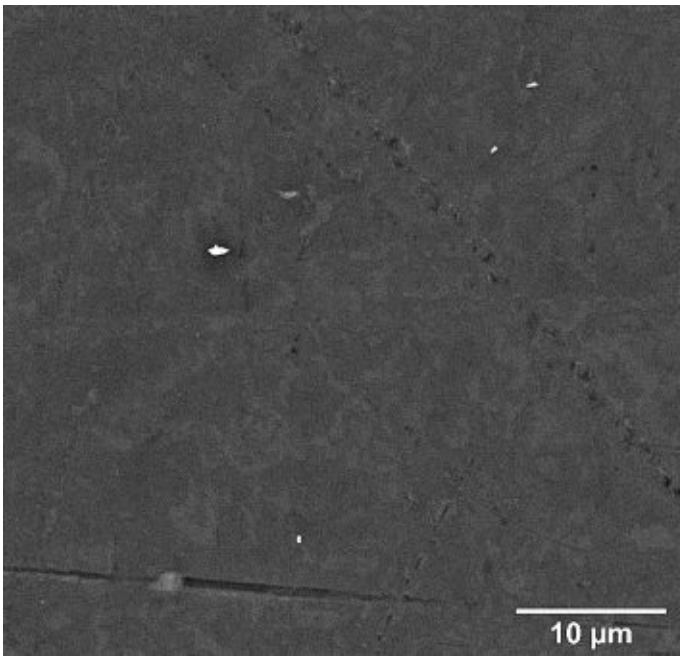

Figure 4.16: Alloy 6082.29, SEM-Observations of heat-treatment 580_4_wq (unetched) show likewise no visible formation of Fe-dispersoids.

4.4 Influence of higher Fe content (6082.30 h)

In comparison to the near-ternary alloy 6082.29, 6082.30 contains a higher Fe content (0.18 %). The Fe content is typical for some industrial 6082 alloys made from both recycled and primary Al.

4.4.1 Microstructure of the as cast state

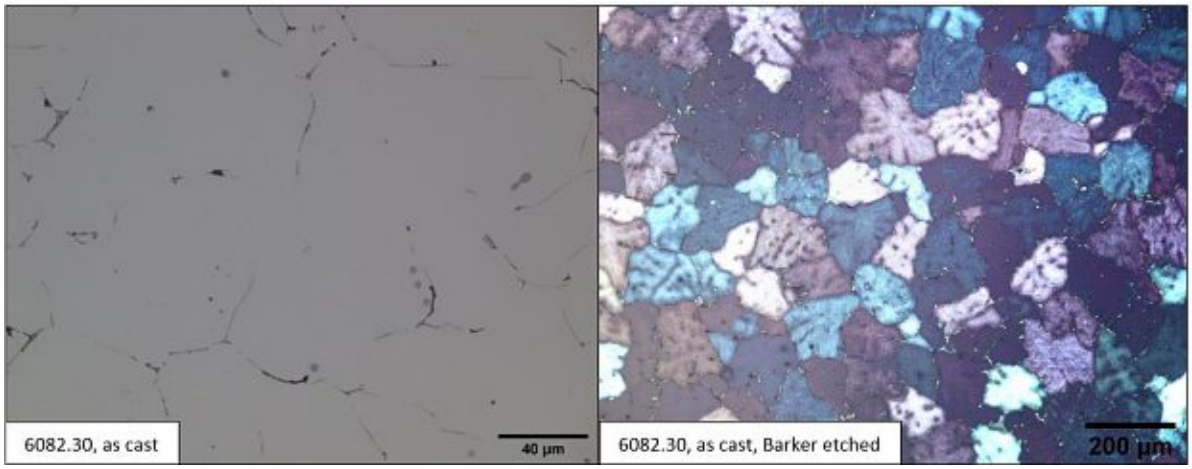

Figure 4.17: as cast state of alloy 6082.30 (left, unetched) grey structures at the grain boundaries are Al-Fe-Si phases, black dots at the Al-Fe-Si phases are primary Mg-Si phases, on the right picture the grain structure of as-cast 6082.30 is shown, which is made visible by electro-polishing the specimen using Barker's reagent.

Figure 4.17 shows, that in the as cast state of alloy 6082.30 more Al-Fe-Si and Mg-Si phases are present than in alloy 6082.29, which can clearly be attributed to the higher Fe content. The higher Fe-content enables formation of more Al-Fe-Si phases, which act as heterogenous nucleation sites for Mg-Si precipitation during solidification and cause more formation of primary Mg-Si phases.

4.4.2 El. conductivity and metallography

As for the previous alloy 6082.29, the values in Table 4 allow to calculate the el. conductivity for the alloy in a certain-state (as-cast state and post heat-treatment) by making assumptions of the expected state of the alloying-elements (in solid-solution or in precipitated-state). In this chapter those calculated values were compared with the measured values for the el. conductivity. In addition, the measured el. conductivity values were compared to the measured el. conductivity values of the as-cast state.

For the calculation of the el. conductivity of the as-cast state of alloy 6082.30 two cases were calculated. In the first case it was assumed that Fe is out of solution (in form of Al-Fe-Si phases), whereas Mg and Si are completely in supersaturated solid-solution. This case sets a possible "lower-limit" for the el-conductivity. For the second case it was assumed that Fe, Mg and Si are completely in the undissolved state, this case should set a possible "upper-limit" for the el. conductivity. Figure 4.18 shows the comparison of the three results. It is obvious that the as-cast state is best described by the assumption that Fe is out of solution, whereas Mg and Si are mostly in supersaturated solution.

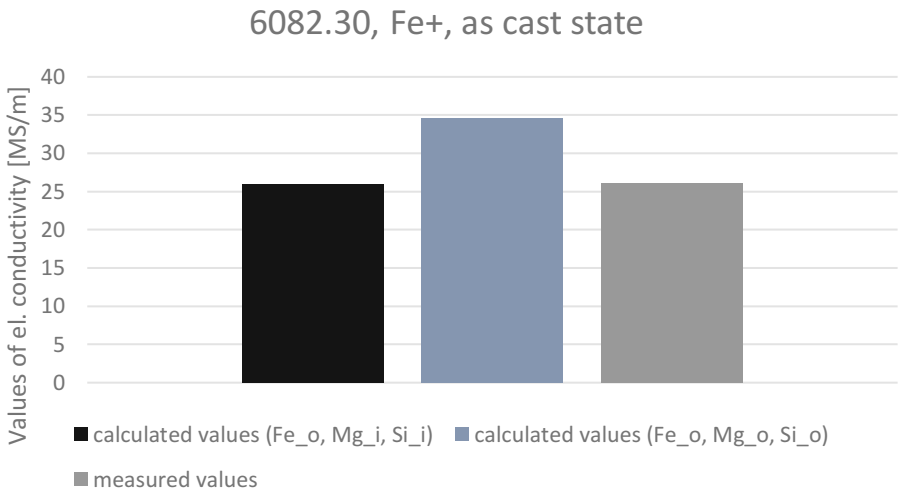

Figure 4.18: Values of el. conductivity of alloys 6082.30 of the as-cast state (bars for standard-deviation of the measured values are excluded since they were too small to be seen in this figure).
Abbreviations:
Element_o = Element out of solution
Element_i = Element in solid solution (super-saturated-solution).

For all five heat-treatments expected el. conductivity values for the post heat-treatment state were calculated using Table 4 and compared to the measured-values post heat-treatment.

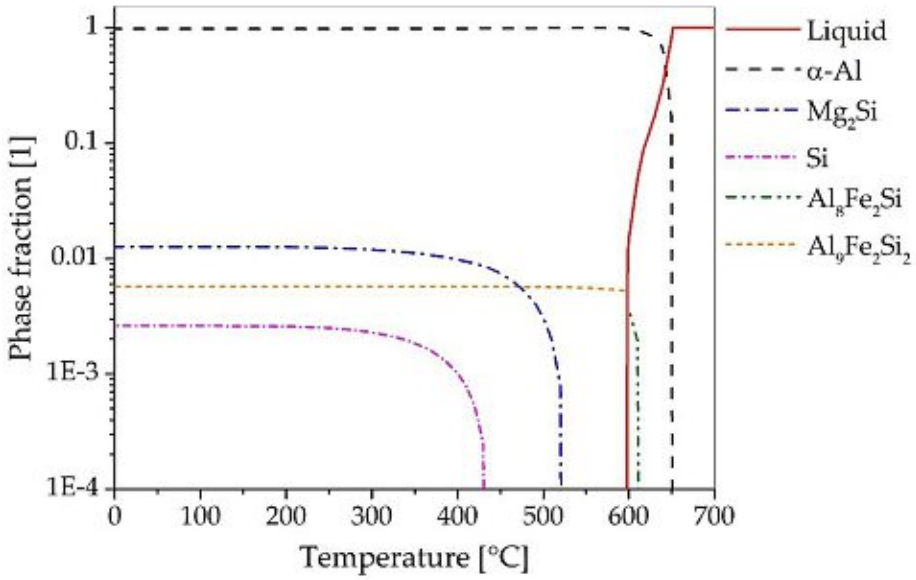

Figure 4.19: Thermo-Calc calculations of the phase-composition depending on temperature for alloy 6082.30 (the solvus line for Mg_2Si is reached at a temperature of 525 °C).

It must be kept in mind, that the measurement of the el. conductivity only shows the sum of all influences of the alloying elements on el. conductivity. Their specific state after a certain heat-treatment (whether in precipitated form or in dissolution) has to be considered applying metallurgical knowledge of the alloying-system (Figure 4.19). The Al_8Fe_2Si and $Al_9Fe_2Si_2$ phases in Figure 4.19 are assumed to be Al-Fe-Si phases of different stoichiometry. For Mg_2Si a solvus temperature of 525 °C was obtained, for excess Si which is not incorporated during Mg_2Si formation a solvus-temperature of 430 °C was obtained.

Table 13 shows the assumptions which were made for the different alloying elements (in solid-solution or in precipitated form) for the post heat-treatment state.

Table 13: Assumed state of the alloying elements for the calculation of el. conductivity values after corresponding heat-treatments.
Abbreviation:
Element_o = out of solution
Element_i = Element in solid-solution

Heat-treatments	Fe	Si	Mg
580_0_wq	Fe_o	Si_i	Mg_i
580_0_f	Fe_o	Si_o	Mg_o
530_4_wq	Fe_o	Si_i	Mg_i
580_4_wq	Fe_o	Si_i	Mg_i
580_4_f	Fe_o	Si_o	Mg_o

Figure 4.20 shows the differences in el. conductivity of the calculated values and measured values. The differences should give insight on how much the assumed states of the alloying elements (in solid-solution or in precipitated-state) for the calculation differ from their state in the specimen obtained through measurement. Differences in el. conductivity of the post heat-treatment and as-cast state are shown in Figure 4.21. Explanations for the results in Figure 4.20 and Figure 4.21 are given in the following sections of this chapter

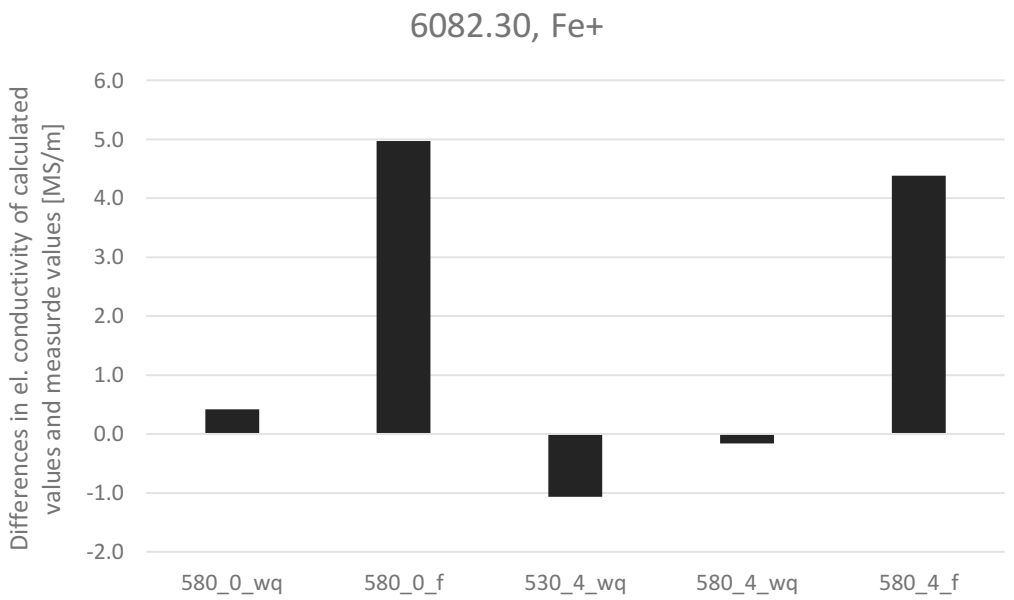

Figure 4.20: Differences in el. conductivity (Δσ) of calculated values (of assumed states of the alloying elements) after heat-treatment and the according measured values post heat-treatment.

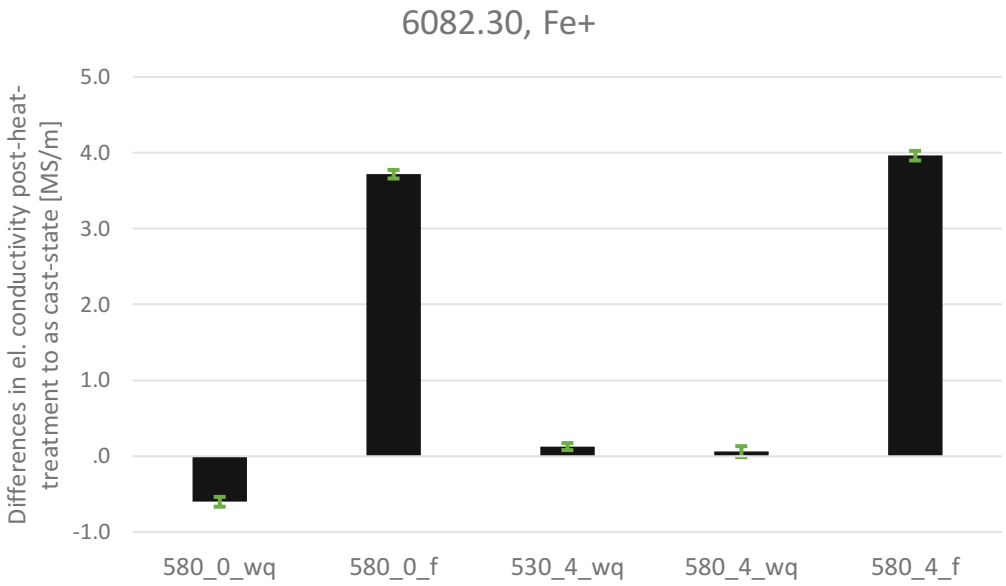

Figure 4.21: Differences in el. conductivity (Δσ) post-heat-treatments and as cast state of the according specimens of alloy 6082.30 (green bars indicate standard-deviations of Δσ and were calculated using Gaussian-error propagation).

Heat-treatment 580_0_wq

Differences in el. conductivity of the calculated values and measured values (Figure 4.20)

For this heat-treatment it was assumed, that Fe is completely out of solution (in form of Al-Fe-Si phases) whereas Mg and Si are completely dissolved in the Al-matrix and remain in this state upon water-quenching the specimen. However, the reason for the slightly positive value in Figure 4.20 remains unclear. The measured value had a slightly lower value than the calculated value, which in this case could only be explained by the fact, that Fe remains also in solid solution to a certain degree and causes an additional drop in el. conductivity of the specimen. If the incorporation of Si-atoms into Al-Fe-Si phases would be considered, the value for Δσ in Figure 4.20 would even be higher (since less Si would be available for the formation of a solid-solution with the Al-matrix) and would make the obtained result even more unclear.

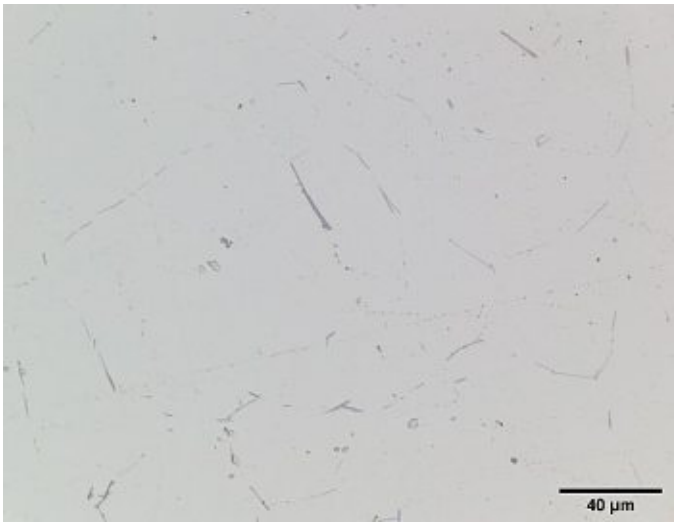

Figure 4.22: Post heat-treatment 580_0_wq (unetched) of alloy 6082.30 reveals, that a high number of Al-Fe-Si phases is formed at the grain-boundaries and that for this heat-treatment an apparent complete dissolution of primary Mg-Si phases occurred (since no visible black-spots/needles at Al-Fe-Si phases are visible).

Differences in el. conductivity of the measured-values post heat-treatment and the as-cast state (Figure 4.21)

The value of Δσ in Figure 4.21 can be explained by the fact, that primary Mg-Si phases (which are visible for the specimen in the as cast-state) form a solid-solution with the Al-matrix. This additional incorporation of Mg and Si into the Al-matrix, causes the value for the el. conductivity of the post heat-treatment state to be lower, than for the as-cast state. It has to be mentioned, that during heating-up of the specimen, secondary Mg-Si phases precipitate in the Al-matrix (from supersaturated solid-solution) but are dissolved again when the temperature is above the solvus-line (525°C). Since a rather short-time period for the precipitates is available to grow to larger phases before reaching the solvus-temperature, their size is expected to be rather small, therefore their dissolution after exceeding the solvus-temperature is expected to happen rather quickly. The post heat-treatment state should therefore be similar to the as-cast state, with the difference, that primary Mg-Si phases additionally form a solid-solution with the Al-matrix.

Heat-treatment 580_0_f

Differences in el. conductivity of the calculated values and measured values (Figure 4.20)

For the calculation of this heat-treatment, it was assumed that upon cooling-down, the whole Mg and Si content of the specimen precipitates as Mg-Si-phases (when reaching temperatures below the solvus-temperature of 525 °C). The high value for Δσ in Figure 4.21 can be explained by the fact, that probably only a minor part of Mg-Si phases is precipitated. When the time-temperature curve for this heat-treatment is observed (Figure 3.2) it can be expected, that the specimen remains approximately twice as long at temperatures above the solvus-line than for heat-treatment 580_0_wq. Mg and Si atoms have therefore significantly more time for diffusion-processes and for the formation of solid-solutions with the Al-matrix. During cooling down of the specimen the diffusion of alloying elements is significantly lowered and when the temperature is below the solvus-line, Mg-Si phases start to precipitate. The precipitation is inhibited when reaching a certain temperature since the diffusion-processes become too slow. This partial precipitation could explain the results for this heat-treatment.

Figure 4.23 shows a metallographic observation of an according specimen. Larger Mg-Si needles are spread within the grains, whereas those larger needles are surrounded by what seems to be smaller Mg-Si needles. As already mentioned, the smaller needles may just have precipitated when the temperature has fallen below the solvus-temperature but didn't have enough time to grow in size because necessary diffusion to do so was inhibited upon further cooling. The higher number of the smaller Mg-Si needles could in addition be explained by the formation of small Fe-dispersoids, which act as nucleation sites for Mg-Si precipitation. This assumption will further be clarified in later sections (for heat-treatment 530_4_wq and 580_4_wq).

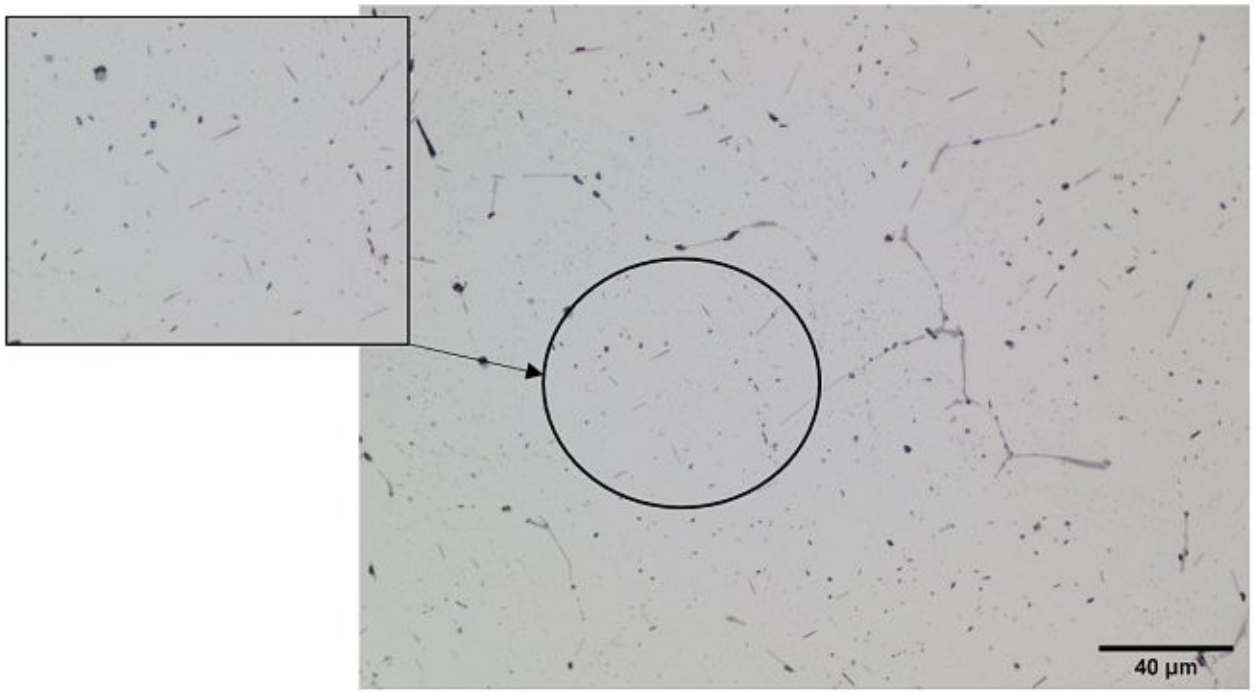

Figure 4.23: Post heat-treatment 580_0_f of alloy 6082.30, Mg-Si needles can be seen (small picture), surrounded by small needles, which could be smaller Mg-Si needles.

Differences in el. conductivity of the measured-values post heat-treatment and the as-cast state (Figure 4.21)

The high value for Δσ in Figure 4.21 could be explained by the same processes as already mentioned in the previous section. Primary Mg-Si phases are dissolved upon exceeding the solvus-temperature during heating up. Mg-Si phases which have precipitated during heating-up from the supersaturated-solution are also dissolved upon exceeding the solvus-temperature during heating-up. When the specimen is cooled-down Mg-Si phases start to precipitate, causing the el. conductivity to increase (compared to the as-cast state, in which Mg and Si are – despite primary Mg-Si mostly in supersaturated-solution). If formation of small and finely dispersed Fe-dispersoids occurs during the heat-treatment, those Fe-dispersoids might act as nucleation sites for Mg-Si phases, causing the necessary activation-energy for Mg-Si precipitation to be lowered through heterogenous nucleation. This process might cause the formation of a high number of small Mg-Si precipitates, which could explain the higher value of Δσ for alloy 6082.30 compared to alloy 6082.29 (which only had approximately 1/3 of the iron-content of alloy 6082.30).

Heat-treatment 530_4_wq

Differences in el. conductivity of the calculated values and measured values (Figure 4.20)

For this heat-treatment the assumption was made, that Fe is out of solution (in form of Al-Fe-Si phases) and Mg and Si are completely in solid solution (since the solvus temperature for Mg_2Si of 525°C is exceeded). The negative value for Δσ in Figure 4.20 shows, that the measured value for the el. conductivity was higher than the calculated value. This could be explained by partial dissolution of Mg-Si compared to the assumed full-dissolution of Mg-Si phases for the calculated value. As already mentioned for alloy 6082.29, the temperature of 530°C for this heat-treatment is only slightly above the solvus-temperature of Mg_2Si (525 °C). Dissolution processes of Mg-Si phases at this temperature are thermodynamically favored but the temperature might be too low as to enable diffusion of atoms to be high enough as to allow for full dissolution of Mg-Si phases. In addition it has to be mentioned, if Fe-dispersoid formation occurs, those dispersoids might include the incorporation of Si atoms (analogous to the stoichiometry of Al-Fe-Si phases) which disables the full precipitation and dissolution of Mg-Si phases, since the required Si-atoms are consumed by Fe-dispersoid formation. Figure 4.24 indicates that such Fe-dispersoid formation might have occurred for this alloy and heat-treatment.

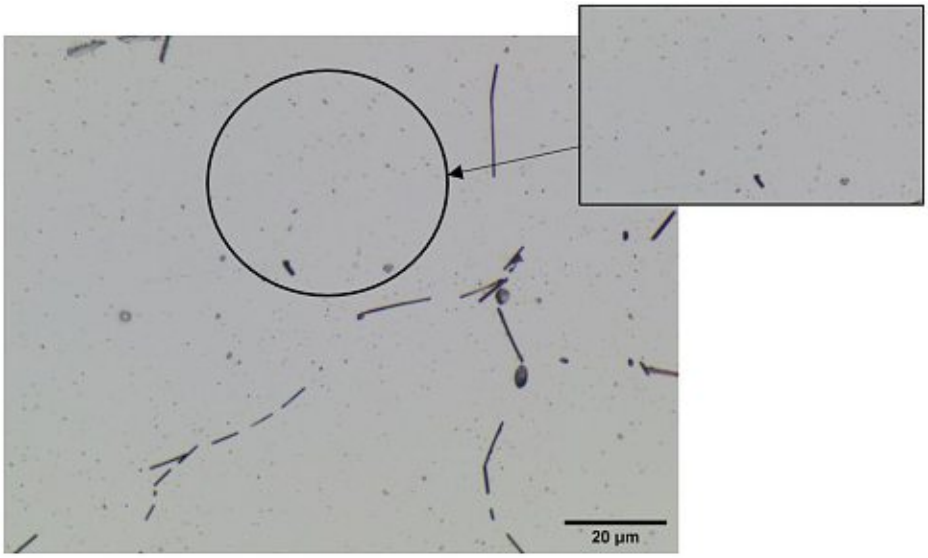

Figure 4.24: Post heat-treatment 530_4_wq of alloy 6082.30 (etched with H_2SO_4), small black dots (small picture) appear what could be formation of small, finely-dispersed Fe-dispersoids.

Differences in el. conductivity of the measured-values post heat-treatment and the as-cast state (Figure 4.21)

The value for Δσ in Figure 4.21 (which is almost zero in this case), indicates, that the sum of all processes which occur during the heat-treatment leads to a value for the el. conductivity as in the as-cast state. As mentioned in the previous section, this result could be explained by only partial dissolution of Mg-Si phases, or the formation of Fe-dispersoids (Figure 4.24), which consume Si atoms for their formation if their stoichiometry is similar to those of the Al-Fe-Si phases. The formed Fe-dispersoids would therefore lead to a lesser incorporation of Mg-Si phases into the Al-matrix. This effect could level-out the dissolution of primary Mg-Si phases and could therefore cause the el. conductivity to remain almost the same compared as to the as-cast state.

Heat-treatment 580_4_wq

Differences in el. conductivity of the calculated values and measured values (Figure 4.20)

For this heat-treatment and for the calculation of the el. conductivity it was assumed, that the high temperature of this heat-treatment is enough, as to cause the full dissolution of Mg-Si phases (since the homogenization temperature of 580 °C is significantly above the solvus-temperature of 525 °C and diffusion at this temperature should be high enough as to allow for full dissolution). The value for Δσ is in this case almost zero, which could mean, that the assumption of fully dissolved Mg-Si phases and fully dissolved Fe in the form of Al-Fe-Si phases is reasonable and that the processes in the specimen during the heat-treatment are close to this assumption. On the other hand, formation of Fe-dispersoids might cause the consumption of Mg and Si atoms and therefore allow for less dissolution of Mg-Si phases. The dissolution of primary Mg-Si phases and the possible formation of Fe-dispersoids (which consumes approximately the same amount of Mg-Si) might level-out each other's effect on the el-conductivity and lead to a value which is almost the same as compared to the as-cast state. Figure 4.25 would indicate this assumption.

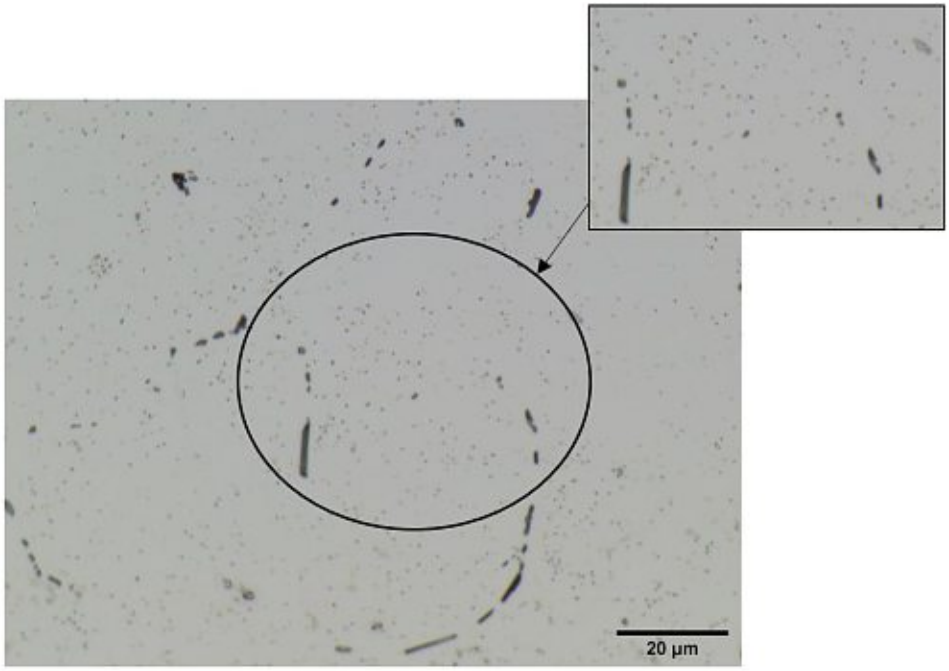

Figure 4.25: Heat-treatment 580_4_wq of alloy 6082.30 (etched with H_2SO_4), small black dots (small picture) appear what could be formation of small, finely-dispersed Fe-dispersoids.

Differences in el. conductivity of the measured-values post heat-treatment and the as-cast state (Figure 4.21)

The value of Δσ in Figure 4.21 remains almost the same for the post heat-treatment state as for the as cast state. As already mentioned in the previous section, this heat-treatment should cause all available Mg and Si atoms to form a solid solution with the Al-matrix. However, as Figure 4.26 indicates the formation of Fe-dispersoids, the formation of those dispersoids might consume Mg and Si atoms and therefore reduce the available Mg and Si atoms for the formation of a solid-solution with the Al-matrix. This process might be compensated almost exactly by the addition of Mg and Si atoms through the dissolution of primary Mg-Si phases and therefore cause the value of the el. conductivity to remain almost the same as compared to the as-cast state. However, it remains unclear, why heat-treatment 530_4_wq and 580_4_wq show almost the same result, as it would be expected, that either all Mg-Si atoms are in solid solution for 580_4_wq (due to the higher temperature and therefore stronger diffusion) and therefore the value for Δσ should be higher for 580_4_wq as for 530_4_wq. This could maybe be explained by the fact, that formation of Fe-dispersoids might cause a significant amount of Mg and Si atoms to be consumed for their formation. This missing part of Mg and Si may cause the effect, that the remaining part of Mg and Si atoms for formation of a solid-solution with the Al-matrix is lowered. The higher temperature compared to 530_4_wq might allow for more significant formation of Fe-dispersoids and therefore further decrease of available Mg and Si for solid-solution formation. The effect of lower Mg-Si incorporation and higher number of Fe-dispersoids on el. conductivity might level out, causing the el. conductivity to reach the same value as for the as-cast state.

Heat-treatment 580_4_f

Differences in el. conductivity of the calculated values and measured values (Figure 4.20)

The high value for Δσ can be explained by the same explanation which was given for heat-treatment 580_0_f. For this heat-treatment it was assumed that all Mg and Si atoms precipitate in the form of Mg-Si phases during cooling-down and it was addidtionally assumed that Fe precipitates fully in the form of Al-Fe-Si phases at the grain boundaries. The high value for Δσ shows, that the measured-value was significantly lower than the calculated value, which means, that probably only a minor part of Mg and Si atoms is precipitated and that the precipitation process is inhibited at a certain temperature since diffusion becomes too weak to allow further precipitation. If the assumption is made that all Mg and Si atoms remain in solid-solution and el. conductivity is calculated for this assumption and compared to the measured value, a comparison with the results of Figure 4.20 would give a rough estimation that 50 % of Mg-Si remain in solid-solution. The lower value of Δσ compared to 580_0_f could again be explained due to the possible formation of Fe-dispersoids. If those dispersoids enable heterogenous nuclation of Mg-Si, this effect may cause more Mg-Si phases to be precipitated, which would cause an increase of el. conductivity compared to 580_0_f (for which formation of Fe-dispersoids might occur too, but the required time for formation could be too high as to allow significant formation of those for 580_0_f).

The absence of longer Mg-Si needles in Figure 4.27 further indicates the possible formation of Fe-dispersoids and their role acting as nucleation-agents for heterogenous Mg-Si precipitation. Figure 4.27 reveals the presence of small and finely-dispersed needles which indicate, that nucleation occurred at a significantly higher number of spots as compared to 580_0_f (Figure 4.23).

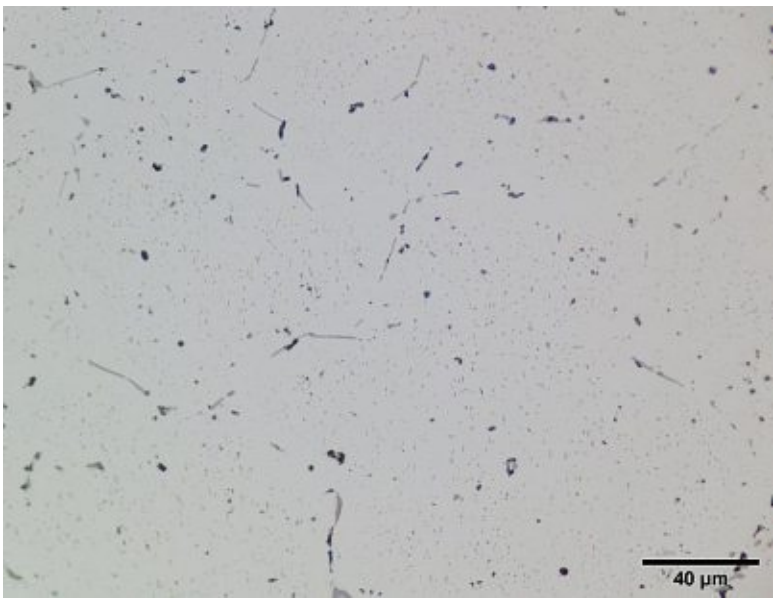

Figure 4.27: Post heat-treatment of 580_4_f of alloy 6082.30, small and finely-dispersed needles and the absence of larger needles indicate if those needles represent Mg-Si phases that nucleation occurred at a higher number of spots than was the case for heat-treatment 580_0_f.

Differences in el. conductivity of the measured-values post heat-treatment and the as-cast state (Figure 4.21)

Heat-treatment 580_4_f causes the el. conductivity to significantly increase compared to the as cast-state. Mg and Si atoms which are mostly in supersaturated-solid-solution in the as cast state, are dissolved during the heat-treatment and in addition, primary Mg-Si phases (which were already present as precipitated phases in the as cast state) are dissolved during the heating-period and are later precipitated upon furnace-cooling. As was already mentioned in the previous section, a rough estimation leads to the assumption, that probably 50 % of possible Mg-Si precipitation occurs for this heat-treatment. The higher value of $\Delta\sigma$ for this heat-treatment compared to 580_0_f could be explained by the fact, that Fe-dispersoids are formed, which than enable heterogenous nucleation of Mg-Si phases at those dispersoids and therefore cause more precipitation of Mg-Si phases.

4.4.3 SEM-Observation

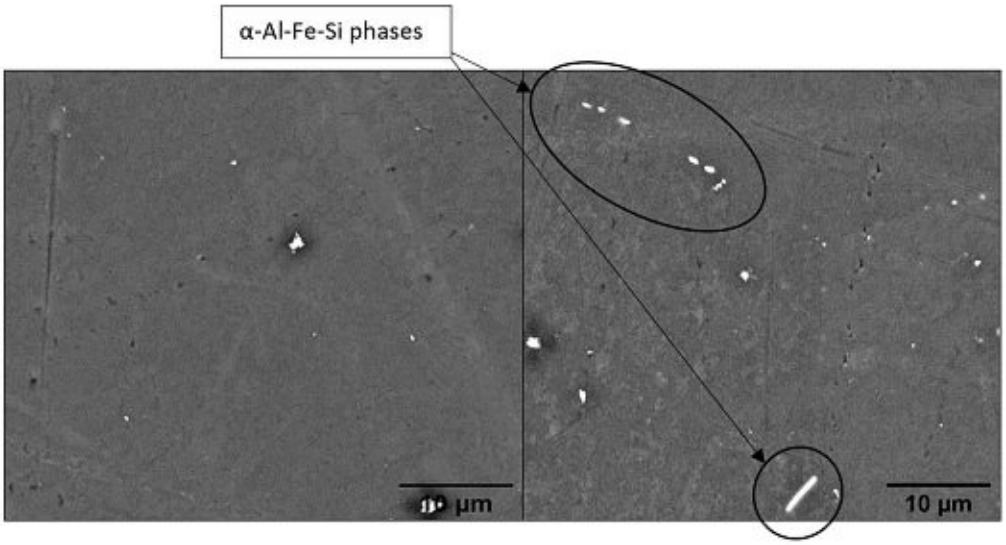

Figure 4.28: SEM observation of alloy 6082.30, of heat-treatment 530_4_wq (unetched).

Figure 4.28 shows that for heat-treatment 530_4_wq formation of Fe-dispersoids is not visible (only Al-Fe-Si-phases are visible) through SEM-observation. Since the specimen in this case was unetched, the question is raised, which effect the etching with H_2SO_4 has on the apparent size of dispersoids. During this etching technique, etching pits are produced around the dispersoids, since the reaction rates between the dispersoids and aluminum matrix differ [73]. The dispersoids have a higher electro-chemical potential compared to the surrounding Al-matrix. In this case the dispersoids act as cathodic reaction sites, at which hydrogen evolution occurs, which stimulates the anodic dissolution of the surrounding aluminum [73]. The etching process causes a detachment of dispersoids from the matrix, which causes the formation of etching pits in the etched surface. Those type of pits can grow up to 10 µm in diameter, making the dispersoids appear significantly larger [73].

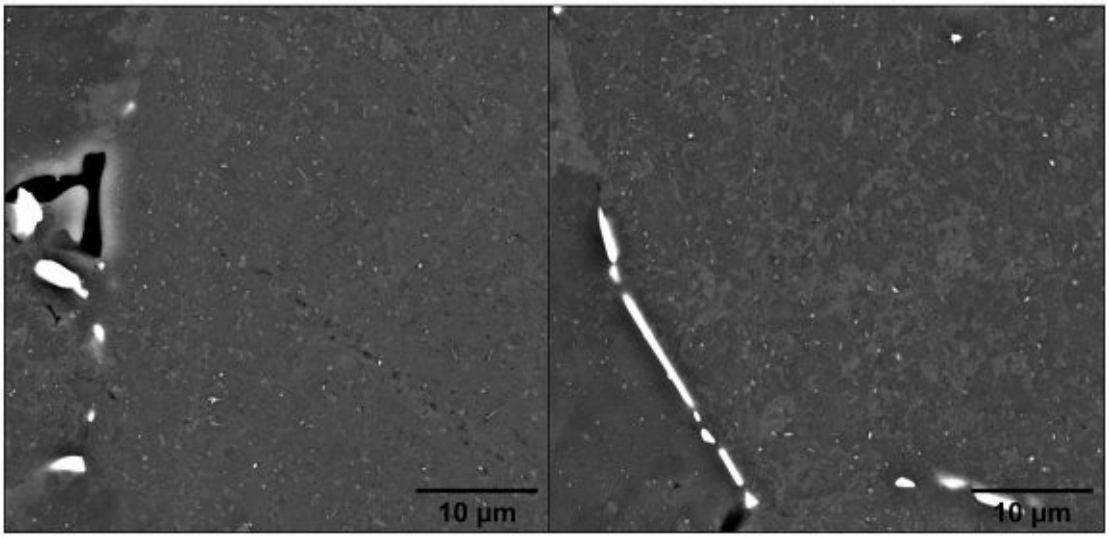

Figure 4.29: SEM observation of alloy 6082.30 after heat-treatment 580_4_wq (unetched), both pictures show the formation of dot-like phases (white dots), which could indicate the formation of Fe-containing dispersoids.

Figure 4.29 shows the formation of dot-like phases, which could be Fe-containing dispersoids. Their spread is concentrated along the grain boundaries which could be explained by the fact, that if Fe-containing dispersoids also contain Si their higher number density at the grain boundaries is caused by the gradient of Si, which shows higher concentrations of Si at the grain boundaries than in the center of the grains [Figure 2.6].

4.5 Alloy 6082.47: Influence of Cr additions

4.5.1 Microstructure of the as cast state

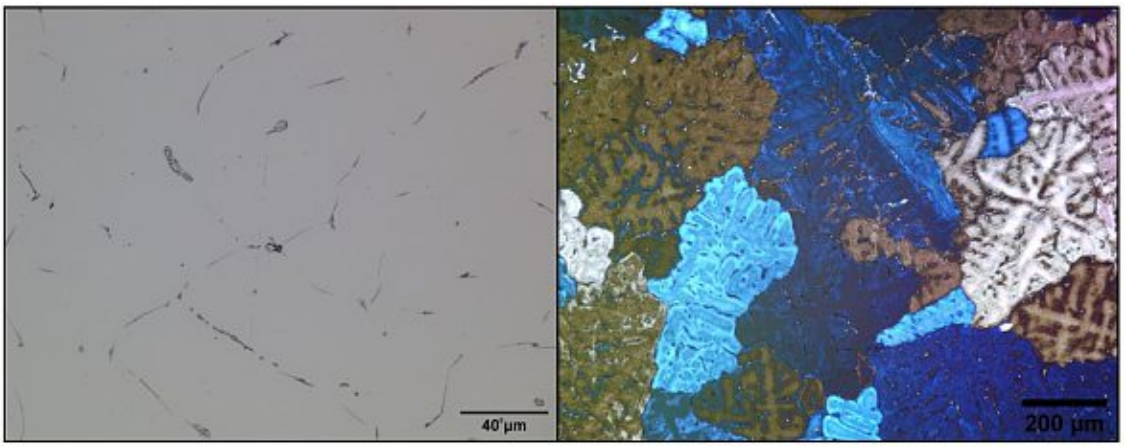

Figure 4.30: Left picture shows the as-cast state of alloy 6082.47 (unetched), grey structures are Al-Fe-Si phases, which lie at the grain-boundaries, small black dots at Al-Fe-Si indicate primary Mg-Si phases, right picture shows the grain structure of alloy 6082.47 (made visible by electro-polishing the specimen using Barker's reagent), compared to the previous alloys the grain-size is significantly increased upon Cr-addition.

Figure 4.30 shows the Barker-etched specimens. It is obvious that additional Cr has a strong impact on the grain size of the alloy and causes the grain size to increase significantly. An increase in grain size can be achieved by increasing the solidification interval/region during casting, which can be obtained by adding slow diffusing elements such as Cr (Figure 2.5).

4.5.2 El. conductivity and metallography

As in the previous chapters, the values in Table 4 were used to calculate el. conductivity values for the as-cast state and for the post heat-treatment state. Those results were compared with the results obtained through measurement.

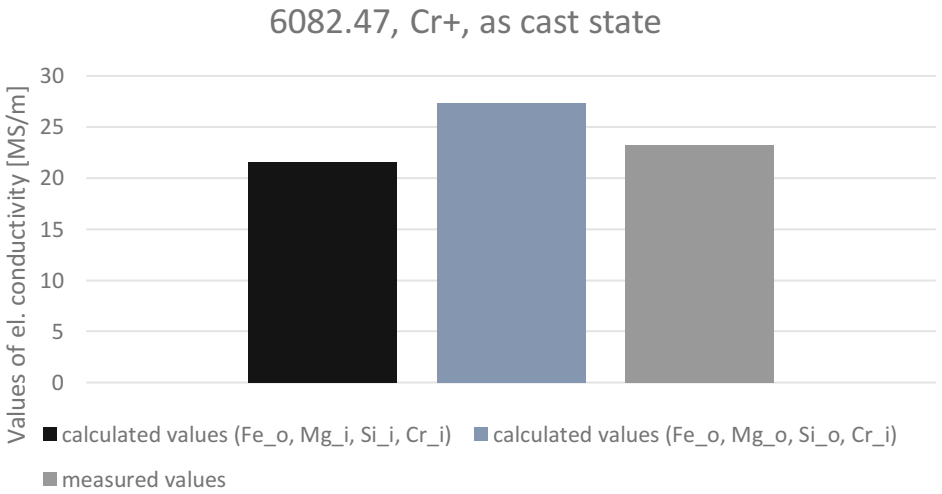

Figure 4.31: Values of el. conductivity of alloys 6082.47 of the as-cast state (bars for standard-deviation of the measured values are excluded since they were too small to be seen in this figure).
Abbreviations:
Element_o = Element out of solution
Element_i = Element in solid solution (super-saturated-solution).

For the as-cast state of alloy 6082.47 it was assumed, that Mg, Si and Cr are in supersaturated-solid-solution, whereas Fe is fully precipitated in the form of Al-Fe-Si phases (the incorporation of Si for the formation of Al-Fe-Si phases was neglected, since only a rough estimation was desired at this stage). The assumption that Cr remains in supersaturated-solid-solution was made, since Cr shows diffusion rates, which are several magnitudes lower compared to the other alloying elements (Figure 2.5).This assumption sets a lower limit for the el. conductivity. The upper limit is set by the assumption that the fast-diffusing elements Mg and Si can precipitate fully during casting (since only a rough estimation is expected this rather unrealistic assumption should set the highest possible value for the el. conductivity). The results shown in Figure 4.31 indicate, that the measured value is between those two limits but rather closely to the lower limit. For further discussions and explanations, it is therefore assumed, that a rather high amount of Mg and Si is in supersaturated-solid solution in the as-cast state and only a minor amount is precipitated as primary Mg-Si phases, whereas Fe is precipitated in form of Al-Fe-Si phases and Cr remains in supersaturated solid-solution.

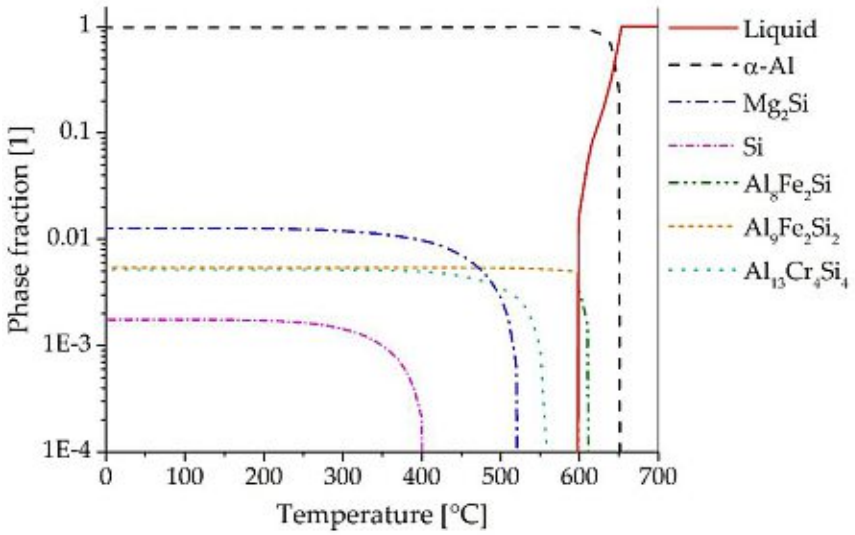

Figure 4.32: Thermo-Calc calculations of the phase-composition depending on temperature for alloy 6082.47.

Figure 4.32 shows the results of ThermoCalc calculations carried out for alloy 6082.47. The $Al_{13}Cr_4Si_4$ phase was the only known Cr-containing phase for this database, however it is assumed, that this is only one of several Cr-containing phases, since the dissolution of this phase at approximately 560 °C is in complete contradiction to the known behavior of Cr-containing phases/dispersoids. It is known that Cr-dispersoids remain in precipitated state in the alloy even upon reaching temperatures close to the melting point of the alloy. The solvus line for Mg_2Si is reached at a temperature of 525 °C, for excess Si which is not incorporated during Mg_2Si formation showed a solvus-temperature of 400 °C. Al_8Fe_2Si $Al_9Fe_2Si_2$ are assumed to be Al-Fe-Si phases of different stoichiometry.

In the next section, the calculated values for the el. conductivity post heat-treatment compared to the measured values post heat-treatment should be discussed (Figure 4.33). Table 14 shows the corresponding assumed states for each alloying element after heat-treatment. In addition, the differences in el. conductivity post heat-treatment and as-cast state should be discussed (Figure 4.34).

Table 14: Assumed state of the alloying elements for the calculation of el. conductivity values after corresponding heat-treatments for alloy 6082.47.
Abbreviations:
Element_o = out of solution
Element_i = Element in solid-solution

Heat-treatments	Fe	Si	Mg	Cr
580_0_wq	Fe_o	Si_i	Mg_i	Cr_i
580_0_f	Fe_o	Si_o	Mg_o	Cr_i
530_4_wq	Fe_o	Si_i	Mg_i	Cr_o
580_4_wq	Fe_o	Si_i	Mg_i	Cr_o
580_4_f	Fe_o	Si_o	Mg_o	Cr_o

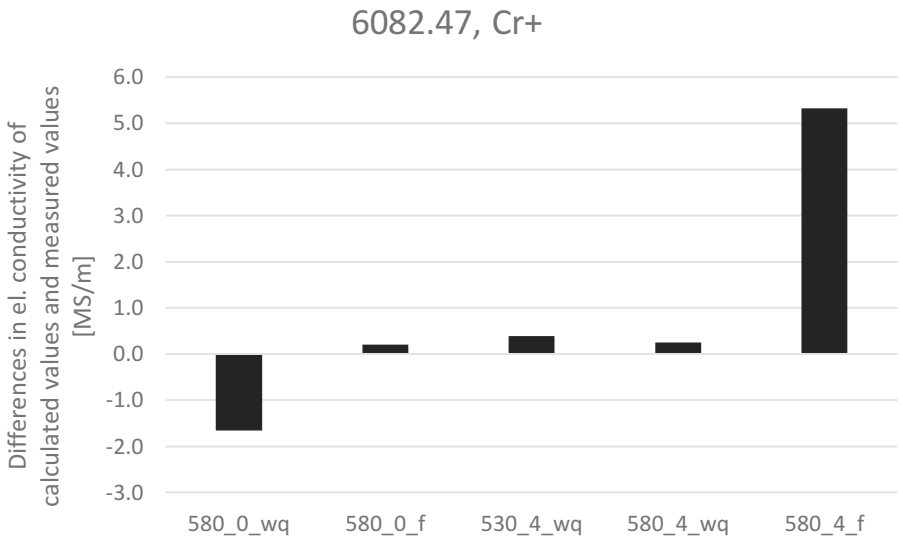

Figure 4.33: Differences in el. conductivity (Δσ) of calculated values (of assumed states of the alloying elements) after heat-treatment and the according measured values post heat-treatment.

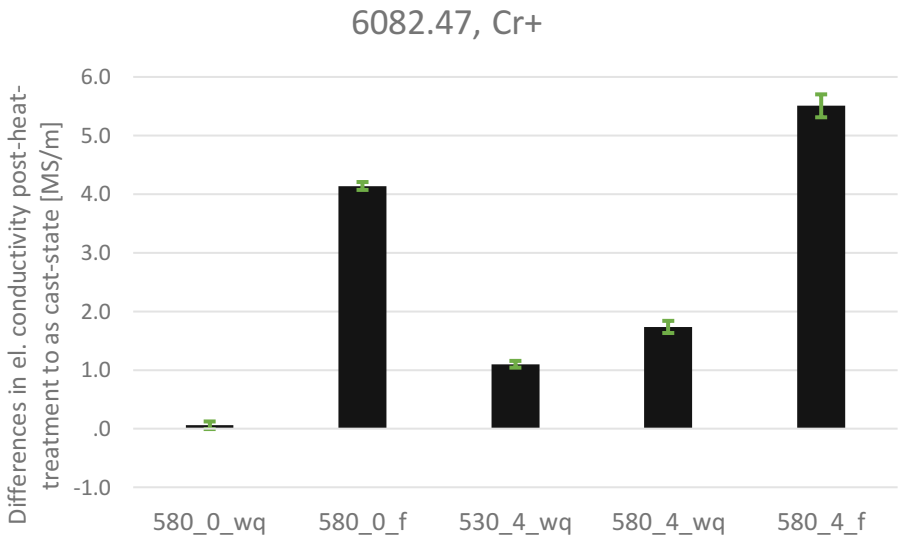

Figure 4.34: Differences in el. conductivity (Δσ) post-heat-treatments and as cast state of the according specimens of alloy 6082.47 (green bars indicate standard-deviations of Δσ and were calculated using Gaussian-error propagation).

Heat-treatment 580_0_wq

Differences in el. conductivity of the calculated values and measured values (Figure 4.33)

For this heat-treatment the value of Δσ in Figure 4.33 shows a negative value. It was assumed, that Cr, Mg and Si are in solid solution, whereas for Fe the assumption was made that Fe is precipitated in form of Al-Fe-Si phases at the grain-boundaries (again neglecting the incorporation of Si and further alloying elements for those phases in order to make calculation easier). Mg and Si are assumed to form a solid-solution upon exceeding the solvus-temperature, whereas Cr is expected to remain in supersaturated solid-solution, since the diffusion rate of Cr is considerably low. The negative value can be explained due to the fact, that the measured value is higher than the calculated value. This higher value for the el. conductivity can be explained due to only partial dissolution of Mg-Si phases upon exceeding the solvus temperature (525 °C). Mg and Si atoms which are in supersaturated-solid-solution in the as-cast state, start to precipitate upon heating-up (Figure 4.32, which only shows the Mg_2Si equilibrium phase since the precursor phases ß' and ß'' were not known to the Database). Those phases then form a solid-solution upon exceeding the solvus-temperature. If those phases are only partially dissolved since the time-period above solvus-temperature is rather short, a higher value for the el. conductivity compared to the calculated value is caused. In addition, if the Δσ value for this alloy is compared to alloy 6028.30, the lower value for 6082.47 could be explained due to partial precipitation of Cr in the form of Cr-containing phases/dispersoids thereof. Since Cr has a strong influence on el. conductivity, even minor precipitation in form of dispersoids could cause the el. conductivity to considerably increase. If Mg-Si dissolution occurred fully, the precipitation of Cr-dispersoids could cause the el. conductivity to outweigh the dissolution of primary Mg-Si phases

Differences in el. conductivity of the measured-values post heat-treatment and the as-cast state (Figure 4.34)

The value for the el. conductivity remains in this case almost the same as in the as-cast state. This behavior could be explained by the dissolution of primary Mg-Si phases (which have been in precipitated form in the as-cast state) and partial precipitation of Cr-containing phases. Those two processes could level out each other's effect on el. conductivity and cause the el. conductivity to reach a value as in the as-cast state.

Heat-treatment 580_0_f

Differences in el. conductivity of the calculated values and measured values (Figure 4.33)

For this heat-treatment it was assumed that Cr remains in supersaturated-solid-solution (due to its low diffusion-coefficient and short-time-period at elevated temperatures for this heat-treatment) and that Mg, Si and Fe are all precipitated completely. The value for Δσ is slightly above zero for this heat-treatment. Since only a certain amount of Mg and Si will form Mg-Si precipitates during cooling-down (due to reaching diffusion-rates at a certain temperature level which are too low as to allow for further precipitation) a certain amount of Mg-Si will remain in solid solution. This process itself could not describe the value for Δσ to remain slightly above zero. In addition, at least partial precipitation of Cr-containing phases could level out the mentioned effects and cause the value of Δσ to remain slightly above/almost zero.

Differences in el. conductivity of the measured-values and the as-cast state (Figure 4.34)

This heat-treatment causes the value for Δσ to reach a high value. Upon heating-up the Mg-Si phases are precipitated from supersaturated-solid-solution. Those phases are dissolved again upon exceeding the solvus-temperature of 525 °C. During cooling-down Mg-Si phases are precipitated upon reaching temperatures below the solvus-temperature. However, upon reaching a certain temperature, diffusion-rates will become too low as to allow full precipitation. Therefore, only a certain part of possible Mg-Si precipitates is formed. This partial precipitation of Mg-Si phases compared to the as-cast state (in which almost a fully supersaturated solid-solution of all Mg and Si atoms within the Al matrix can be assumed) explains the high value for Δσ in Figure 4.34.

Heat-treatment 530_4_wq

Differences in el. conductivity of the calculated values and measured values (Figure 4.33)

For this heat-treatment is was assumed that Mg, Si are in solid solution and that Cr and Fe are fully precipitated as phases containing atoms thereof (taking the ThermoCalc calculation of Figure 4.32 into consideration). The value of Δσ is slightly positive. Although the calculation assumes that Mg and Si are completely in solid-solution, most likely only a certain amount is dissolved since the temperature is only slightly above the solvus-temperature of 525 °C and the diffusion rate at this temperature may require long heating-periods (even longer than the four hours for this heat-treatment). The full precipitation of Cr may also only occur to a certain degree, since Cr is an element which has a significantly low diffusion rate and precipitation processes may require long time-periods even at elevated temperatures. The formation of Cr-containing phases may therefore only occur to a certain degree, which would cause the el. conductivity to remain lower than calculated. The sum of the mentioned processes could explain the slightly positive value for Δσ.

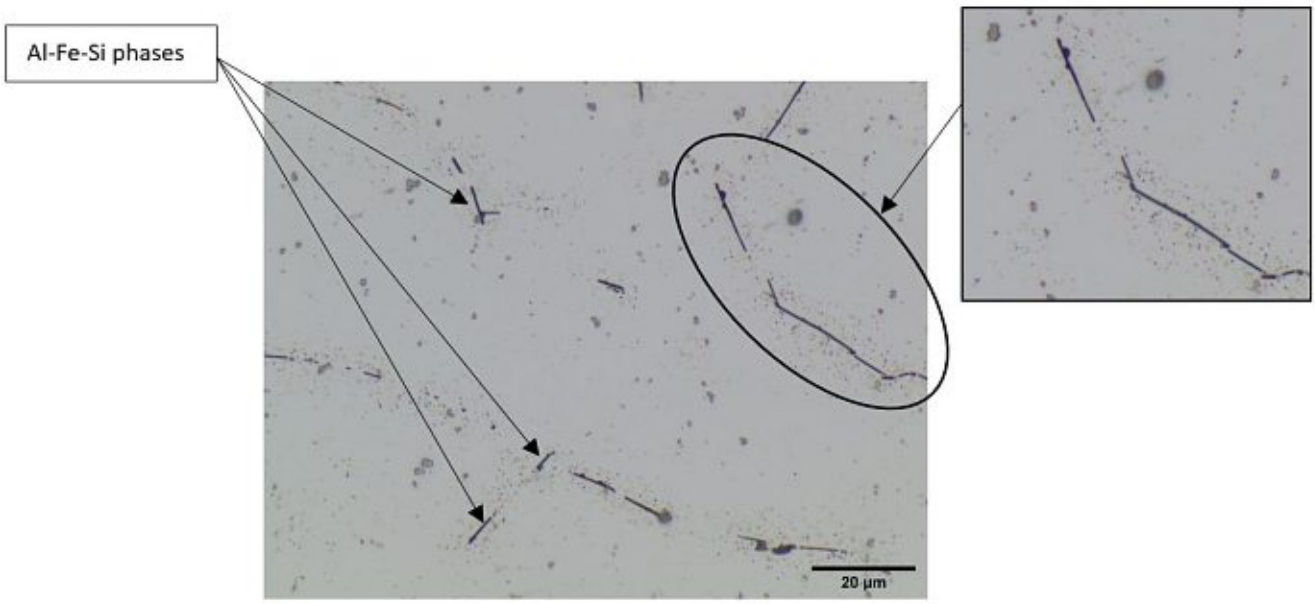

Figure 4.35: Post heat-treatment 530_4_wq of alloy 6082.47 (etched with H_2SO_4), small black dots besides the Al-Fe-Si phases (zoomed-out picture) indicate possible formation of Cr-containing dispersoids.

Differences in el. conductivity of the measured-values and the as-cast state (Figure 4.34)

The difference in el. conductivity for this heat-treatment show a positive value. Since the value of Δσ is significantly higher than for the previously mentioned alloys, the shift to higher values for Δσ can be attributed by the presence of Cr in this alloy. In the previous chapters the partial dissolution of Mg-Si phases (which upon heating-up are precipitated from supersaturated-solid-solution from the as-cast state) upon exceeding the solvus-temperature has been discussed. The results so far indicate that only partial dissolution of Mg-Si phases for heat-treatments at 530 °C and duration of four hours occur. The shift towards a positive value for Δσ in this case could be attributed to the fact that Cr-containing dispersoids are formed which cause the el. conductivity to increase compared to the non Cr-containing alloys. The metallographically observation in Figure 4.35 would affirm this assumption.

Heat-treatment 580_4_wq

Differences in el. conductivity of the measured-values post heat-treatment and the as-cast state (Figure 4.33)

For the calculation of the value of el. conductivity for this heat-treatment, complete precipitation of Cr (in form of Cr-containing phases/dispersoids) and Fe (in form of Al-Fe-Si phases) was assumed. For Mg and Si the complete dissolution of those alloying elements was assumed, since the heat-treatment is well above the solvus temperature of 525 °C and diffusion rates at 580 °C should be high enough as to allow for complete dissolution.

The value for Δσ is slightly positive but close to zero for this heat-treatment. The mentioned assumptions could therefore describe a state of the alloying elements post water-quenching, which is close to the real state of those elements. The higher number-density of black spots in Figure 4.36 compared to Figure 4.35 would indicate, that a higher number of Cr-containing dispersoids was precipitated for this heat-treatment.

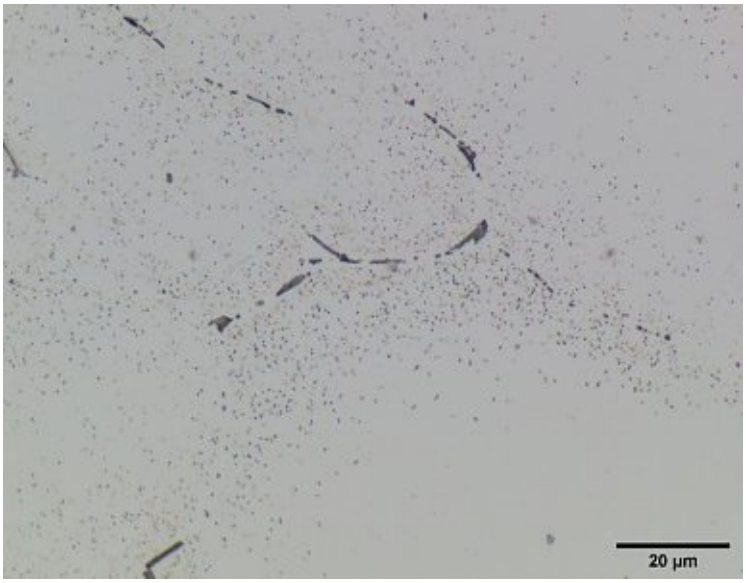

Figure 4.36: Post-heat treatment 580_4_wq of alloy 6082.47 (etched with H_2SO_4), small black dots indicate precipitation of phases, which could be Cr-containing dispersoids.

Differences in el. conductivity of the measured-values and the as-cast state (Figure 4.34)

Figure 4.34 shows a positive value for Δσ, which is higher than for heat-treatment 530_4_wq. The positive value can be explained due to full dissolution of Mg-Si phases, meaning, that primary Mg-Si phases from the as-cast state, as well as secondary Mg-Si phases which were in the supersaturated state in the as-cast state – form a solid-solution with the Al-matrix. In addition, the higher precipitation of Cr-containing phases – compared to heat-treatment 530_4_wq could explain the higher value for Δσ for this heat-treatment. Figure 4.36 indicates, that the higher number-density of black spots would indicate the stronger precipitation of Cr in form of Cr-containing dispersoids.

Heat-treatment 580_4_f

Differences in el. conductivity of the calculated values and measured values (Figure 4.33)

Figure 4.33 shows, that Δσ reaches a high value for this heat-treatment. For the calculation of the el. conductivity of this heat-treatment it was assumed that all elements (Fe, Cr, Mg, Si) are in precipitated state. It was assumed, that all Cr and Fe atoms in the specimen are in precipitated state (in the form of Cr-containing phases and Al-Fe-Si phases respectively) and Mg and Si fully precipitate upon cooling-down and reaching temperatures below the solvus-temperature. The high value of Δσ for this heat-treatment shows, that this assumption is far off the true state of the alloying elements in the specimen post heat-treatment. It is from a metallurgical point of view clear, that the precipitation of Mg-Si phases will not occur completely, since diffusion of the elements is inhibited at a certain temperature during cooling-down and the precipitation-process is stopped at this stage. In addition, if Cr remains only to a minor degree in solid solution, this could be enough as to cause a high decrease of el. conductivity for the measured value.

Differences in el. conductivity of the measured-values post heat-treatment and the as-cast state (Figure 4.34)

The value for Δσ of this heat-treatment shows the expected positive value, meaning, that the expected precipitation of phases occurred during the heat-treatment and that those processes occurred to a large degree, causing a higher value for the el. conductivity compared to the as-cast state. It is interesting to note, that the values of Δσ for heat-treatments 580_0_f and 580_4_wq combined, nearly equal the value of Δσ for heat-treatment 580_4_f. If complete dissolution of Mg-Si phases for 580_0_f and 580_4_f is assumed (above solvus-temperature) and almost the same amount of precipitated Mg-Si phases is assumed for both heat-treatments, then the difference of those two heat-treatments could be explained by the formation of Cr-containing dispersoids. The effect on the el. conductivity by the precipitation of Cr-containing dispersoids is given by heat-treatment 580_4_wq. If the values for Δσ of 580_0_f and 580_4_wq are combined, their sum should closely equal to the value for Δσ of 580_4_wq, which is the case in Figure 4.34.

4.5.3 SEM-Observation

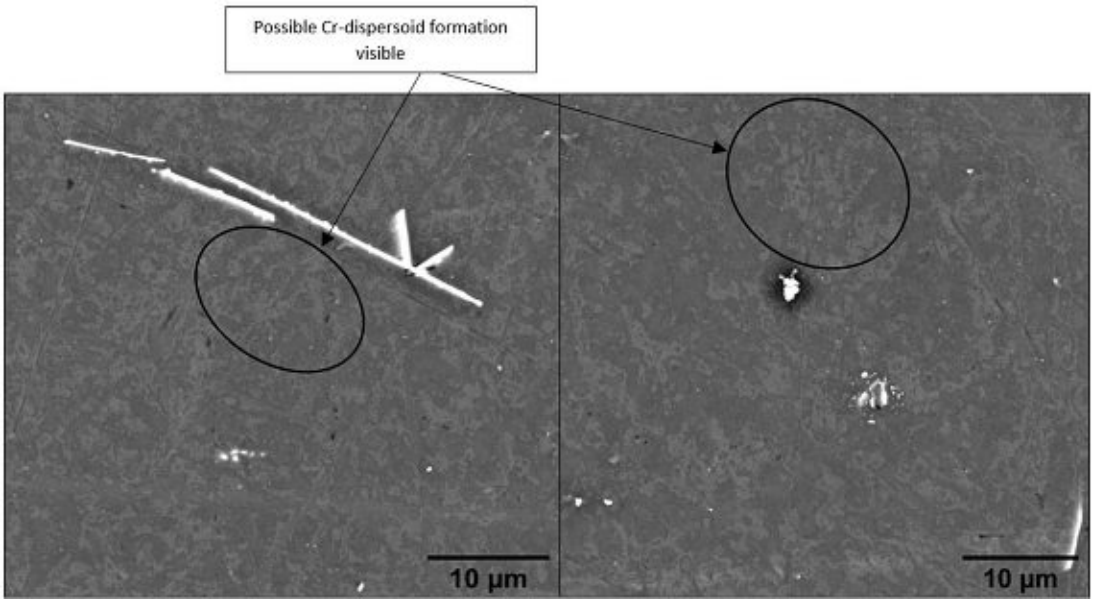

Figure 4.37: Alloy 6082.47, SEM observation of a specimen post heat-treatment 530_4_wq (unetched).

Although metallographic investigations of etched specimens of heat-treatment 530_4_wq clearly indicate the possible formation of Cr-containing dispersoids (Figure 4.35), SEM-observation of heat-treatment 530_4_wq show almost no such phases (Figure 4.37, white dots could also be impurities stemming from preparation).

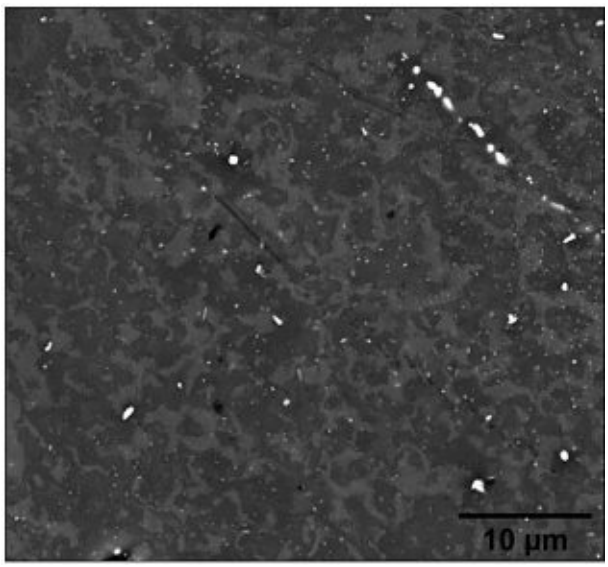

Figure 4.38: Alloy 6082.47, SEM-Observation of 580_4_wq, Cr-containing dispersoids are visible as small white dots.

Figure 4.38 clearly shows the formation of what appears to be Cr-containing dispersoids (white dots). The dispersoid-phases are more densely spread near the grain boundaries than towards the grain center.

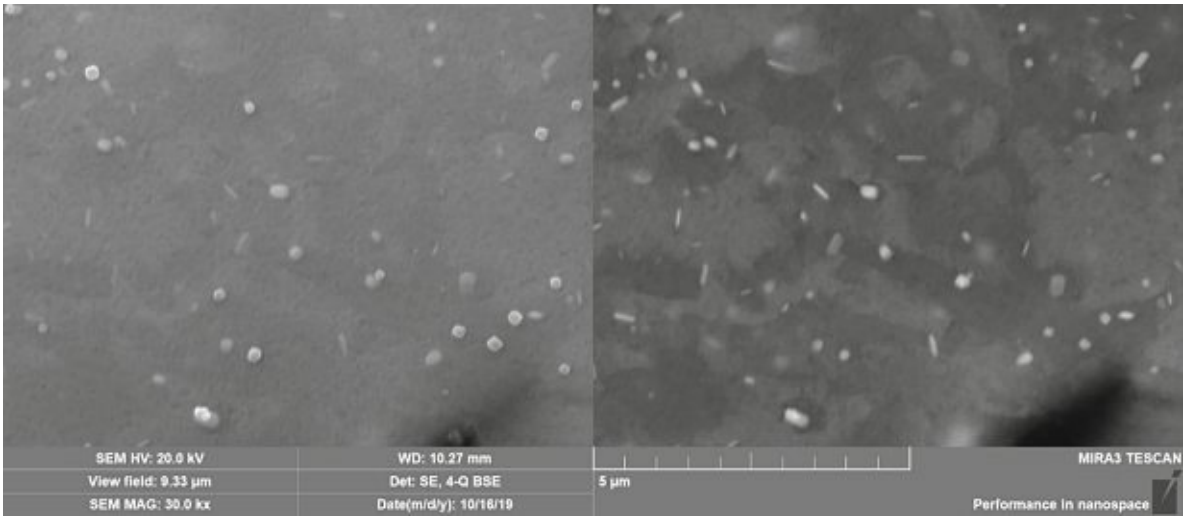

Figure 4.39: comparison of secondary electron measurement (left) and backscatter-mode (right) of alloy 6082.47.

Figure 4.39 shows the comparison of two different modes of measurements using a SEM. The left picture shows the secondary electron mode, which usually gives information of the surface-near section of the specimen, since only the secondary electrons which are produced near the surface have kinetic energies which allow them to escape the surface of the specimen.

The right picture shows the backscattered electron mode. Primary electrons from the electron beam of the electron-gun have high kinetic energies (several keV) which allow them to penetrate the surface of the specimen and get backscattered to the detector. Because of the higher energies of primary electrons compared to secondary electrons information for higher depths of the specimen is obtained.
Figure 4.39 shows that in this case the secondary electron-mode also gave a good insight of the specimen, which can only be achieved in specimens with very good surface quality. In contrast, the backscattered electron mode is more robust and surface contaminations have far less influence.

4.6 Alloy 6082.48: Effects of additional Cu addition

4.6.1 Microstructure of the as cast state

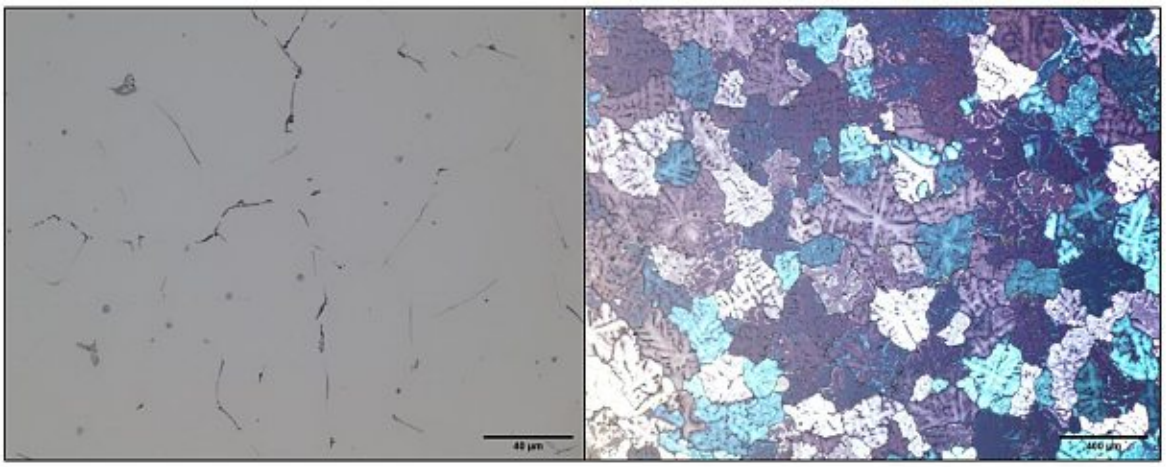

Figure 4.40: As-cast state of alloy 6082.48 (left, unetched), grey structures are Al-Fe-Si phases, which lie at the grain-boundaries, small black dots at Al-Fe-Si indicate primary Mg-Si phase, electro-polishing of an as-cast specimen (using Barker's reagent as polishing agent) of alloy 6082.48 (right) reveals the grain-structure of the as-cast state.

Figure 4.40 shows the as-cast state of alloy 6082.48. Interestingly, upon addition of Cu, the grain size is reduced dramatically (right part of Figure 4.41) and reaches almost the same value as for alloy 6082.30 (i.e., the alloy without Cr). It seems that the higher diffusion rate of Cu levels out the effects of the slower diffusing Cr (Figure 4.30).

4.6.2 El. conductivity and metallography

In this chapter insights which where generated through measurements of the el. conductivity of the specimens should be discussed. First, the as-cast state of the specimens should be discussed. Since the as-cast state shows no visible formation of larger Cr or Cu-containing phases (no significant difference compared to alloys 6082.29 and 6082.30) two cases were assumed for the calculation of the el. conductivity of the as-cast state. For the first case its was assumed, that all elements despite Fe are in supersaturated solid-solution, this should set a lower-limit for the value of el. conductivity. For the second case, it was assumed, that Fe, Mg and Si are in precipitated stage(in form of Al-Fe-Si phases or primary Mg-Si, respectively) whereas Cu and Cr remain in supersaturated-solution, since no significant formation of precipitated phases thereof could be seen in Figure 4.40. This assumption should set an upper-limit for the el. conductivity.

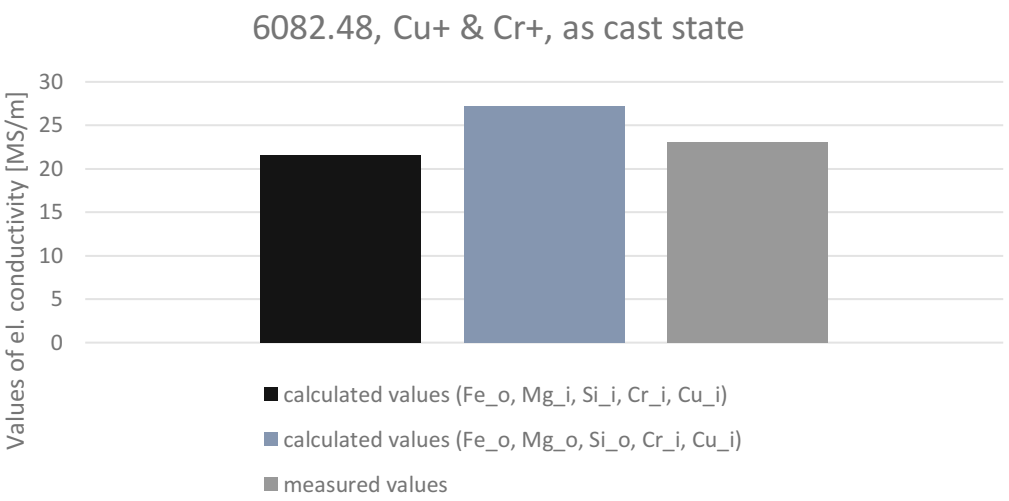

Figure 4.42: Values of el. conductivity of alloys 6082.48 of the as-cast state (barrs for standard-deviation of the measured values are excluded since they were too small to be seen in this figure).
Abbreviations:
Element_o = Element out of solution
Element_i = Element in solid solution (super-saturated-solution).

Figure 4.42 shows the results of the two assumed states of the as-cast state, as well as the measured value. It is evident, that the true state of the alloying elements is roughly in the middle between the two assumed limits however, since the measured-values is closer to the lower-limit, it is assumed that the assumptions made for the lower level describe the true state of the as-cast state more closely.

Figure 4.43 shows the calculation of the phase-composition depending on temperature carried out using ThermoCalc. The solvus line for Mg_2Si is reached at a temperature of 525 °C, the $Al_{13}Cr_4Si_4$ was the only known Cr-containing phase for this Database, however it is assumed, that this is only one of several Cr-containing phases, since the dissolution of this phase at approximately 560 °C is in complete contradiction to the known behavior of Cr-containing phases/dispersoids. It is known that they remain in precipitated state in the alloy even upon reaching temperatures close to the melting point of the alloy. $Al_9Fe_2Si_2$ and Al_8Fe_2Si are assumed to represent Al-Fe-Si phases of different stoichiometry. The Q-phase is the thermodynamically stable Cu-containing phase, which has a solvus-temperature of 334 °C. Pure Si represents excess Si of the alloy which is not consumed during Mg_2Si formation (solvus-temperature 400 °C).

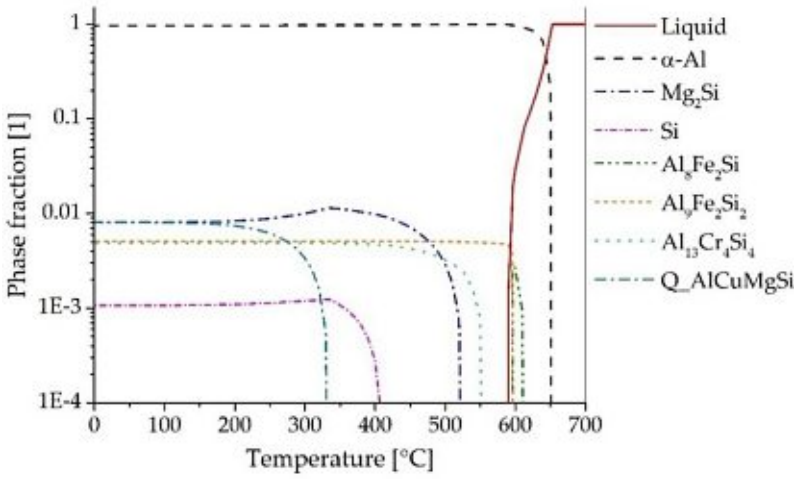

Figure 4.43: Thermo-Calc calculations of the phase-composition depending on temperature for alloy 6082.48.

Table 15: Assumed state of the alloying elements for the calculation of el. conductivity values after corresponding heat-treatments for alloy 6082.48.
Abbreviations:
Element_o = out of solution, Element_i = Element in solid-solution

Heat-treatments	Fe	Si	Mg	Cr	Cu
580_0_wq	Fe_o	Si_i	Mg_i	Cr_i	Cu_i
580_0_f	Fe_o	Si_o	Mg_o	Cr_i	Cu_i
530_4_wq	Fe_o	Si_i	Mg_i	Cr_o	Cu_i
580_4_wq	Fe_o	Si_i	Mg_i	Cr_o	Cu_i
580_4_f	Fe_o	Si_o	Mg_o	Cr_o	Cu_i

Table 15 shows the assumed state of the alloying elements post heat-treatments. Figure 4.43 shows the presence of the Q-phase, which can have different composition, one of which has been reported as $Al_4Mg_8Si_7Cu_2$ [2]. In addition Figure 4.43 shows that the Q-phase is dissolved upon reaching a temperature of 334°C. Therefore it was assumed that every heat-treatment which was applied causes Cu to form a solid solution with the Al-matrix.

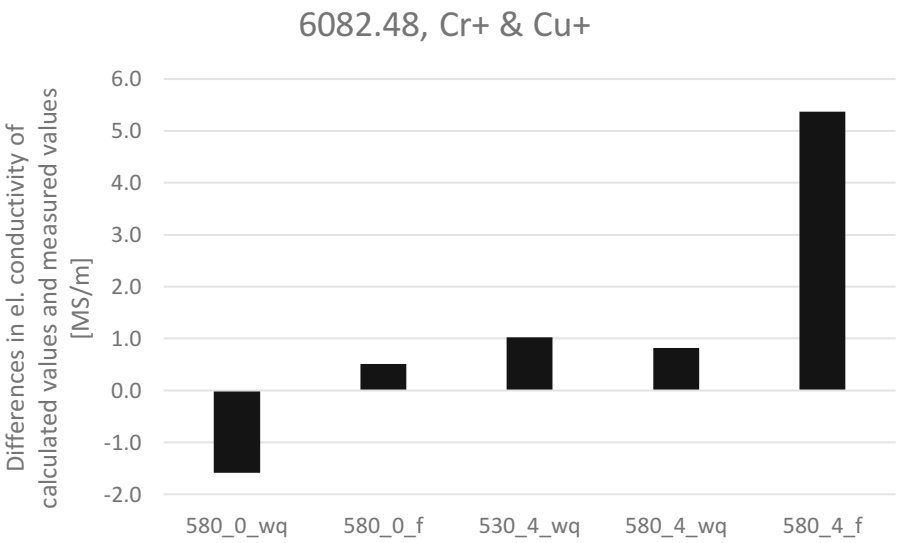

Figure 4.44: Differences in el. conductivity (Δσ) of calculated values (of assumed states of the alloying elements) after heat-treatment and the according measured values after heat-treatment.

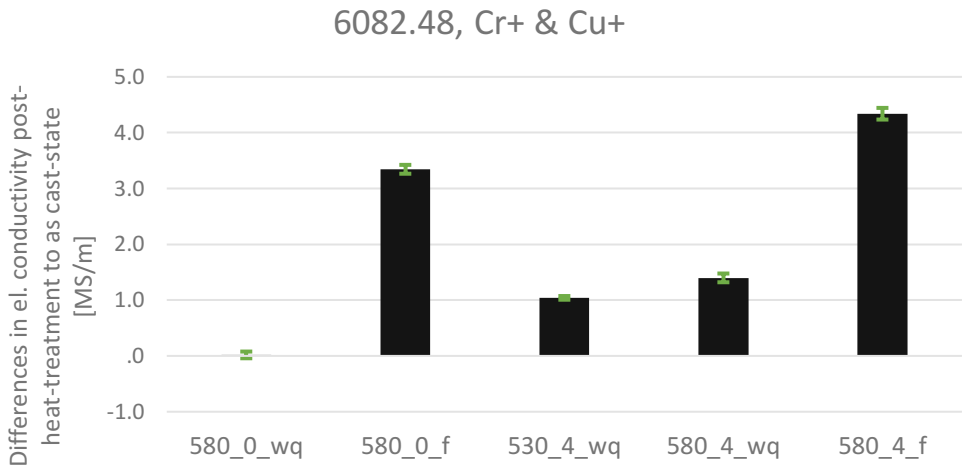

Figure 4.45: Differences in el. conductivity (Δσ) of measured values post-heat-treatments and as cast state of the according specimens of alloy 6082.48 (green bars indicate standard-deviations of Δσ and were calculated using Gaussian-error propagation).

Heat-treatment 580_0_wq

Differences in el. conductivity of the calculated values and measured values (Figure 4.44)

Figure 4.44 shows for this heat-treatment a significant negative value for Δσ. For the calculated value of the el. conductivity the assumption was made that Fe is in precipitated state in the form of Al-Fe-Si phases (due to the low solubility of Fe in Al). For the rest of the alloying elements it was assumed that they form a solid-solution with the Al-matrix. This assumption was made because the diffusion-rate of Cr is rather low and although elevated temperatures are applied for this heat-treatment it is assumed that most of the available Cr remains in supersaturated-solid-solution. For Cu, Mg, Si it is assumed, that all three elements are precipitated during heating-up, but are dissolved upon reaching solvus-temperatures (330°C for the Cu-containing Q-phase and 525°C for Mg_2Si) and since their diffusion-rates are rather high (Figure 2.5) full dissolution of those elements is assumed. The negative value for Δσ could be explained by the fact, that the assumed full dissolution of Mg and Si happens only to a certain degree, causing the measured value of el. conductivity to be higher than the calculated value. On the other hand, if almost complete dissolution of Mg and Si occurred, even minor precipitation of Cr-containing phases would cause el. conductivity to rise significantly (since the influence of Cr on el. conductivity is high). This second assumption could therefore also explain the negative value for Δσ in Figure 4.44.

Differences in el. conductivity of the measured-values post heat-treatment and the as-cast state (Figure 4.45)

The value for Δσ in Figure 4.45 is almost zero. This could be explained by the fact, that probably Mg, Cu and Si phases are precipitated during heating-up from supersaturated-solid-solution but are dissolved again upon exceeding the solvus-temperature. Additionally, if primary Mg-Si phases from the as-cast state form a solid-solution, a decrease for Δσ is expected. However, since Cr has a strong impact on the el. conductivity (Figure 2.21), even a slight precipitation of Cr-containing phases would create a significant increase in el. conductivity. This increase caused by Cr-precipitation could outweigh the effect of primary Mg-Si dissolution and could cause the value for Δσ to become very low or almost zero.

Heat-treatment 580_0_f

Differences in el. conductivity of the calculated values and measured values (Figure 4.44)

The value for Δσ is only slightly positive for this heat-treatment. For the calculation of the el. conductivity it was assumed, that Fe, Mg and Si are precipitated completely. For Fe the precipitation could occur completely during casting in the form of Al-Fe-Si phases, or during heating-up in the form of Fe-containing dispersoids. However, once Fe is precipitated during heating-up or casting, it should remain in precipitated phases since the solubility of Fe in Al is rather low and Thermo-Calc calculations show likewise no unexpected behavior from this assumption. For Mg and Si the precipitation from supersaturated-solid solution during heating-up is expected. The precipitated Mg-Si phases should dissolve again upon exceeding the solvus-temperature (525 °C) and precipitate again during cooling-down. For Cr and Cu it is assumed that those elements remain in solid-solution (Cr is assumed to remain in the supersaturated as-cast state). This assumption is based on the low diffusion-rate of Cr and although Cu should precipitate in form of the Q-phase according to the ThermoCalc-calculation in Figure 4.43, it is assumed that diffusion for the rest of the necessary elements at those temperatures is too low as to allow for significant precipitation processes. Although calculated and measured value are of similar magnitude for this heat-treatment, it is rather expected, that Mg and Si only precipitate partially. The effect on el. conductivity caused by this partial precipitation, could be outweighed by partial precipitation of Cr-containing phases/dispersoids. Since Cr has a high influence on el. conductivity, precipitation of Cr might outweigh the partial precipitation of Mg and Si and cause the measured value to be close to the calculated value (for which full precipitation of Mg and Si and full remainder of Cr in solid-solution was assumed).

Differences in el. conductivity of the measured-values post heat-treatment and the as-cast state (Figure 4.45)

For this heat-treatment Δσ shows a significant positive value, indicating that the post heat-treatment state has a higher el. conductivity than the as-cast state. This could be explained by the fact, that Mg-Si phases are precipitated when the specimen is cooled-down in the furnace. Upon heating-up, secondary Mg-Si phases are precipitated from the supersaturated solid-solution, but are again dissolved upon exceeding the solvus-temperature of 525°C. In addition, primary Mg-Si phases which were present in the as-cast state are dissolved. Those dissolved phases precipitate partially when the specimen is cooled-down in the furnace once the temperature falls below the solvus-temperature. Figure 4.46 indicates, that rather long-needles of Mg-Si precipitates were formed (zoomed-out picture), which could be explained by the fact that nucleation of those phases occurred homogeneously. If a significant amount of Cr-containing dispersoids would have been available at the stage of precipitation, rather small and finely dispersed Mg-Si needles could have been expected. Figure 4.46 therefore indicates, that significant formation of Cr-containing dispersoids did not occur for the short heating-period of heat-treatment 580_0_f.

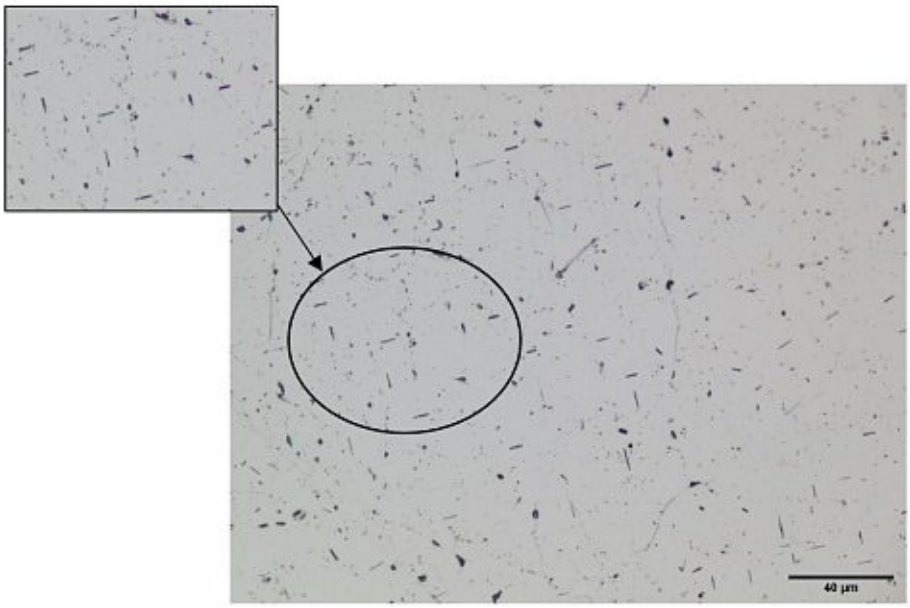

Figure 4.46: Post heat-treatment 580_0_f of alloy 6082.48, long needles indicate possible precipitation of Mg-Si phases (black-needles in zoomed-out picture).

Heat-treatment 530_4_wq

Differences in el. conductivity of the calculated values and measured values (Figure 4.44)

The value for Δσ shows a positive value, meaning, that the calculated value was higher than the measured value for this heat-treatment. For the calculated value it was assumed that Fe and Cr are completely in precipitated-state (in form of Al-Fe-Si phases and Cr-containing phases/dispersoids, respectively) and Mg, Si and Cu form solid-solutions with the Al-matrix. In this case, a reasonable explanation for the positive value for Δσ is the partial precipitation of Cr. Since Cr has a low diffusion-constant this heat-treatment could indicate, that the temperature of 530 °C and hold-period of four hours is not enough as to allow for full precipitation of Cr-containing phases. In previous works the formation temperature for Cr-dispersoids was mentioned to be in the range of 490-550 °C [27]. Figure 4.47 indicates possible formation of Cr-containing dispersoids. Comparison of analogously prepared metallographic specimens of heat-treatment 580_4_wq should reveal, if a significantly higher amount of Cr-containing dispersoids was formed for a temperature of 580 °C.

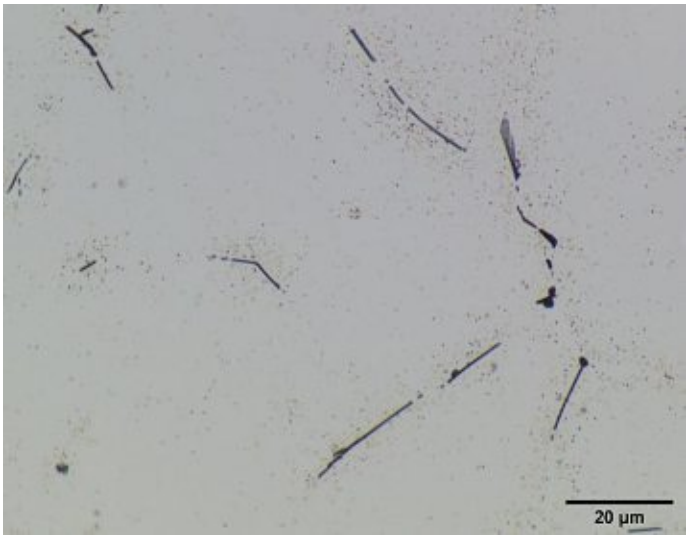

Figure 4.47: Post heat-treatment 530_4_wq of alloy 6082.48 (etched with H_2SO_4), black dots besides Al-Fe-Si phases (long-black-needles) indicate possible formation of Cr-containing dispersoids.

Differences in el. conductivity of the measured-values post heat-treatment and the as-cast state (Figure 4.45)

The value for Δσ in this case is positive. In the previous section it was mentioned, that for Cr only partial precipitation in form of Cr-containing dispersoids is considered. If Mg, Si and Cu form solid-solutions with the Al-matrix, then the positive value for Δσ can be explained by Cr-precipitation. Even if primary Mg-Si precipitates which are present in the as-cast state fully dissolve for this heat-treatment, the effects of those phases on el. conductivity can be outweighed by Cr-precipitation. Even if minor Cr precipitation occurs, the high influence of Cr on el. conductivity could easily outweigh the formation of solid-solution of primary Mg-Si phases.

Heat-treatment 580_4_wq

Differences in el. conductivity of the calculated values and measured values (Figure 4.44)

The value for Δσ is positive for this heat-treatment. For this heat-treatment it was assumed that Fe and Cr are in precipitated state (as Al-Fe-Si phases and Cr-containing phases/dispersoids, respectively). For Mg, Si and Cu full dissolution was assumed. As already mentioned for heat-treatment 530_4_wq, the positive value for Δσ in this case can be attributed to partial precipitation of Cr. Since the value for Δσ is slightly lower than for 530_4_wq, the measured-value is therefore closer to the calculated value than for 530_4_wq, indicating, that the higher temperature of 580_4_wq allowed for more precipitation of Cr-containing phases. Figure 4.48 shows, that the higher number density of what is assumed to be Cr-containing dispersoids precipitates compared to heat-treatment 530_4_wq would further confirm this assumption.

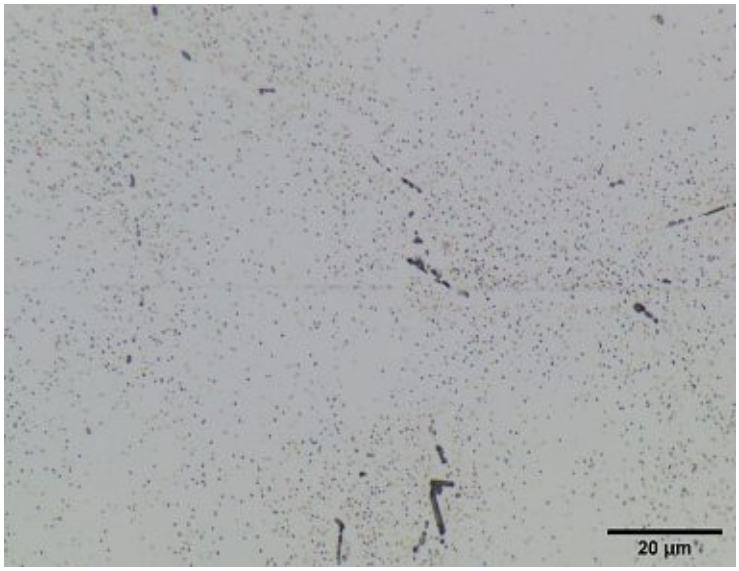

Figure 4.48: Post heat-treatment 580_4_wq (etched with H_2SO_4), black dots indicate possible formation of Cr-containing dispersoids of which the number density appears to be significantly higher than for heat-treatment 530_4_wq (Figure 4.47).

Differences in el. conductivity of the measured-values post heat-treatment and the as-cast state (Figure 4.45)

Δσ is positive for heat-treatment 580_4_wq. As already mentioned for heat-treatment 530_4_wq, the positive value can be explained by the precipitation of Cr-containing phases. Figure 4.48, indicates that for 580_4_wq more precipitates are formed than for 530_4_wq (Figure 4.47). The higher value for Δσ compared to 530_4_wq would further indicate, that more Cr-phases were precipitated for 580_4_wq, causing a higher increase in el. conductivity compared to 530_4_wq.

Heat-treatment 580_4_f

Differences in el. conductivity of the calculated values and measured values (Figure 4.44)

For this heat-treatment it was assumed, that only Cu remains in solid-solution during cooling-down, whereas Mg and Si are precipitated fully during cooling-down. For Fe the complete precipitation in form of Al-Fe-Si phases was assumed (which for the remainder of Fe in supersaturated solid-solution is expected to occur rather quickly during heating-up) and for Cr full precipitation in form of Cr-containing phases/dispersoids is assumed. The high value for Δσ indicates, that the measured value was significantly lower than the calculated value. This could be explained, by only partial precipitation of Mg-Si phases, since the precipitation process might be stopped at a certain temperature because diffusion is slowed down too much as to allow further precipitation. In addition, the slow diffusing Cr could remain to a certain degree in solid solution. Since Cr has a strong effect on el. conductivity, even a minor amount of Cr in solid solution could cause the value for el. conductivity to decrease significantly. Figure 4.49 indicates formation of Mg-Si phases, which appear as short and finely dispersed needles in the grain. This pattern of Mg-Si precipitates indicates, that nucleation of those phases could have occurred at Cr-dispersoids (of which formation is expected due to the results in Figure 4.48). For Cu it was assumed, that Cu-atoms remain in solid-solution during cooling-down, since diffusion of other necessary atoms for formation of Cu-containing phases (Mg and Si) is expected to come to a halt at a certain temperature, which makes formation of Cu-containing phases upon further cooling-down very unlikely to form.

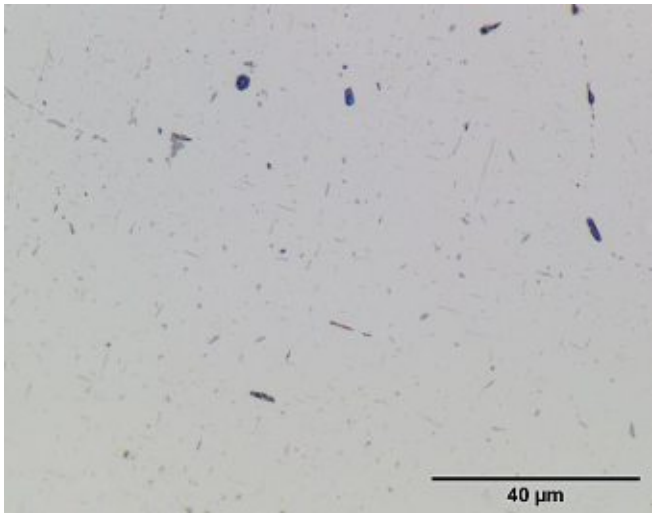

Figure 4.49: Post heat-treatment 580_4_f of alloy 6082.48 (unetched), small-white needles indicate Mg-Si precipitation during cooling-down.

Differences in el. conductivity of the measured-values post heat-treatment and the as-cast state (Figure 4.45)

The value for Δσ is significantly positive for heat-treatment 580_4_f, indicating, that the value for el. conductivity post heat-treatment is significantly higher than for the as-cast state. This could be explained by the fact, that Mg-Si is significantly precipitated from solid-solution during cooling-down, and Cr precipitates in form of Cr-containing dispersoids (as indicated by Figure 4.47 and Figure 4.48). The difference in Δσ between 580_4_f and 580_0_f could be ascribed to the precipitation of Cr-containing phases/dispersoids which occur during the four hours. It has to be noted, that the difference between 580_0_f and 580_4_f is approximately equivalent to the value for Δσ of 580_4_wq. This indicates, that the difference in Δσ between 580_0_f and 580_4_f can be attributed to the precipitation of Cr-containing phases/dispersoids. Figure 4.49 indicates, that Mg-Si precipitation occurred at formed Cr-dispersoids, since Mg-Si formed short and finely-disperses needles, which indicates that the number of nucleation spots was considerably higher than for 580_0_f (Figure 4.46). This assumes, that finely dispersed Cr-containing precipitates might act as nucleation-sites for Mg-Si precipitation.

4.6.3 SEM-Observation

The SEM micrographs in Figure 4.50 show no significant changes compared to the previous specimens for heat-treatment 530_4_wq. It is evident, that etching with H_2SO_4 causes dispersoids to appear significantly larger in size, due to the effect that dispersoids act as cathode during etching with H_2SO_4, which causes anodic dissolution of the surrounding Al-matrix [73]. Figure 4.47 shows the formation of what is assumed to be Cr-containing dispersoids, whereas no such phases are visible in Figure 4.50. The comparison of those two figures makes clear, that the etching-pits of dispersoids are significantly larger than the dispersoids themselves, since even SEM micrographs show no evident dispersoid-formation for 530_4_wq, whereas the etching pits can even be detected by light-microscope observation (Figure 4.47).

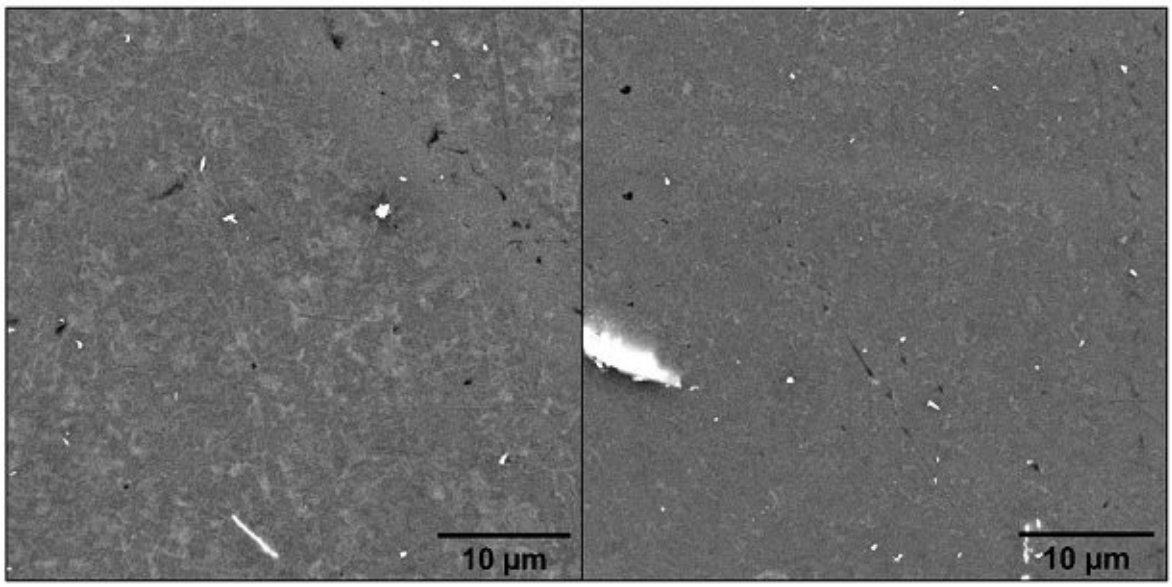

Figure 4.50: Backscattered SEM micrographs of alloy 6082.48, post heat-treatment 530_4_wq (unetched), white dots are assumed to be rather impurities than Cr-containing dispersoids.

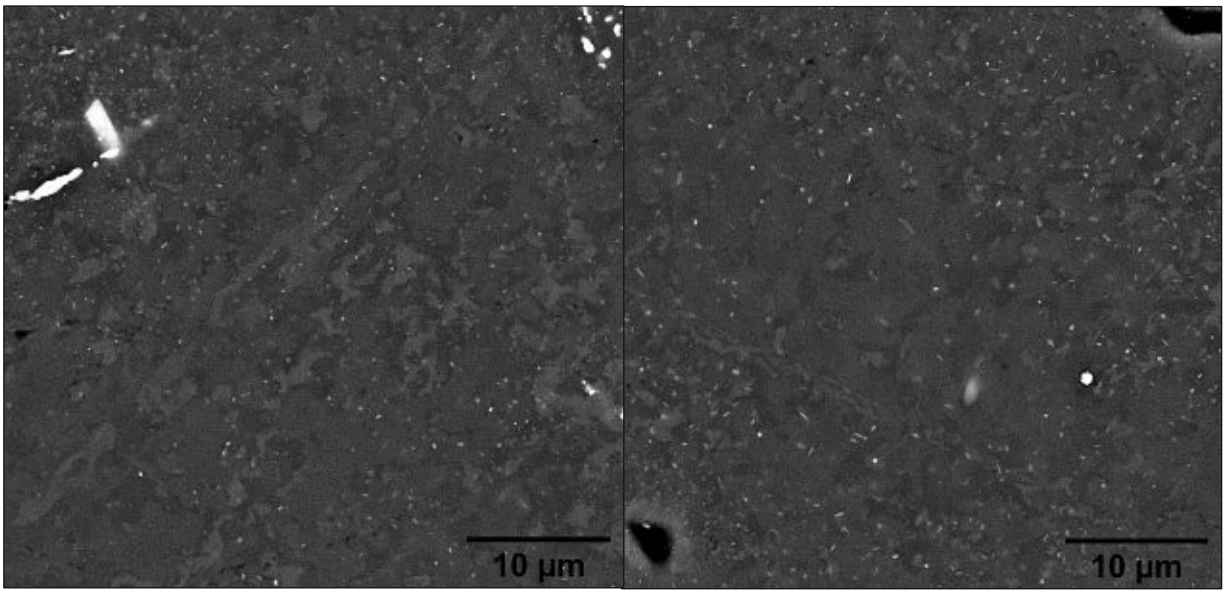

Figure 4.51: Backscattered SEM micrographs of alloy 6082.48, post heat-treatment 580_4_wq (unetched).

The dispersoid pattern in Figure 4.51 shows a similar pattern compared to alloy 6082.47. The higher homogenization temperature of 580 °C allowed for formation of a high number of finely dispersed phases (white dots), which are assumed to be Cr-containing dispersoids. It is again visible that formed dispersoids are concentrated at the grain boundaries.

4.7 Alloy 6082.49: Effect of Mn additions instead of Cu and Cr

4.7.1 Microstructure of the as cast state

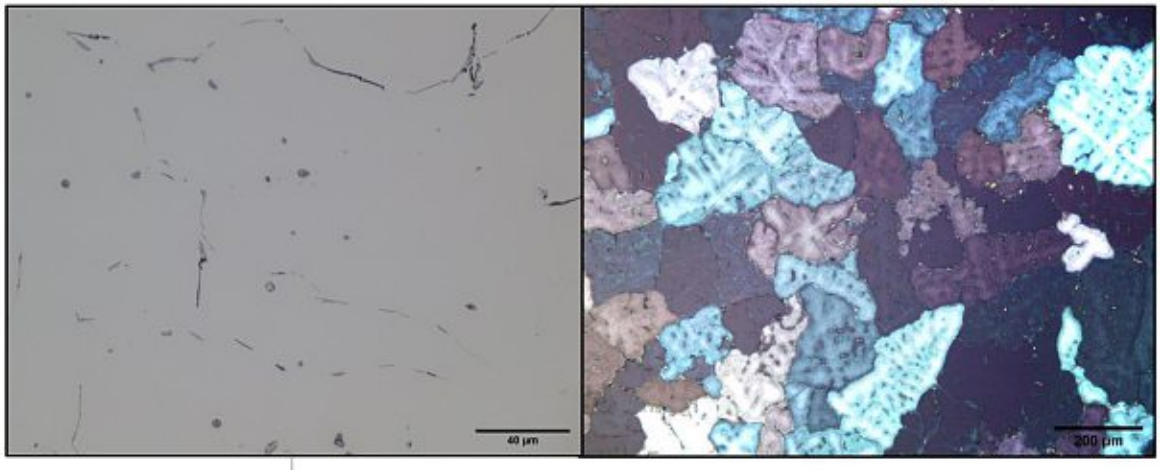

Figure 4.52: As-cast state of alloy 6082.49, left (unetched), grey structures are Al-Fe-Si phases, which lie at the grain-boundaries, small black dots at Al-Fe-Si indicate primary Mg-Si phases, right, grain-structure of alloy 6082.49, made visible by electro-polishing the specimen using Barker-reagent.

Figure 4.52 shows that alloy 6082.49 exhibits roughly the same grain size as alloys 6082.48 & 6082.30. Since Mn has a higher diffusion rate (roughly one magnitude for all temperatures) than Cr, the grain size reaches similar values as for the non-Cr-containing alloys.

4.7.2 El. conductivity and metallography

At the beginning of this chapter the el. conductivity of the as-cast state of alloy 6082.49 should be discussed. For the calculation of the el. conductivity of the as-cast state, two assumptions for the as-cast state were made. The first assumption – which sets a lower limit for the el. conductivity assumes that Fe is completely precipitated in form of Al-Fe-Si phases, whereas Mg, Si and Mn remain in supersaturated-solid-solution. The second assumption setting an upper limit for the el. conductivity assumes that only the slow diffusing Mn (Figure 2.5) remains in supersaturated-solid-solution, whereas the faster diffusing elements Fe, Mg and Si precipitate completely (Fe in form of Al-Fe-Si phases and Mg and Si in form of Mg-Si phases). For both assumptions the incorporation of Si in the Al-Fe-Si phases was neglected, since only a rough estimation of the as-cast state should be made.

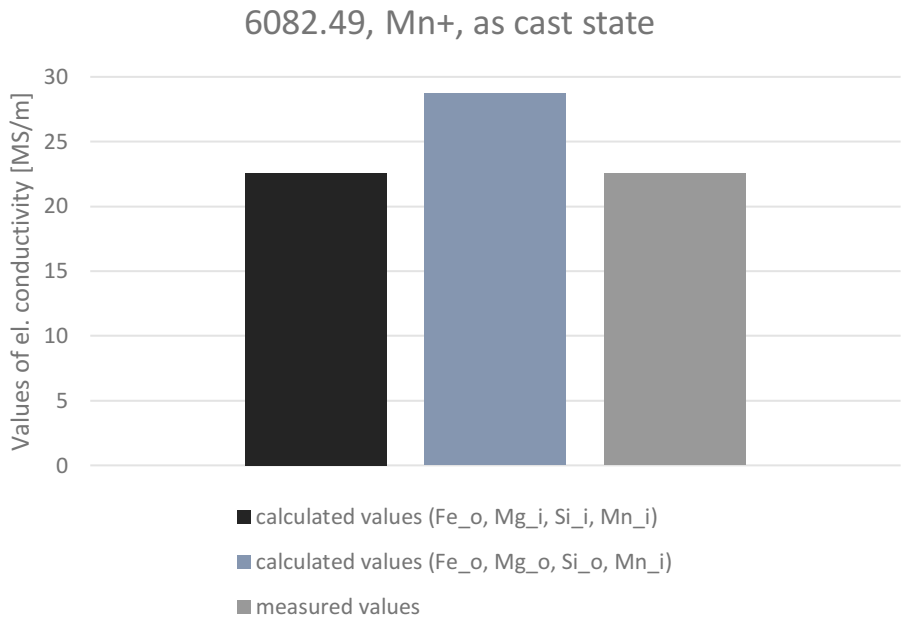

Figure 4.53: Values of el. conductivity of alloys 6082.49 of the as-cast state (bars for standard-deviation of the measured values are excluded since they were too small to be seen in this figure).
Abbreviations:
Element_o = Element out of solution
Element_i = Element in solid solution (super-saturated-solution).

Figure 4.53 reveals, that the assumptions made for the lower limit of the el. conductivity describe the true as-cast state (obtained by measurement) reasonably better, than the assumptions made for the upper limit. However, since the measurement only delivers the sum of alloying elements in solid-solution or in precipitated form, the true-state of the as-cast state is rather to be expected between the two assumed states of alloy 6082.49. Although the assumptions made for the lower limit are rather unrealistic (since Figure 4.52 reveals, that Mg and Si are also in present in precipitated form as primary Mg-Si phases at Al-Fe-Si phases) Figure 4.54 reveals, that those assumptions describe the true-state of the as-cast state reasonably well. For further discussions it should be assumed, that Mg and Si are mostly in supersaturated solid-solution in the as-cast state.

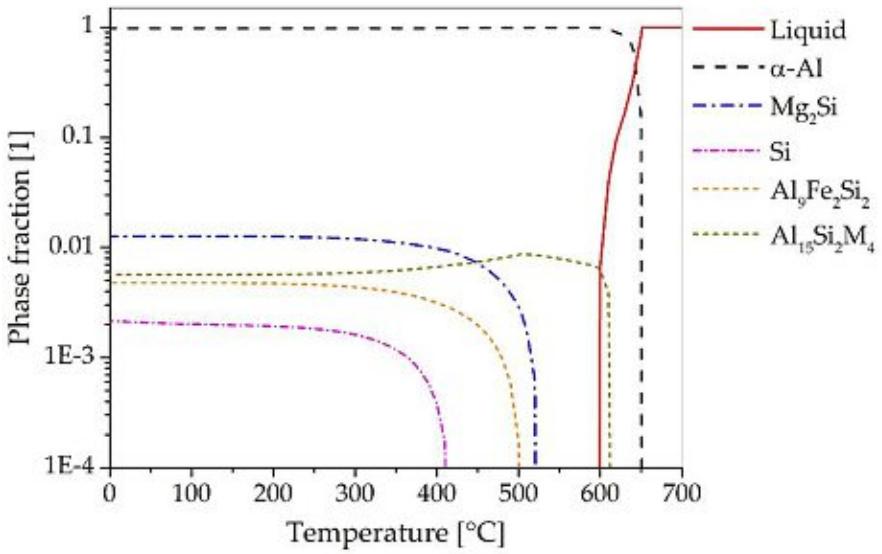

Figure 4.55: ThermoCalc calculation of the phase-composition depending on temperature for alloy 6082.49.

For the heat-treatments applied, analogous assumptions for the post-heat treatment states of the alloying elements were made and compared to the measured-values. For the assumption the results of the ThermoCalc calculation of alloy 6082.49 were considered (Figure 4.55). The $Al_{15}Si_2M_4$ phase is considered to be one of the Mn-containing phases, which are expected to precipitate during heat-treatments in form of Mn-dispersoids. The dissolution of the $Al_9Fe_2Si_2$ (and incorporation in the $Al_{15}Si_2M_4$ phase) is rather unlikely to occur, but of all results considered during calculation, this result delivered the most reasonable result. It was rather expected, that the major Fe-containing phases, remain precipitated in the Al-matrix in form of Al-Fe-Si phases, and that Mn-containing phases form independently of Fe-containing phases. The solvus-temperature for the Mg_2Si phase is 525 °C. The excess Si which is not consumed for Mg_2Si formation has a solvus temperature of 400 °C.

Table 16 shows the assumptions which were made for the post heat-treatment state of the alloying elements.

Table 16: Assumed state of the alloying elements for the calculation of el. conductivity values after corresponding heat-treatments for alloy 6082.49.
Abbreviations:
Element_o = out of solution
Element_i = Element in solid-solution

Heat-treatments	Fe	Si	Mg	Mn
580_0_wq	Fe_o	Si_i	Mg_i	Mn_i
580_0_f	Fe_o	Si_o	Mg_o	Mn_i
530_4_wq	Fe_o	Si_i	Mg_i	Mn_o
580_4_wq	Fe_o	Si_i	Mg_i	Mn_o
580_4_f	Fe_o	Si_o	Mg_o	Mn_o

In the following sections the difference in el. conductivity of the calculated values post heat-treatment and the measured values post heat-treatment should be discussed (Figure 4.56). Additionally, the differences in el. conductivity of the measured values post heat-treatment and as-cast state should be discussed (Figure 4.57).

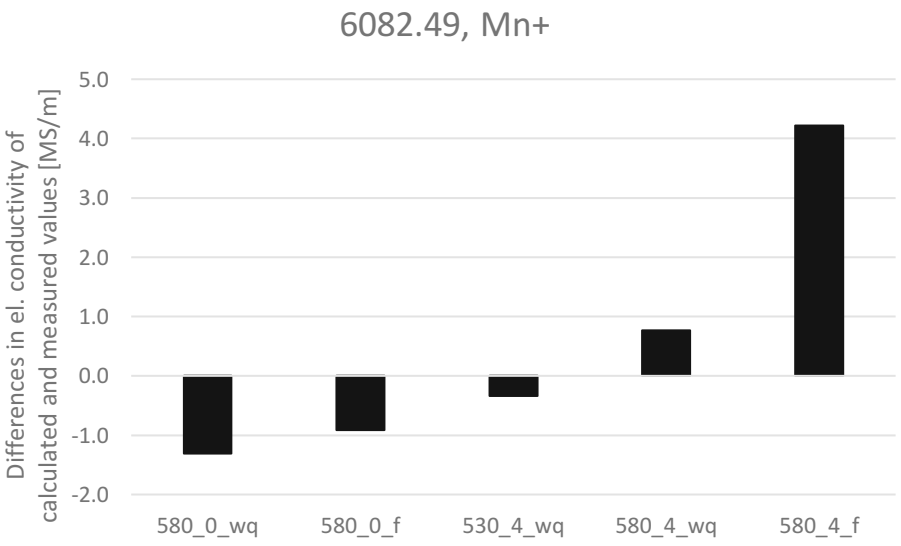

Figure 4.56: Differences in el. conductivity (Δσ) of calculated values (of assumed states of the alloying elements) after heat-treatment and the according measured values post heat-treatment.

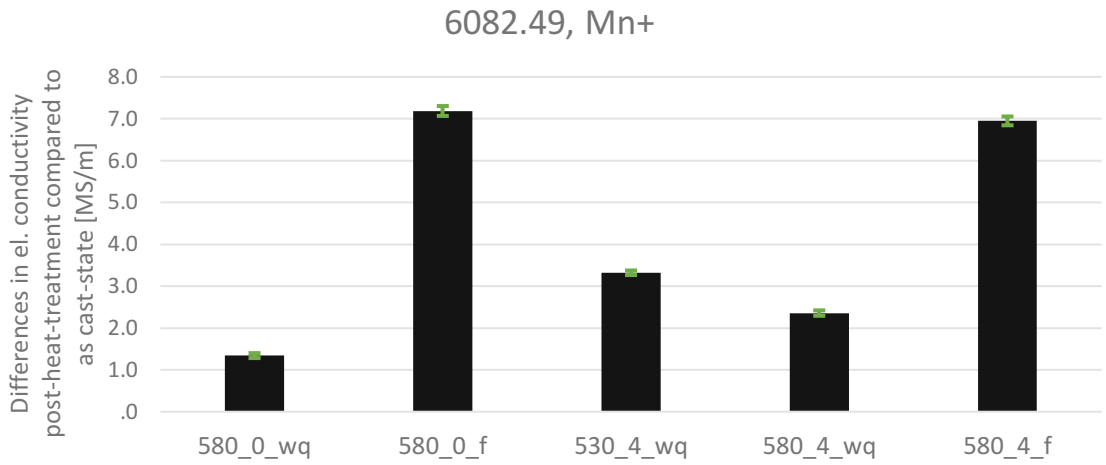

Figure 4.57: Differences in el. conductivity (Δσ)post-heat-treatments and as cast state of the according specimens of alloy 6082.49 (green bars indicate standard-deviations of Δσ and were calculated using Gaussian-error propagation).

Heat-treatment 580_0_wq

Differences in el. conductivity of the calculated values and measured values (Figure 4.56)

For the calculation of the el. conductivity of this heat-treatment, it was assumed, that Fe fully precipitates in form of Al-Fe-Si phases (neglecting the consumption of Si for the formation of those phases in order to make calculation easier), whereas Mg and Si form a solid-solution upon exceeding the solvus-temperature of 525 °C (after being precipitated as secondary Mg-Si phases from supersaturated solid-solution during heating-up). For Mn the assumption was made, that all of Mn remains in supersaturated solid solution, since the diffusion-rate of Mn is rather low and the time-period at elevated-temperatures which would allow for precipitation since diffusion is enhanced is rather short.

The negative value for Δσ in Figure 4.58 reveals, that the measured value was significantly higher than the calculated value. This could be described due to the fact, that probably not all of the Mg-Si phases which precipitate during heating-up are dissolved fully upon exceeding the solvus-temperature of 525°C. In addition although no precipitation of Mn-containing phases was considered precipitation of Mn-containing phases may have occurred. Even if precipitation of Mn-containing phases occurs only to a minor degree, the high influence on el. conductivity of Mn would cause the el. conductivity to significantly increase (Figure 2.21). Therefore slight precipitation of Mn-containing phases and partial dissolution of Mg-Si phases could describe the result in Figure 4.59 for this heat-treatment.

Differences in el. conductivity of post-heat-treatment and as cast-state (Figure 4.57)

The value for Δσ Figure 4.57 is slightly positive, indicating, that the el. conductivity is higher for the post heat-treatment state, than for the as-cast state. This could be explained by dissolution of primary Mg-Si phases, which are present as precipitates at Al-Fe-Si phases in the as-cast state. Those Mg-Si phases could be dissolved additionally to the secondary Mg-Si phases (which precipitate during heating-up but are dissolved again upon exceeding the solvus-temperature). In addition, precipitates containing Mn could have formed. Even if the slow diffusing Mn forms precipitates during this heat-treatment, their influence on el. conductivity would be significant, giving an additional explanation for the value of Δσ in Figure 4.57.

Heat-treatment 580_0_f

Differences in el. conductivity of the calculated values and measured values (Figure 4.56)

For the calculation of the el. conductivity of this heat-treatment, it was assumed, that during heating-up Mg-Si precipitates from supersaturated solid-solution (ThermoCalc calculation in Figure 4.55) are formed and fully dissolve upon exceeding the solvus-temperature of 525 °C. During cooling-down Mg-Si phases are again precipitated when the temperatures becomes lower than the solvus-temperature. For this calculation the full precipitation of Mg-Si phases was assumed. For Fe the full precipitation in form of Al-Fe-Si phases was expected (again neglecting the incorporation of Si for the formation of Al-Fe-Si phases since only a rough estimation is considered). For Mn it was assumed, that all of Mn remains in supersaturated-solid-solution, since the diffusion rate for Mn is considerably low compared to the other alloying elements of alloy 6082.49. Even if the assumption of complete inhibition of Mn-precipitation is rather unlikely to occur, this assumption should set a lower possible limit for the el. conductivity post heat-treatment.

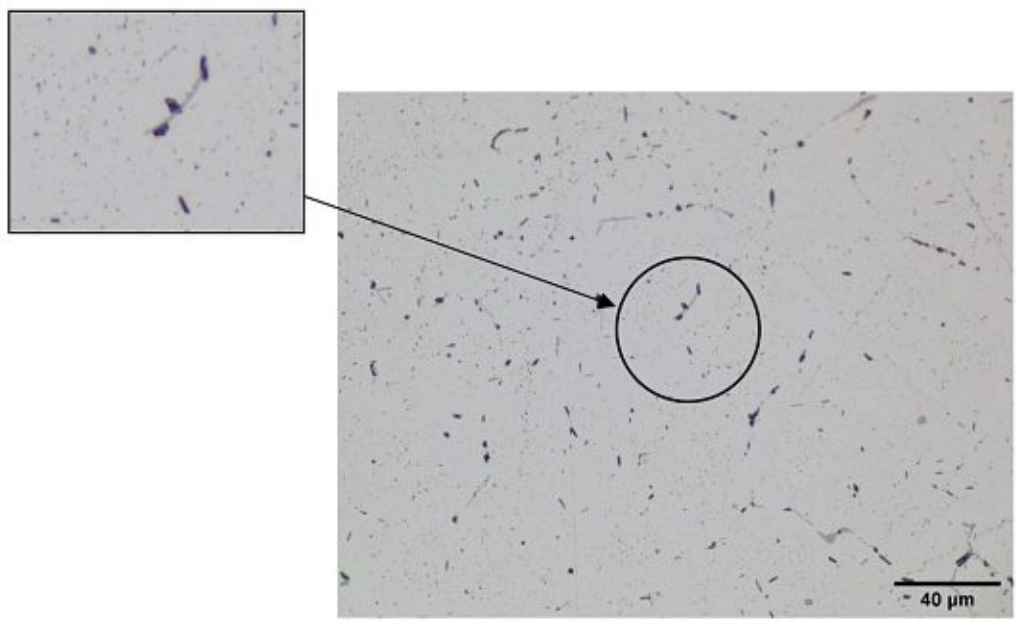

Figure 4.60: Post heat-treatment 580_0_f of alloy 6082.49. Zoomed-out picture indicates, that Mg-Si precipitation occurred in the form of small-needles, indicating, that Mn-dispersoids (which might have precipitated) acted as nucleating-agents, causing Mg-Si to precipitate as finely dispersed, small needles.

The negative value of Δσ indicates that the measured value is higher than the calculated value. This could only be explained by the fact, that precipitation of Mn occurred. Since the time-period at elevated temperatures (in this case, for the precipitation of Mn-phases elevated temperatures are considered to be as high as 400 °C, since in previous works it has been mentioned that at those temperatures Mn-precipitates start to form) is approximately twice as long as for 580_0_wq (heating-up period and Newtonian cooling-down curve) Mn precipitation could explain the negative value for Δσ for this heat-treatment [27].

Differences in el. conductivity of post-heat-treatment and as cast-state (Figure 4.57)

For this heat-treatment Δσ shows a significant high value, meaning that the el. conductivity of the alloy post heat-treatment is significantly higher compared to the as-cast state. This could be explained by significant precipitation of Mg-Si phases during cooling-down of the heat-treatment, as well as by at least partial precipitation of Mn-containing phases, which was already considered in the previous section. Even if for 580_0_wq full dissolution of Mg-Si phases (upon exceeding the solvus temperature) was not expected to occur (since alloy 6082.29 indicated rather partial dissolution), heat-treatment 580_0_f keeps the specimen approximately twice as long above the solvus-line, allowing more Mg-Si phases to be dissolved compared to 580_0_wq. If Mn-containing precipitates have formed during the heat-treatment, they might act as nucleating agents for Mg-Si phases to be formed and therefore allow for a high content of Mg and Si atoms to be in precipitated state at the end of the heat-treatment.

Heat-treatment 530_4_wq

Differences in el. conductivity of the calculated values and measured values (Figure 4.56)

The value for Δσ is slightly negative for this heat-treatment. For this heat-treatment it was assumed that Fe and Mn are completely precipitated in form of Al-Fe-Si phases and Mn-containing phases, respectively. For Mg and Si full dissolution was assumed. The solvus-temperature of 525 °C for Mg_2Si was only slightly exceeded for this heat-treatment, even if full dissolution of Mg-Si phases could be questioned for this temperature and time-period, full dissolution of Mg-Si phases was assumed. The slight negative value could be explained, due to the fact, that possibly Mg-Si remains to some extend undissolved. However, since the value for Δσ is only slightly negative, the assumptions made for this heat-treatment could mean, that the true state of alloy post heat-treatment is well described by the assumptions made. Figure 4.61 indicates, that significant precipitation of phases occurred, which appear to be Mn-containing dispersoids.

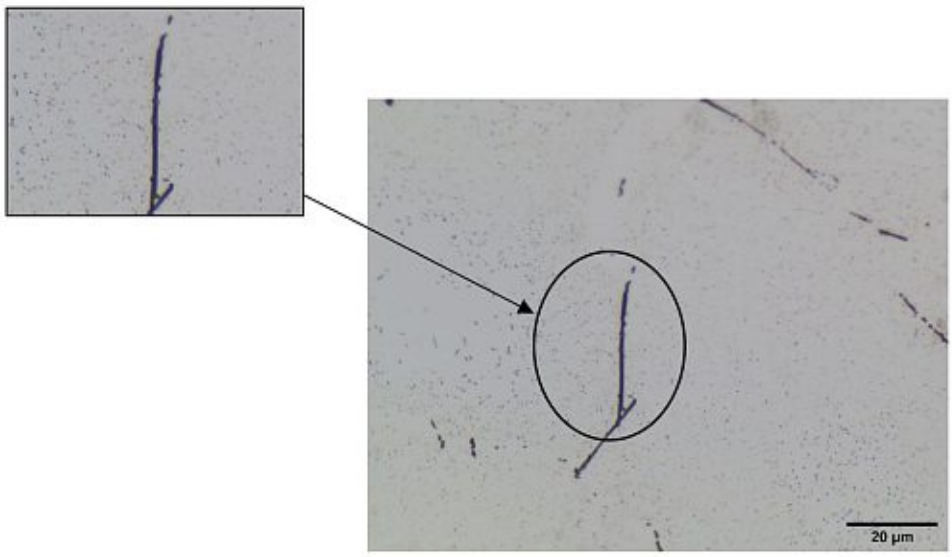

Figure 4.61: Post-heat treatment 530_4_wq of alloy 6082.49 (etched with H_2SO_4), black dots (small picture) indicate possible formation of Mn-containing dispersoids.

Differences in el. conductivity of post-heat-treatment and as cast-state (Figure 4.57)

The difference in el. conductivity for the post heat-treatment and as-cast state of this heat-treatment show a positive value. If significant dissolution of secondary Mg-Si phases can be considered, than the change in el. conductivity for this heat-treatment could be attributed to the precipitation of Mn-containing phases. In the previous section full precipitation of Mn & Fe was assumed, as well as full dissolution of secondary Mg-Si phases. This assumption lead to a small value for Δσ, indicating that the assumptions made could come close to the true-state of the alloying elements post heat-treatment. Figure 4.61 also indicates possible formation of Mn-containing dispersoids. The result in this section would further indicate, that the visible precipitates in Figure 4.61 could be Mn-dispersoids.

Heat-treatment 580_4_wq

Differences in el. conductivity of the calculated values and measured-values (Figure 4.56)

The differences in el. conductivity between the calculated and measured-values for this heat-treatment show a slightly positive value for Δσ. For the calculated value it was assumed that Fe and Mn are completely precipitated (in form of Al-Fe-Si phases and Mn-containing dispersoids, respectively), for Mg and Si complete dissolution of secondary Mg-Si phases was assumed, since the hold-temperature of this heat-treatment of 580 °C is well above the solvus-temperature of 525 °C for Mg_2Si. The positive value for Δσ indicates that the calculated value was slightly higher than the measured value. This could be explained due to incomplete precipitation of Mn-containing phases/dispersoids. Since Mn has a high influence on el. conductivity, even a minor amount of Mn which remains in solid solution would cause the el. conductivity of the measured value to be lower than the value for the assumed state (which assumed full precipitation of Mn). The high number of precipitates in Figure 4.62 indicates possible formation of Mn-containing dispersoids.

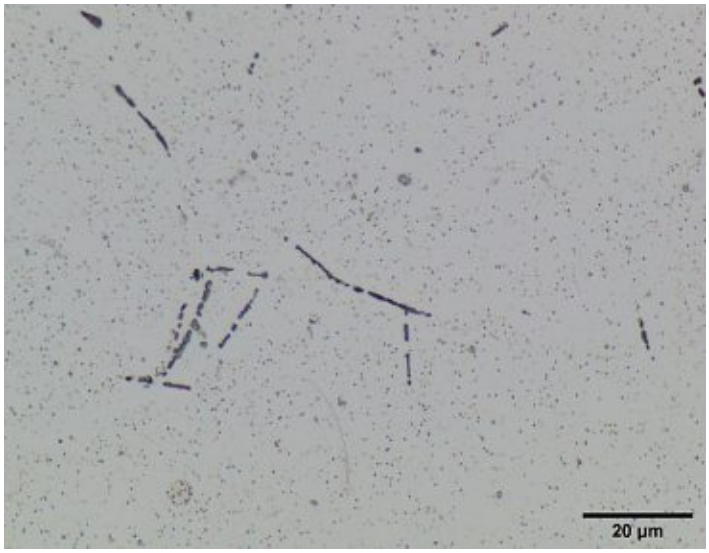

Figure 4.62: Post heat-treatment 580_4_wq of alloy 6082.49 (etched with H_2SO_4), the high number of black dots indicates possible formation of Mn-containing dispersoids.

Differences in el. conductivity of post-heat-treatment and as cast-state (Figure 4.57)

The value for Δσ is positive for this heat-treatment, indicating that the post heat-treatment value for el. conductivity is higher than the value for the as-cast state. The higher value of Δσ for heat-treatment 530_4_wq compared to 580_4_wq indicates that the lower-temperature may have caused more precipitation of phases. However, this result may have been caused due to a phase-change in Mn-containing Mg-Si alloys which was observed in previous works [27]. In their work Strobel et. al. found out, that for lower temperatures and shorter homogenization-periods higher dispersoid number densities and lower particle-sizes have been obtained.

In addition, the stoichiometry of the formed dispersoids has been analyzed. It was detected that for lower temperatures the $Al_{15}(MnFe)_3Si_2$ structure with a high Mn:Fe ratio was obtained, whereas for higher homogenization temperatures and longer durations the $Al_{12}(MnFe)_3Si$ structure was obtained which showed a low Mn:Fe ratio of approx. 1:1. It is assumed that the growth of Mn-dispersoids is controlled by the diffusion of Fe to the particles and the subsequent substitution of Mn. It therefore explains that for lower temperatures such as for 530_4_wq more Mn is used for the formation of dispersoids and is substituted by Fe for higher temperatures such as for 580_4_wq. This process explains the higher change in conductivity for 530_4_wq than for 580_4_wq.

Heat-treatment 580_4_f

Differences in el. conductivity of the calculated values and measured values (Figure 4.56)

The value for Δσ shows a significant high value for this heat-treatment. For the calculated value of el. conductivity full precipitation of all alloying elements was assumed. Fe and Mn are assumed to precipitate in the form of Al-Fe-Si phases and Mn-containing phases/dispersoids, respectively. For Mg and Si full precipitation in form of Mg-Si phases was assumed. The high value for Δσ indicates, that the measured value is significantly lower than the calculated value. The results of heat-treatment 580_4_wq indicated, that Mn is not fully precipitated in the form of Mn-containing dispersoids. However, the results showed that only a minor amount should remain in solid-solution. The results in Figure 4.62 also indicate precipitation of what seems to be of a high number of Mn-containing dispersoids. Therefore, the result for this heat-treatment and section could be explained by partial precipitation of Mg-Si containing phases.

Differences in el. conductivity of post-heat-treatment and as cast-state (Figure 4.57)

Δσ shows a significant positive value for this heat-treatment, indicating, that a high content of alloying elements is in precipitated state in the post heat-treatment state compared to the as-cast state. As in the previous section, this could be attributed to a high amount of Mg-Si phases, which precipitate upon cooling-down once the temperatures falls below the solvus-temperature of 525 °C. In addition, Mn-containing precipitates may have formed, Figure 4.62 indicates that such precipitates may have formed. Compared to the previous alloys it has to be mentioned, that Δσ shows almost the same value for 580_0_f as for 580_4_f. This could mean, that the short-heating-period for 580_0_f was enough, as to cause the alloying elements to reach the same state as for 580_4_f. Since the diffusion-rate for Mn is approximately an order of magnitude higher than for Cr, the higher diffusion-rate might allow Mn to precipitate significantly during 580_0_f. In addition, those Mn precipitates might act as nucleation sites for Mg-Si precipitation and allow the same amount of Mg-Si to precipitate, as for 580_4_f.

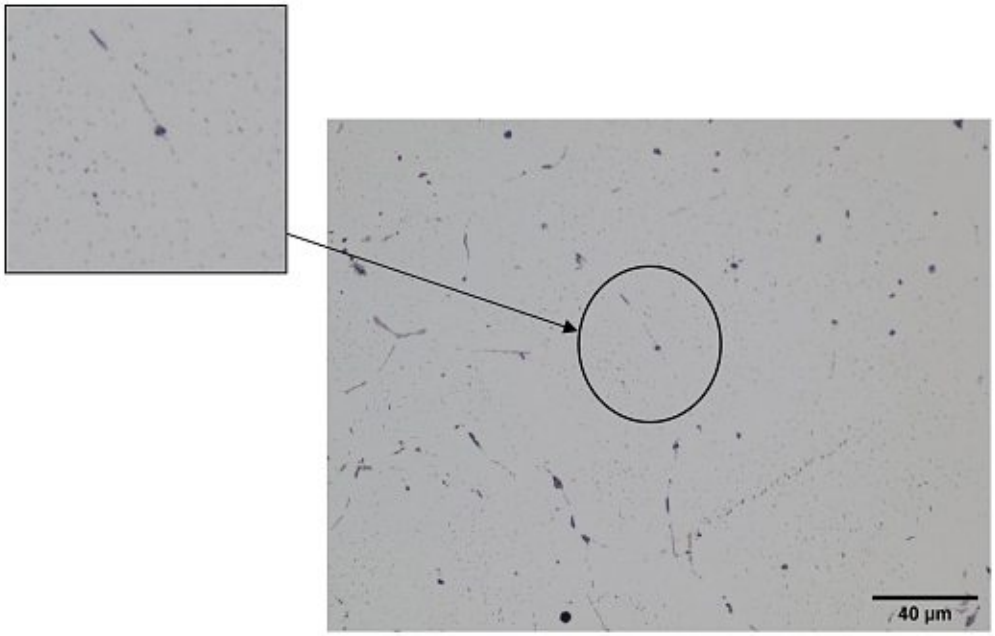

Figure 4.63: Post heat-treatment 580_4_f of alloy 6082.49. Small-sized precipitates (zoomed-out picture) indicate that Mg-Si precipitation might have occurred in the form of short-needles, which could indicate, that Mg-Si nucleates at Mn-dispersoids during cooling-down.

Figure 4.63 shows, that Mg-Si occurred in the form of small-sized needles, which are finely dispersed throughout the grain. This precipitation pattern would further indicate, that Mn-dispersoids might act as nucleation sites for Mg-Si precipitation. In addition, Figure 4.60 shows a similar pattern for Mg-Si precipitates, indicating, that the short-time period for 580_0_f might be enough to cause the alloying elements to take the same state (in solution or in precipitated form) as for 580_4_f.

4.7.3 SEM-Observation

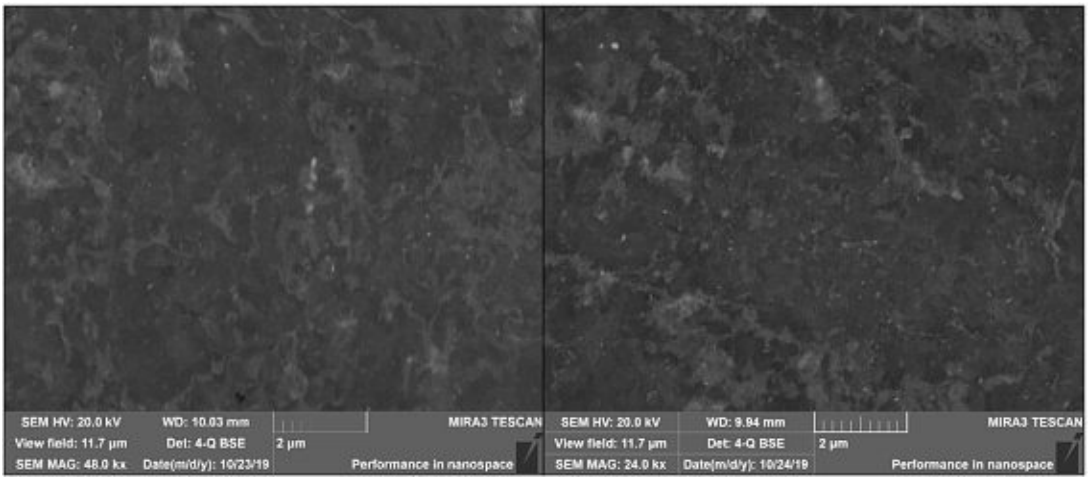

Figure 4.64: Backscattered SEM micrographs post heat-treatment 530_4_wq of alloy 6082.49. Small white dots indicate possible formation of Mn-containing dispersoids.

Figure 4.64 shows that in contrast to the previous alloys the low temperature of 530_4_wq was high enough to produce precipitates, which could possibly be Mn-containing dispersoids which are large enough to be seen with SEM-Observation. However, a high magnification had to be applied to make the dispersoids visible (the same magnification was applied for the alloys post heat-treatment 530_4_wq before but no dispersoid formation was visible).

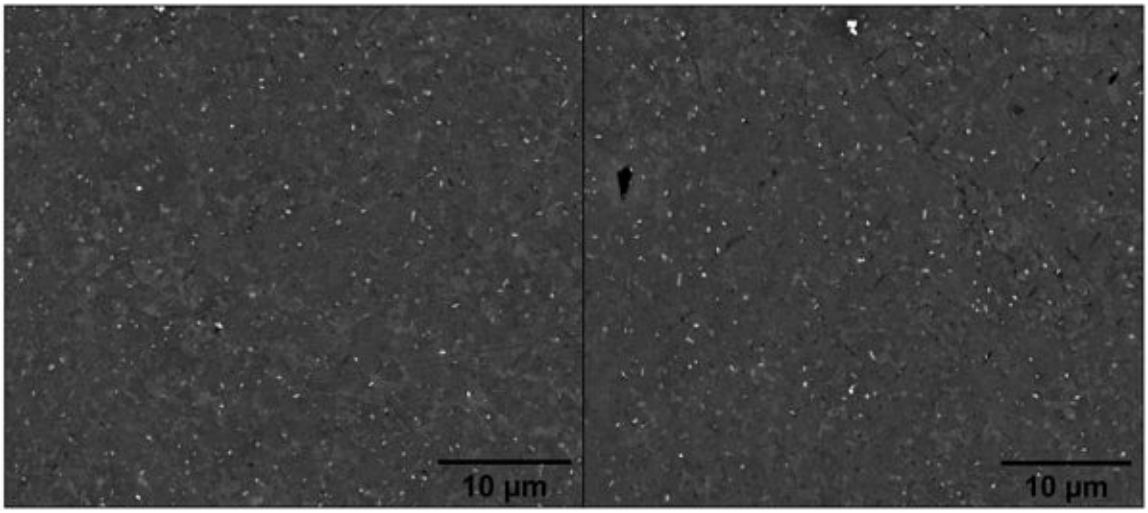

Figure 4.65: SEM-observation post heat-treatment of 580_4_wq of alloy 6082.49. White dots which are homogeneously spread within the grains indicate possible formation of Mn-containing dispersoids.

Figure 4.65 shows the formation of phases for heat-treatment 580_4_wq, which could be Mn-dispersoids. In this case the dispersoids are not concentrated along the grain boundaries but rather spread throughout the whole grain. Figure 2.6 shows a high homogeneity for Mn within a specimen. It could therefore mean that a high homogeneity for a certain element in the as cast stage causes a more uniform distribution of dispersoids upon homogenization.

4.8 Effect of higher Fe-content on el. conductivity

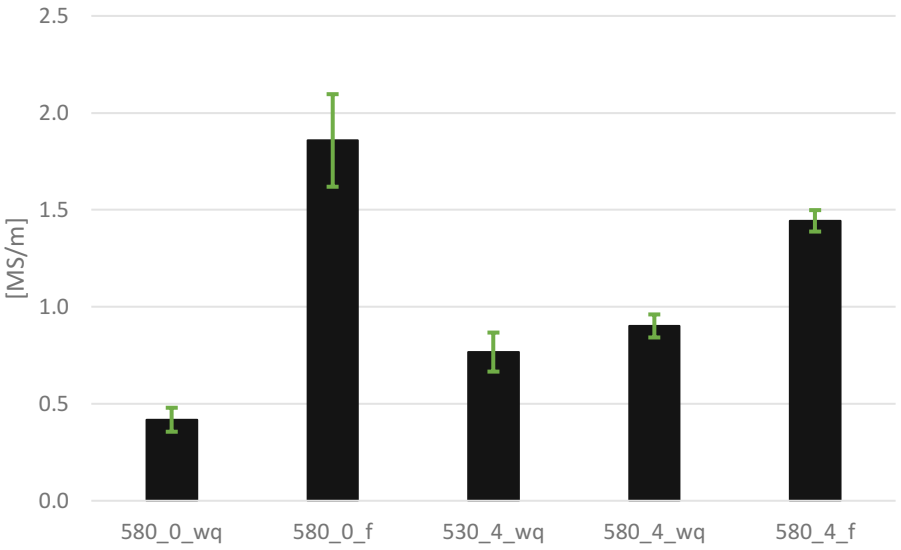

Figure 4.66: Values for Δσ of measured values post heat-treatment and measured-values of the as-cast state of alloy 6082.29 were subtracted from the according Δσ-values of alloy 6082.30 (Values of Δσ in Figure 4.7 are subtracted from according values in Figure 4.21, green bars indicate standard-deviations, which were calculated using Gaussian-error propagation).

The values of Δσ of the measured-values of el. conductivity post heat-treatment and measured-values of the as-cast state of alloy 6082.29 were subtracted from the according values for alloy 6082.30 in order to investigate the effect of higher Fe-content on el. conductivity. Figure 4.66 shows the according results. It is evident, that a higher Fe- content, causes the value for Δσ for each heat-treatment to become significantly higher. The higher values for heat-treatments 580_0_w, 530_4_wq and 580_4_wq could be attributed to the higher amount of Fe-containing precipitates which are expected to be formed for those heat-treatments. The higher value in Figure 4.66 for 530_4_wq compared to 580_0_wq could be attributed to the longer duration of homogenization for 530_4_wq and therefore allow more Fe-containing phases to be precipitated. The higher value for 580_4_wq compared to 530_4_wq could be explained by the stronger diffusion of Fe for the higher temperature of 580 °C and therefore making precipitation of Fe-containing phases easier to occur.

The higher value for 580_0_f in Figure 4.66 could be explained by the influence of Fe-containing precipitates/dispersoids which could act as nucleation sites for Mg-Si precipitation. If Fe-dispersoids are formed for heat-treatment 580_0_f, the higher Fe content of alloy 6082.30 (which has a Fe-content of 0.18 mass-%, which is approximately three-times as high as for alloy 6082.29, which has a Fe-content of 0.06 mass-%) could allow for significantly higher number-density of Fe-dispersoids to be precipitated for alloy 6082.30 for heat-treatment 580_0_f. If dispersoids enhance Mg-Si precipitation, this higher number-density of Fe-dispersoids would also increase Mg-Si precipitation and therefore cause a higher value for Δσ to be obtained for 6082.30 than for 6082.29.

If the values in Figure 4.66 of 580_4_f and 580_0_f are compared, it is evident, that the difference in el. conductivity becomes less, if the time period of heat-treatment becomes longer. If Fe-dispersoid formation occurs for alloy 6082.30 during 580_4_f (which Figure 4.25 indicates for etched

metallographic specimens post heat-treatment of 580_4_wq), the low Fe-content of alloy 6082.29 would make the necessary time for Fe-dispersoid formation to be higher than for alloy 6082.30. Although no visible Fe-dispersoid formation could be detected for alloy 6082.29, their size may be too small to be detected by metallographic or SEM-observation. If however, a significantly higher number of small Fe-dispersoids was precipitated for 580_4_f than for 580_0_f, they might act as nucleation-sites for Mg-Si precipitation, causing the value in Figure 4.66 to be lower for 580_4_f than for 580_0_f, since more Mg-Si phases are precipitated in this case for alloy 6082.29.

4.9 Effect of Cu-addition on el. conductivity

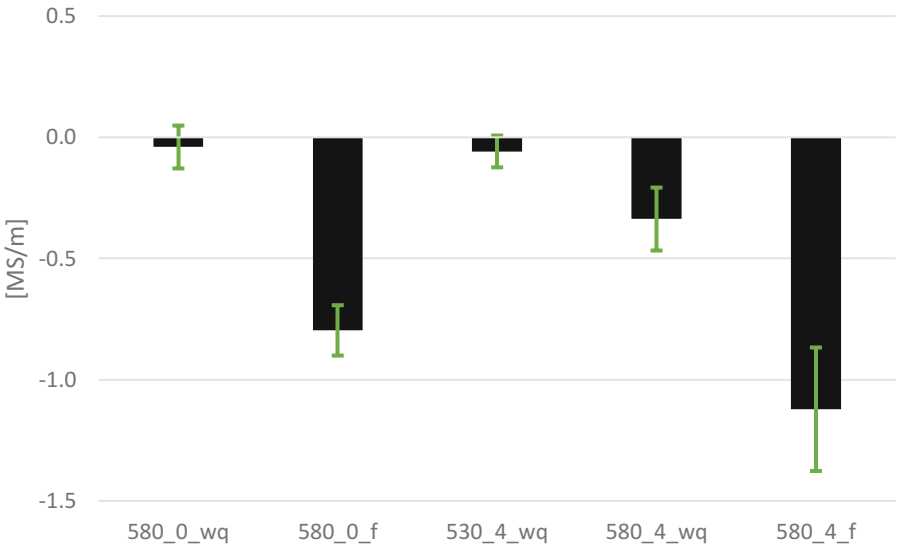

Figure 4.67: Values for Δσ [y-axis, MS/m] of measured values post heat-treatment and measured-values of the as-cast state of alloy 6082.47 were subtracted from the according Δσ-values of alloy 6082.48 (Δσ-values in Figure 4.34 were subtracted from according values in Figure 4.57, green bars indicate standard-deviations, which were calculated using Gaussian-error propagation).

In order to compare the differences on el. conductivity which are caused by Cu addition, Δσ-values of measured post heat-treatment and as-cast state of alloy 6082.47 were subtracted from the according values of alloy 6082.48 (Figure 4.67). In this chapter only the main-differences between those alloys should be discussed. Alloys 6028.48 and 6082.47 showed significant differences in conductivity for 580_0_f and 580_4_f (Figure 4.67). The high difference for those heat-treatments can probably be attributed to Cu, which remains in solution for those heat-treatments. The high diffusion-rate of Cu might cause the fast-diffusing Cu-atoms to inhibit the precipitation of Mg-Si phases. This would explain that heat-treatments 580_0_f and 580_4_f show a significantly lower change for Δσ in conductivity for alloy 6082.48. Although the cooling-down for those two heat-treatments happens reasonably slow, the cooling-down curve is still an exponential Newtonian cool-down curve. This means that at the beginning of the cooling-down the high temperatures are passed more quickly than the lower temperatures. Therefore, precipitation processes are inhibited after a certain duration since diffusion comes to a halt at a certain temperature. If fast-diffusing Cu-atoms collide with Mg and Si atoms at a high frequency during-cooling-down the precipitation of Mg-Si phases might be inhibited, since the necessary frequency of collisions with Mg and Si atoms for the precipitation of according phases could be reduced significantly upon Cu-addition. Since this process has only a limited time window the lack of Mg and Si collisions might cause a significant inhibition of their according phase-precipitations. The high value for Δσ of 580_4_f indicates, that the Δσ value of alloy 6082.47 was significantly higher than for alloy 6082.48 for this heat-treatment. This indicates, that significantly more Mg-Si precipitates were

formed for alloy 6082.47 for this heat-treatment. This effect could be caused, due to the fact that a significant number of Cr-dispersoids was formed compared to 580_0_f. Formed Cr-dispersoids might act as nucleation sites for Mg-Si precipitates. Although the number of formed Cr-dispersoids for alloy 6082.47 and 6082.48 might be the same for 580_4_f, the mentioned interference of Cu on Mg-Si precipitation might cause significantly less Mg-Si precipitates to be formed for alloy 6082.48 (although Cr-dispersoids could act as nucleation sites). Since for alloy 6082.47 no such interference occurs for Mg-Si precipitations, alloy 6082.47 might form a significantly higher number of Mg-Si precipitates compared to 6082.48. In addition it has to be noted, that the value of Δσ for 580_4_f roughly equals the addition of Δσ values of 580_0_f and 580_4_wq. It is assumed that Δσ-values obtained by 580_4_wq can mostly be attributed to the formation of dispersoids. If dispersoids act as nucleation sites for Mg-Si precipitation, the addition of Δσ-values of 580_0_f and 580_4_wq should roughly equal the Δσ-value for heat-treatment 580_4_f (since for 580_4_f the same number of dispersoids as for 580_4_wq should be formed, which during-cooling down can act as nucleation sites for 580_4_f). Since this is the case for 580_4_f, the higher Δσ value compared to 580_0_f is attributed to the higher number-density of dispersoids, which act as nucleation-sites during Mg-Si precipitation.

4.10 Comparison of the influence on el. conductivity upon Mn-addition or Cr-addition

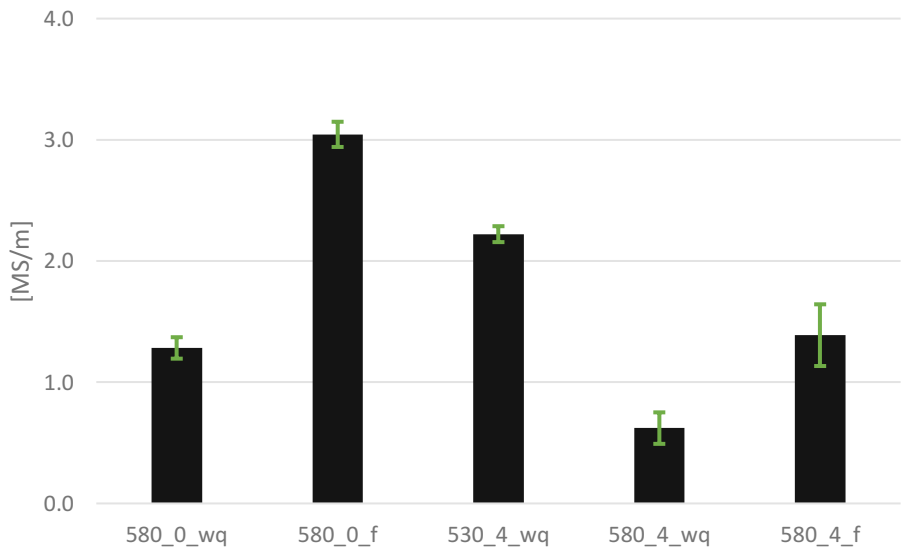

Figure 4.68: Values for Δσ of measured values post heat-treatment and measured-values of the as-cast state of alloy 6082.47 were subtracted from the according Δσ-values of alloy 6082.49 (Δσ-values in Figure 4.34 were subtracted from the according values in Figure 4.57, green bars indicate standard-deviations, which were calculated using Gaussian-error propagation).

Figure 4.68 shows the difference for Δσ of alloys 6082.49-6082.47 for the measured-values of el. conductivity post heat-treatment and the measured values for the as-cast state (Difference of values for Δσ shown in Figure 4.57 and Figure 4.34).

For 580_0_wq the higher change in conductivity can be explained due to the higher diffusion rate of Mn compared to Cr. Therefore, the short heat input for 580_0_wq is enough to produce a considerably higher number of Mn precipitates/dispersoids compared to Cr precipitates/dispersoids formed for this heat-treatment. In addition, the higher number of Mn dispersoids might act as nucleation site for Mg-Si-precipitation, which can be seen for 580_0_f. The change for 530_4_wq could be attributed to the $Al_{15}(MnFe)_3Si_2$ phase which may have formed for the lower-temperature of 530_4_wq [27]. The higher Mn content of dispersoids which are expected to form for this temperature and higher

diffusion-rate to Cr explains the higher amount of precipitated phases for this heat-treatment. 580_4_wq shows that for higher temperatures approximately similar results are obtained for conductivity measurements since the diffusion rate for Cr is also increased and the phase transformation of the Mn-dispersoids decreases the change in conductivity [27]. For higher temperatures as for 580_4_wq phase-change from the $Al_{15}(MnFe)_3Si_2$ structure (with a high Mn:Fe ratio) to the $Al_{12}(MnFe)_3Si_2$ structure (with a low Mn:Fe ratio) was described in previous works [27]. 580_4_f shows that the same reason mentioned for 580_0_f is probably the explanation for the higher change in conductivity for alloy 6082.49. Since the number and size of formed dispersoids becomes similar for both alloys (due to the higher temperature of 580 °C and therefore stronger diffusion for Mn and Cr), the situation for nucleation of Mg-Si during cooling becomes similar (similar number-density of dispersoids for 6082.49 and 6082.47 for this heat-treatment allow for similar number of nucleation-sites for Mg-Si precipitation during cooling-down) and therefore the change for 580_4_f is not as significant as for 580_0_f.

4.11 Average grain size

All alloys showed similar grain-sizes, only alloy 6082.47 showed a significantly larger grain-size. Slow-diffusing elements can cause the solidification-interval to increase during casting, which results in a coarser grain. However, in order to make a representative comparison of the grain-size of each alloy in the as-cast state, the casting process has to be equal for each alloy. It has to be considered if the same amount of TiB_2 was used for each alloy and if the chemical additives were of same age (by chemical additives the chemical-compounds which contain the alloying elements is meant). Since at this stage it cannot be confirmed that these requirements were meat for each alloy, only the qualitative observation is made, that alloy 6082.47 showed a significantly larger-grain size. For future comparison of the grain-size of the as-cast state the mentioned casting-parameters have to be taken additionally into account in order to make a representative comparison.

4.12 DSC Measurements

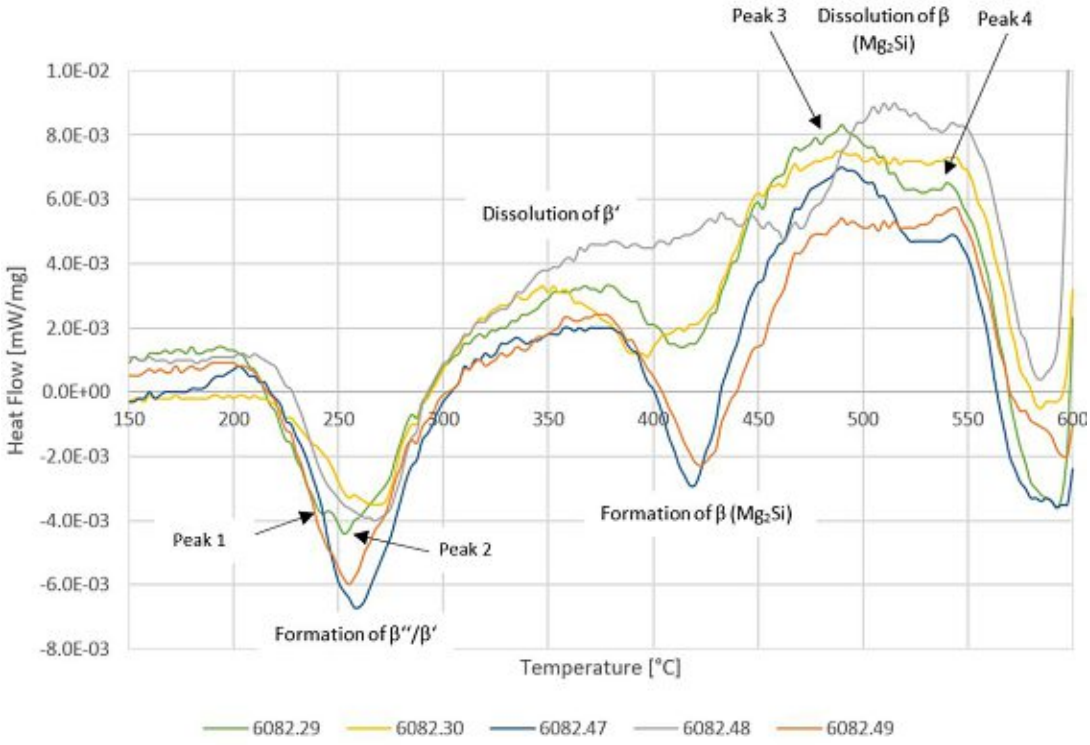

Figure 4.69: First DSC-measurements of all alloys.

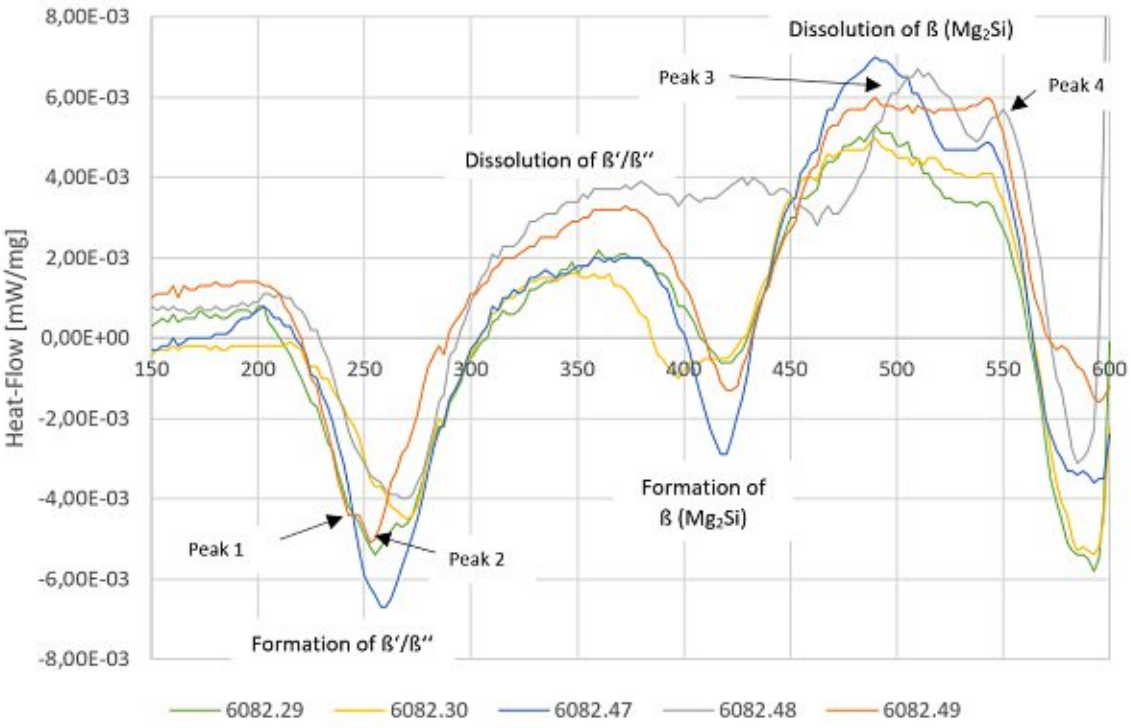

Figure 4.70: Second DSC-measurement of all alloys.

Two DSC-measurements were carried out for all alloys (Figure 4.69 & Figure 4.70). The as cast materials were heated up at a rate of 3K/min till melting occurs/fully melted. As reference material Al of 99.98 % purity was used. The obtained values of the reference material were subtracted from the values of the specimens.

Figure 4.69 & Figure 4.70 show the heat flux from/towards the specimens. Exothermic peaks – which indicate the formation of phases – have a negative heat flux/ a negative slope, while endothermic peaks – which indicate the dissolution of phases – have positive values/ a positive slope of the heat flux. Since the heat flux from formed dispersoids is small compared to the heat-flux from Mg-Si precipitation, in previous trials at LKR it was observed, that the DSC-measurements only give information on the formation of Mg-Si-phases and that the formation of dispersoids may only be detected indirectly through their possible influence on dissolution/precipitation of Mg-Si phases. The formation of Mg-Si-phases and the ultimate stage of the thermodynamically stable phase Mg_2Si are processes which have been investigated for decades and details have been described in chapter 2.1.2.1 [74].

Although the intensity/height of exothermic/endothermic events differ for certain alloys for Figure 4.69 & Figure 4.70, it is evident, that only slight shifts for the peak-temperatures of the reactions are observed between the two figures.

Peak 1 and Peak 2 can be attributed to the formation of ß'' and ß', respectively [74]. The formation of both phases occurs within a temperature-interval of 225 °C – 260 °C. It is evident from both Figures, that formation of both phases occurs at higher temperatures for alloy 6082.30 (approximately 270 °C) than for 6082.29 (approximately 260 °C). It is assumed, that the higher Fe-content of alloys 6082.30 may cause significant formation of Fe-dispersoids in the same temperature-region. Since Si is also necessary for the formation of Fe-dispersoids (it is assumed that their stoichiometry is close to that of Al-Fe-Si phases) this "competition" for necessary Si-atoms for Fe-dispersoid formation or ß'' and ß' phases may shift the peak-temperatures for ß'' and ß' to higher-temperatures.

In contrast, the peak-temperature for the formation of the ß-phase is significantly lower for 6082.30 (peak-temperature of 390 °C) than for 6082.29 (peak-temperature 420 °C). It is assumed, that if Fe-dispersoid formation occurs prior to ß-formation, formed dispersoids might act as nucleation-sites for ß-formation, causing the peak for formation of ß to be shifted towards lower temperatures.

Alloys 6082.29, 6082.47 and 6082.49 show similar peak-temperatures for ß'' and ß' formation. It is assumed that for those three alloys dispersoid-formation occurs at significantly higher temperatures, (or significantly less dispersoids are formed for 6082.29 than for 6082.30) and that therefore ß'' and ß' occurs without any "competing" dispersoid-formation for the same temperature-region as mentioned for 6082.30. The peak-temperature for ß-formation is also similar for those three alloys, indicating, that no major differences occur between the three alloys up to this temperature-region.

Alloy 6082.48 shows a similar peak-temperature for ß'' and ß' formation as alloy 6082.30. It is assumed, that formation of the Q-phase might start to occur at this temperature-region. One stoichiometry for the stable Q-phase which was mentioned is $Al_4Mg_8Si_7Cu_2$ [2]. In chapter 2.1.2.1 the formation sequence for the Q-phase was mentioned. The formation of the Q-phase would therefore create a "competion" for Mg and Si atoms, which are also necessary for ß'' and ß' formation. The shift of the peak-temperatures towards higher temperatures could be explained by this "competition" for necessary atoms. Additionally, since the ß''-phase is one of the necessary intermediate phases for the formation

of the Q-phase, the formation of the Q-phase might occur in competition with the formation of the ß'-phase (which follows the ß''-phase during Mg-Si precipitation), which could further explain the shift towards higher-temperatures for ß'-formation.

The peak for ß-formation occurs in the temperature-range of 380 °C – 430 °C. It is clearly visible that alloy 6082.48 shows a plateau instead of an exothermic peak for the Mg_2Si formation. Both measurements delivered the same result, since it was assumed that inhomogeneous distribution of the elements in this alloy could have caused the results, additional DSC-specimens of alloy 6082.48 of a different part of the bolt were measured twice additionally. Those specimens showed the same results.

The plateau could indicate, that upon Cu-addition the precipitation of Mg-Si phases is inhibited. For alloy 6082.48 the ThermoCalc calculation showed, that the Cu-containing Q-Phase has a solvus-temperature of 334 °C. Since all necessary alloying elements for the formation of the Q-Phase are fast-diffusing elements in an Al-matrix, the formation of one of the intermediate phases might occur during casting.

Upon exceeding the solvus-temperature for the Q-phase of 334 °C it occurs, as if the dissolved Cu-atoms inhibit the formation of the stable ß-phase (Mg_2Si). Since Cu-atoms have a high diffusion rate, their diffusion might inhibit precipitation of Mg-Si phases, since Cu could cause the frequency for necessary collisions of Mg and Si atoms to decrease, causing the necessary time for precipitation of Mg-Si-phases to increase.

The dissolution of the ß-phase occurs within a temperature-range of 460 °C – 560 °C. Alloys 6082.30 and 6082.49 presented additional irregularities. Both specimens show rather a plateau for the β-dissolution instead of the two-peak trend. It is interesting to notice that the remaining/other specimens show a larger Peak 3 than Peak 4 which usually show opposite behavior [31, 75].

In their work, Langkruis et. al. showed, that for precipitates of equal type and for a constant heating-rate, peaks for dissolution of phases can be shifted towards lower temperatures if the according phases are smaller in diameter [75]. It is therefore assumed, that Peak 3 represents the dissolution of small-sized secondary-ß phases, whereas Peak 4 represents the dissolution of larger-sized primary ß-phases. In the case of alloys 6082.30 and 6082.49, the amount of secondary β-phases (precipitated during heating-up) might be significantly lower than for the other alloys. Additionally, secondary β is precipitated almost homogenously in the grains as small needles, whereas primary β is mostly present as larger precipitates at grain boundaries at Al-Fe-Si-phases. If dissolution of ß occurs, secondary β might require significantly less time to fully dissolute due to their smaller dimensions than the larger-sized primary β phases. For alloys 6082.29, 6082.47 (peak-temperature 480 °C) and 6082.48 (peak-temperature 515 °C) the higher value for Peak 3 than for Peak 4 may indicate, that quantitatively more secondary ß-phases were dissolved than primary ß-phases. The plateau-like shape for ß-dissolution for alloys 6082.30 and 6082.49 may be produced by similar amounts of primary and secondary ß-phases, which could cause the two peaks to be of similar intensity. If in addition the size of primary and secondary ß-phases is similar, the shift in temperature for Peak 3 and Peak 4 may not be as significant as for the other alloys, causing the two peaks to create a rather plateau-like behavior.

For alloy 6082.48 the shift of ß-dissolution to higher temperatures (515 °C and 550 °C, respectively), could indicate, that dissolved Cu-atoms may also prohibit the dissolution of phases, causing the necessary temperature for dissolution of phases to be shifted towards higher temperatures.

4.12.1 Comparison of DSC-analysis and measurements of el. conductivity

For the characterization of the reference material in chapter 4.1 specimens in the as-cast state of alloys 6082.30 v and 6082.30 h were heated up with a heating rate of 3 K/min to a certain temperature and were then subsequently quenched in water. Immediately after water-quenching the el. conductivity of the specimens was measured and the value for el. conductivity of the as-cast state was subtracted from those values. In Figure 4.71 only the results for 6082.30 h are shown, since for 6082.30 v no DSC-measurements were carried out.

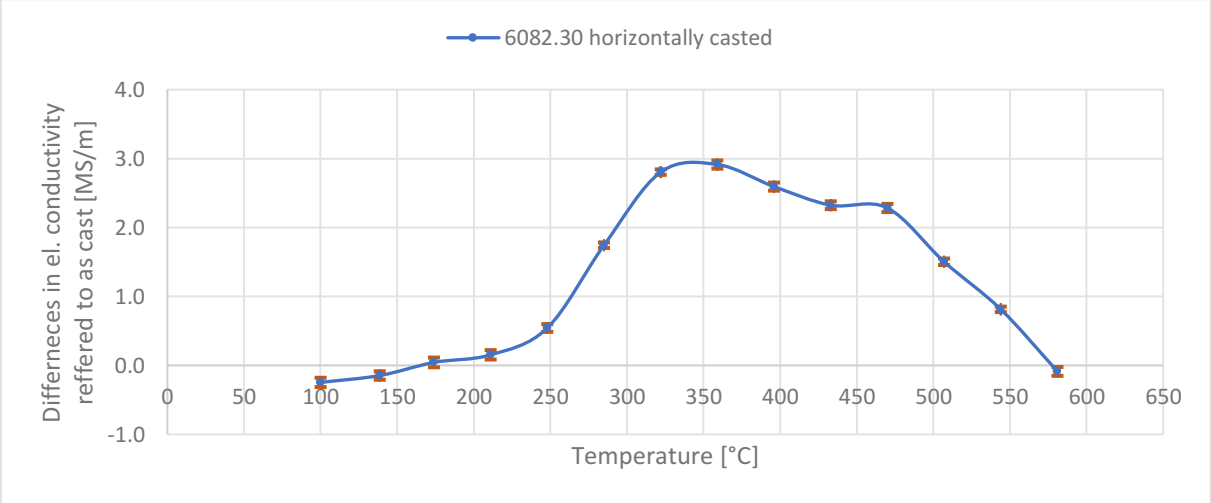

Figure 4.71: Differences in el. conductivity (Δσ, measured with SIGMASCOPE®SMP) post-heat-treatments (after water-quenching) and as-cast state of horizontally casted 6082.30 alloys (red bars for each measurement are standard deviations obtained by Gaussian-error propagation, specimens were heated up to the corresponding temperature and were then subsequently quenched in water and el. conductivity was measured immediately after water-quenching).

Since for the DSC-measurements also as-cast specimens of 6082.30 h were used (heating-up was carried out at a rate of 3 K/min) the results for the two DSC-measurements of this specimen are shown in Figure 4.72. Comparison of the results of Figure 4.71 and Figure 4.72 should be carried out.

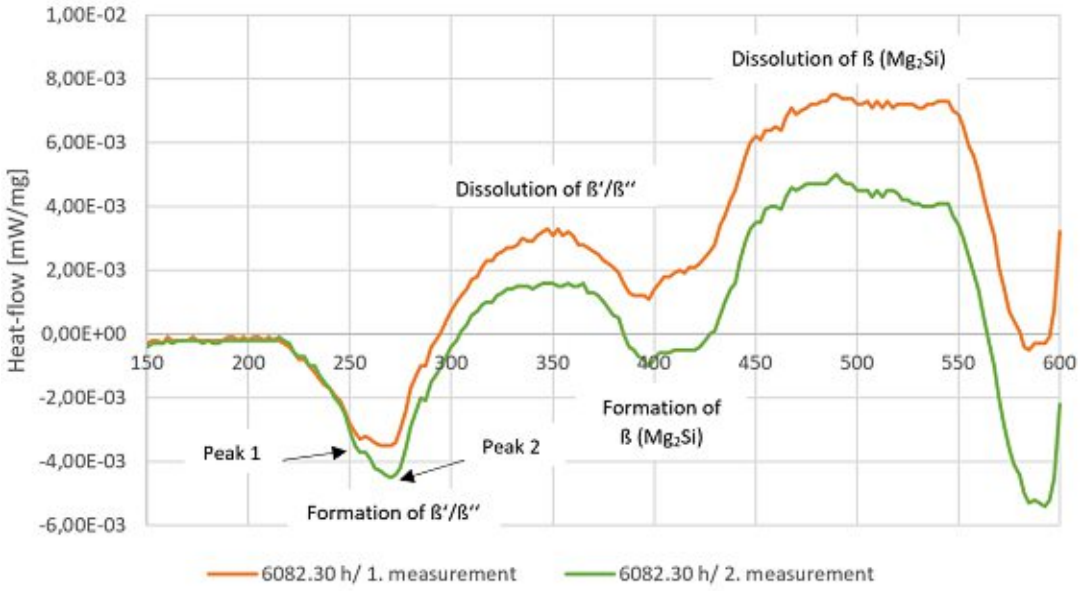

Figure 4.72: DSC-measurements carried out with horizontally casted alloys 6082.30.

Figure 4.71 shows, that the el. conductivity of the specimens starts to increase at a temperature of approximately 175 °C, until reaching a peak at approximately 350 °C. The DSC-measurements in Figure 4.72 show, that for the same temperature-interval the formation of ß'-phases (Peak 1) and ß''-phases (Peak 2) and subsequent dissolution of those phases occurs. Since the el. conductivity increases steadily within this temperature-interval, it is assumed, that Mg-Si atoms from the supersaturated as-cast state steadily precipitate during this temperature-interval. The endothermic-trend of the two lines in Figure 4.72 in the temperature-region 275-350 °C could indicate, that although Mg-Si atoms are further precipitated during this interval (indicated by the increasing trend of el. conductivity) that endothermic phase-transformations of the formed ß' and ß'' occur, which outweigh the exothermic precipitations of Mg-Si atoms.

The temperature interval of 350-425 °C for the el. conductivity shows a decreasing trend. The trend-line of the DSC-measurement shows an exothermic event for the same-temperature region. The formation of the thermodynamically stable Mg_2Si phase which is expected during this temperature-region, could indicate, that during this formation Mg and Si atoms dissolute to a certain degree, causing the value for el. conductivity to decrease for this temperature-interval.

From 450–575 °C the el. conductivity decreases again and reaches the same value as for the as-cast state. During this temperature-interval, the DSC-measurement shows an endothermic trend. It is therefore assumed, that during this temperature-region the dissolution of the Mg_2Si phase occurs, which causes the el. conductivity to decrease for this temperature-region.

For the el. conductivity measurements which were carried out for alloys 6082.29 to 6082.49 it was for heat-treatment 580_0_wq in some cases assumed, that full dissolution of Mg-Si phases did not occur for this heat-treatment. Although DSC measurements of all specimens indicate dissolution of Mg-Si phases, it has to be mentioned, that the chemistry of the specimens which were used for the different heat-treatments could have been slightly different for each specimen (since the specimens represent only a small fraction of the casted bolt). Therefore, the necessary time for dissolution of primary Mg-Si phases might have been slightly different for the specimens, causing the values for el. conductivity the be different than expected.

In addition, alloy 6082.48 showed a different behavior for all DSC-runs. Figure 4.73 shows the comparison of DSC-runs for alloys 6082.30 and 6082.48. It is clearly evident, that alloy 6082.48 shows no clear exothermic-peak for Mg_2Si formation but rather a plateau-like behavior. The values in Figure 4.67 already indicated, that the el. conductivity for each applied heat-treatment is decreased upon Cu-addition. The highest decrease in el. conductivity was observed for 580_0_f and 580_4_f. For those two heat-treatments it was assumed, that Cu atoms inhibit the precipitation of Mg-Si phases during cooling-down. The solvus-temperature for the Cu-containing Q-phase was calculated using ThermoCalc, which gave a solvus-temperature for the Q-phase of 334 °C. It was therefore assumed, that during-cooling down for 580_0_f and 580_4_f all Cu-atoms are completely in dissolved state. During cooling-down, it seems, as if fast-diffusing Cu-atoms inhibit the precipitation of Mg-Si phases. It was assumed, that the Cu atoms might collide frequently with Mg-Si atoms during diffusion, decreasing the number of Mg-Si collisions, which are necessary for Mg-Si phases to form.

The missing of an exothermic-peak for Mg_2Si formation for alloy 6082.48 and rather plateau-like trend for the DSC-line at this temperature-region indicates, that formation of Mg_2Si phases during-heating-up could also be inhibited by the assumed effects mentioned in the previous section. In addition, the peaks for Mg_2Si dissolution are shifted to higher temperatures, which could also indicate, that the

dissolution of phases is inhibited upon Cu-addition and that higher temperatures and longer time-periods are required in order to dissolve phases once Cu is present in solid-solution of an alloy.

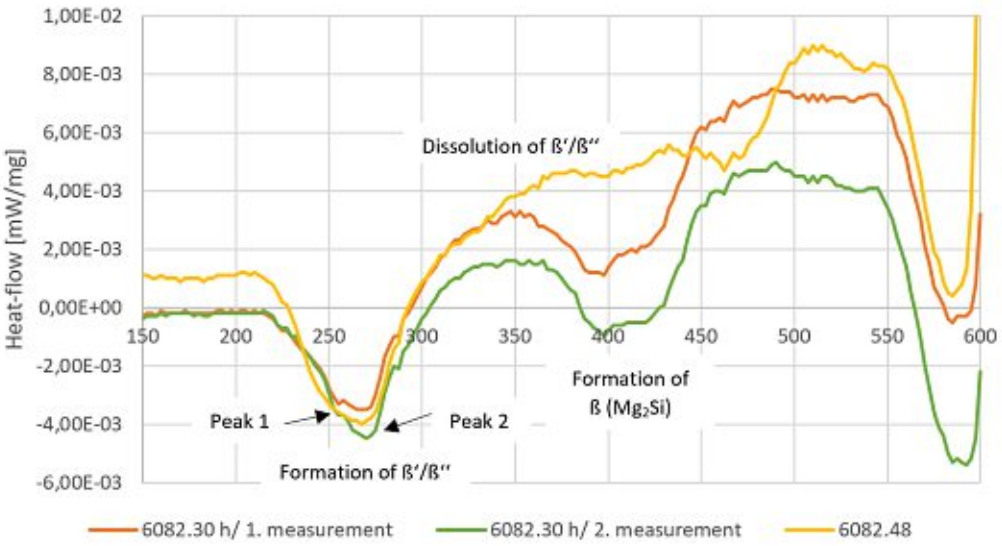

Figure 4.73: DSC-measurements carried out for the according alloys. Specimens were in the as-cast state at the beginning of the DSC-run and heating-rate applied was 3 K/min.

4.13 Size-distribution of dispersoids

SEM-observations which were carried out show, that the distribution of phases which indicate possible formation of dispersoids is not homogenous within the matrix. Therefore, no determination of the size-distribution of the dispersoids was carried out. In order to obtain a representative size distribution for the specimens, lab-scale extrusion of the homogenized specimens should be carried out. Extrusion of the specimens would lead to a more homogenous distribution of dispersoids within the matrix. Image analysis of SEM micrographs of those extruded specimens could give a more representative determination of the size distribution of the particles and would give a more detailed estimation on the dispersoid distribution caused by the different homogenization schemes.

Since SEM of most of the specimens of 530_4_wq showed no dispersoids, higher resolution techniques such as TEM-analysis would be necessary for those specimens.

Metallographic observation of etched specimens (using H_2SO_4) post heat-treatments 530_4_wq and 580_4_wq indicated the formation of dispersoids for alloys except 6082.29. It was already mentioned that etching causes formed dispersoids to appear larger in size, since during etching they act as cathode, while the surrounding Al-matrix acts as anode and is dissolved during etching [73]. Images obtained by metallographic observation of those etched specimens therefore only allow to estimate whether dispersoid formation occurred or not, but no representative quantification of dispersoids can be carried out.

Comparison of metallographic images of the etched specimens of different alloys was not carried out. It appeared, that if the same specimen is etched multiple times, that distribution of formed dispersoids appeared slightly different after each etching process, so no representative comparison between the alloys could be made with images from metallographic observation of etched specimens.

4.14 Mg-Si-precipitation

In chapter 2.1.2.1, the main aspects and effects of Mg-Si-precipitation have been mentioned. Extrusion processes which enable high extrusion speeds require all Mg-Si-phases to be dissolved in solid solution prior to extrusion. The right homogenization scheme in order to obtain such a material behavior requires temperatures which are high enough to reach the solvus temperature of Mg_2Si in order to dissolve primary Mg_2Si (which is mostly present as large precipitates at grain boundaries in the as-cast state). Furthermore, cooling conditions have to be chosen high enough to avoid unnecessarily precipitation of Mg-Si in form of large-sized long-needles. Large-sized precipitates/needles could require long preheat-periods prior extrusion in order to obtain a full solid solution of Mg-Si, which would again decrease the productivity. Since Österreicher et. al. have suggested that existing dispersoids might act as nucleation sites for Mg-Si during cooling, a high number density of dispersoids leads to finer Mg-Si precipitation and therefore shorter heating-up periods are required to dissolve Mg-Si particles before extrusion [31].

ThermoCalc phase-composition of all alloys for the relevant temperature intervals were carried out. The most important aspect of the calculations of those heat-treatments was the solvus-temperature of the Mg_2Si phase. The solvus temperature obtained by ThermoCalc calculations for this phase was 525 °C for all alloys. Although the temperature applied during heat-treatment 530_4_wq is slightly higher than the solvus temperature, the results obtained by measurement of el. conductivity indicated that not all Mg-Si phases are dissolved for this heat-treatment. The duration of four hours for this heat-treatment may be too short as to allow for full dissolution of Mg-Si phases.

Figure 4.74 shows the different patterns of Mg-Si precipitates for 580_0_f and 580_4_f of alloy 6082.29. The comparison shows that 580_4_f causes Mg-Si to precipitate as fine plates or needles within the grains, whereas 580_0_f produces a significant amount of longer Mg-Si plates or needles. The same result was achieved for all alloys. It is therefore assumed, that for 580_4_f the dispersoid-forming elements (Fe, Cr, Mn) cause precipitation of according dispersoids, which then act as nucleation-site for Mg-Si phases during cooling-down. To the best of our knowledge, only Reiso reported the formation of Al-Fe-Si dispersoids for Fe-containing Al-Mg-Si alloys, and their role as nucleation sites for Mg-Si precipitation [9]. Etched metallographic specimens post heat-treatment of 530_4_wq and 580_4_wq indicated the formation of a high number of dispersoids for alloys 6082.30 to 6082.49, and indicate the formation of Fe-dispersoids for alloy 6082.30, as mentioned by Reiso [9]. The change in Mg-Si precipitation (from larger needles/plates to small needles/plates) for longer heat-treatments but same temperature is therefore attributed to the formation of dispersoids, which act as nucleation sites for Mg-Si precipitation. The high number-density of dispersoids could cause Mg-Si phases to nucleate heterogeneously at those dispersoids, causing the formation of a high number of small-sized Mg-Si needles/plates. Although no formation of Fe-dispersoids of etched metallographic specimens post heat-treatment of 530_4_wq and 580_4_wq of alloy 6082.29 could be detected, it is assumed that their size is too small to be detected via metallographic or SEM-observation. Since this alloy showed the same difference in Mg-Si precipitation for 580_0_f and 580_4_f mentioned for the other alloys, it is assumed, that the lower Fe content of 0.06 % (compared to 0.18 % for 6082.30) requires longer heating-periods at high-temperatures in order to create Fe-dispersoids, which then may be visible by metallographic and SEM-observation. In addition, TEM-analysis might give an option to detect assumed small-sized Fe-dispersoids.

The observations made in this thesis agree with the findings of Österreicher et. al. that dispersoids might act as nucleation sites for Mg-Si precipitation. Further, it has to be pointed out, that the

specimens which contained Cr and Mn already for the rather short heat-treatment 580_0_f showed a lower amount of long Mg-Si needles. This observation further underlines the role of dispersoids for Mg-Si precipitation. Even the short period at which those specimens were kept at higher temperatures, could have allowed for nucleation and subsequent growth of small dispersoids, which apparently had an effect on Mg-Si phase formation during cooling-down.

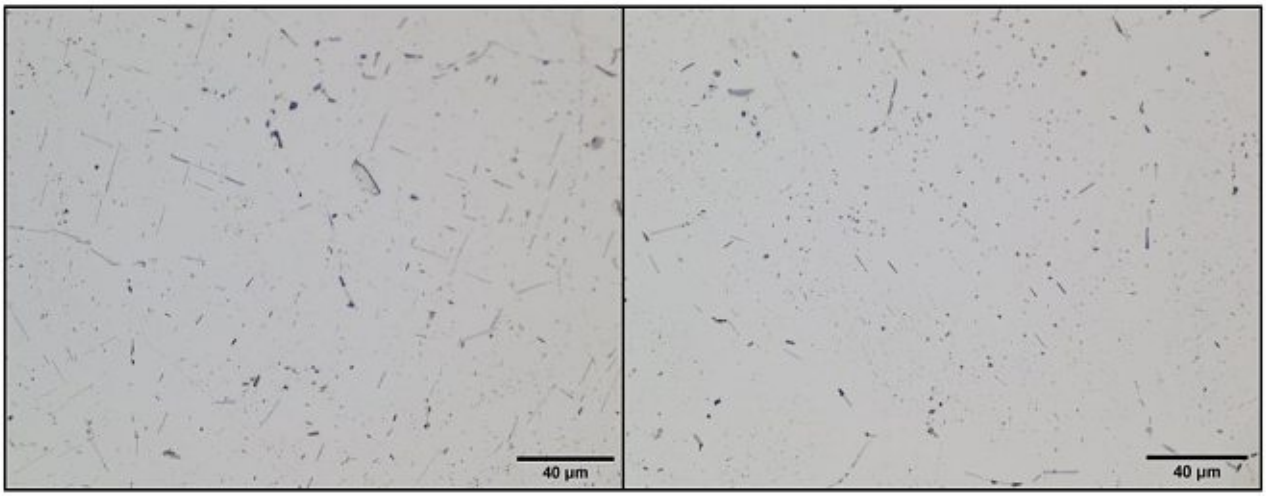

Figure 4.74: Difference in Mg-Si precipitation pattern for 580_0_f (left) and 580_4_f (right) for alloy 6082.29 are visible, the left pictures indicates formation of large-sized Mg-Si needles/plates, whereas the right picture indicates formation of small-sized Mg-Si needles/plates.

4.15 High temperature compression tests

In order to investigate the mechanical properties at higher temperatures, compression tests in a deformation dilatometer of homogenized specimens were carried out. Schiffl. et. al. reported that data obtained by such measurements deliver useful insights for the development of industrial extrusion processes [76].

Out of the five heat-treatments, specimens which underwent heat-treatment 580_4_f were chosen for the compression tests, since this heat-treatment is closely related to the heat-treatments applied for industrial homogenization schemes.

In order to ensure representativeness, three measurements were carried out for each of the most relevant alloys (6082.47, 6082.48 & 6082.49) and for each deformation-temperature (450 °C, 480 °C and 510 °C). The applied strain-rate for each measurement was $\dot{\varphi} = 1.0\ s^{-1}$. Of the three measurements for each temperature the maximum flow-stress was calculated. Of the obtained maximum flow-stress values the mean-value and the standard-deviations of those mean-values were calculated. The mean maximum flow-stress values in dependence of temperature are shown in Figure 4.75.

Figure 4.75 shows, that all alloys have a higher maximum flow-stress for test-temperature 480 °C than for 450 °C. It is expected, that for higher test-temperatures softening of a material occurs. Softening of a material can be explained by annihilation of dislocations and rearrangement of dislocations [77]. Annihilation is caused by reaction of two dislocations, which have the same magnitude but opposite directions of the Burgers-vector [11]. Rearrangement of dislocations can be described by two processes: movement of dislocations within slip-planes (conservative-movement) or climbing of dislocations (non-conservative movement) [33]. The climbing of dislocations can be described by the diffusion of vacancies to the pressure-side of the tension-field of the dislocation. When the vacancy replaces the last atom of the half plane (which ends in the dislocation), the half plane is effectively shortened by one lattice-constant [33]. Since this movement occurs perpendicular to the slip-plane, it is called non-conservative movement. Conservative and non-conservative movement of dislocations can cause additional annihilation of dislocations, but mostly configurations with a lower energy content are formed. Those configurations usually consist of parallel arrangements of dislocations or dislocation-networks, which form low-angle grain-boundaries [33]. The formation of those structures and annihilation of dislocations causes the strength of the material to decrease.

Figure 4.75 shows, that the flow-stress increases from test-temperature 450 °C to temperature 480°C. The expected decrease may not have occurred, since it could be that within this temperature-range the formation of dislocations due to deformation is higher than the annihilation and climbing of dislocations. For test-temperature 510 °C a high decrease of the maximum flow-stress can be seen. It is therefore assumed, that within the temperature range of 480 °C – 510 °C, at a certain temperature the annihilation and climbing of dislocations outweigh the formation of new dislocations and that the strength of the material decreases.

It was further expected, that alloy 6082.48 would have the highest flow-stress values for each-temperature, since it is known that upon Cu addition significant strength-increases are achieved for Al-alloys [2]. However, alloy 6082.49 shows a higher value for maximum flow-stress for test-temperature 480 °C than alloy 6082.48. It is assumed, that Mn-dispersoids in alloy 6082.49 have a higher strengthening-effect than Cu and Cr-dispersoids in alloy 6082.48 for this certain temperature.

Particle-hardening of an alloy can be described by two mechanisms: dislocations can only move within the lattice of the matrix and have to move around existing particles or dislocations are able to cut through existing particles [33]. For the hard and incoherent dispersoids it is expected, that dislocations can only move around existing dispersoids. For alloy 6082.49 and test-temperature 480 °C, it appears as if Mn-dispersoids create a "barrier" for dislocation-movement, which inhibits dislocation movement stronger than Cr-dispersoids and Cu-containing hardening-phases together. In addition, in chapter 4.9 it was mentioned, that the Cu-content in alloy 6082.48 may cause less Mg-Si precipitation during cooling-down for 580_4_f compared to alloy 6082.47. If the amount of formed Mg-Si precipitates is less for 6082.48 compared to 6082.49, an additional barrier for dislocation movement would be available for 6082.49, which in addition could explain the high flow-stress for 6082.49 for 480 °C. For the higher test-temperature of 510 °C the mentioned dislocation-barriers for 6082.49 may be easier for dislocations to bypass than barriers existent in 6082.48, which would explain the lower flow-stress for 6082.49 than for 6082.48 at this-temperature.

Since metallography and SEM-observations showed, that what was expected to be formed Mn-dispersoids alloy 6082.49 indicated larger dimensions of formed dispersoids compared to alloy 6082.47, it is assumed that Mn-dispersoids impose a stronger barrier for dislocation-movement than Cr-dispersoids. This behavior could explain, that for all test-temperatures alloy 6082.49 shows a significantly higher flow-stress compared to alloy 6082.47. It is therefore assumed that a certain Mn-content increases the strength of the material more than the same amount of Cr.

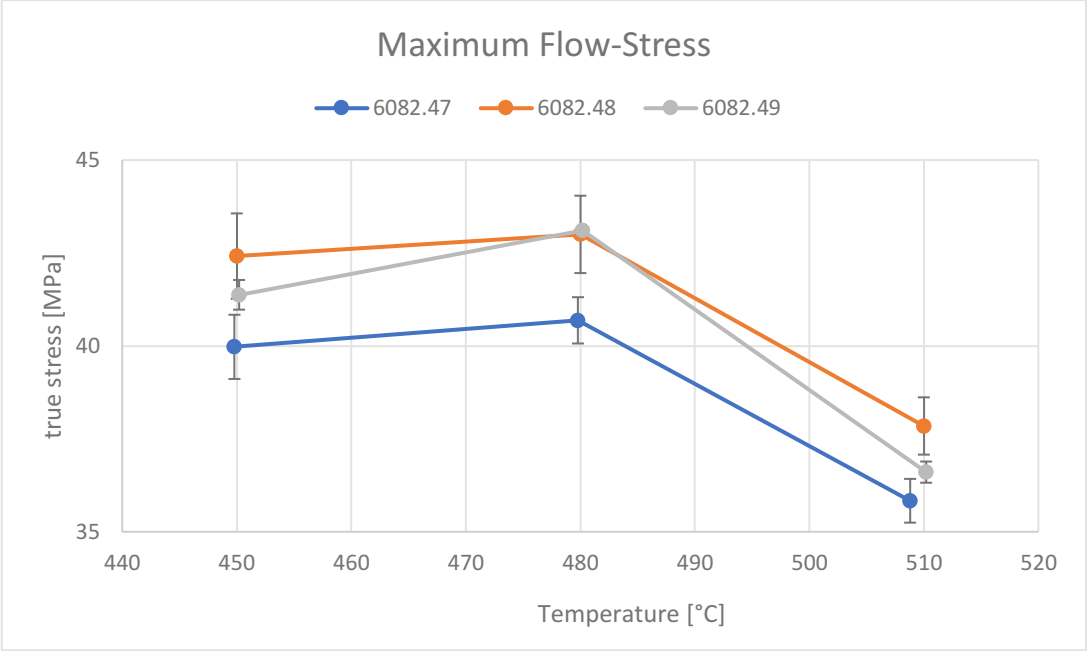

Figure 4.75: Mean maximum flow-stress values for each test-temperature are shown (black-barrs indicate standard-deviation for each value, for each temperature and alloy three compression-tests were carried out. The standard-deviation for alloy 6082.49 and test-temperature 480 °C is too small to be seen).

Figure 4.76 shows one of the obtained flow-stress curves (since all measurements showed similar trends of the curves, only one is shown for discussion). For ductile materials like Al the compressive stress-strain curves are similar for those obtained by testile testing [78]. Figure 4.76 shows that this behavior was obtained for the compression-tests. It is expected, that once the flow-curve reaches the peak flow-stress, the flow-stress remains at this value and a plateau-like trend of the flow-curve is obtained. However, Figure 4.76 shows, that after reaching a peak flow-stress, the curves shift to lower flow-stress values (true strain 0.3 – 0.7). This could be explained by softening of the material, which occurs due to annihilation and climbing of dislocations, causing a decrease in strength of the material. The slight increasing trend after this decline could be explained due to hardening of the material which could occur because of dislocation-formation leveling out the annihilation and climbing of dislocations.

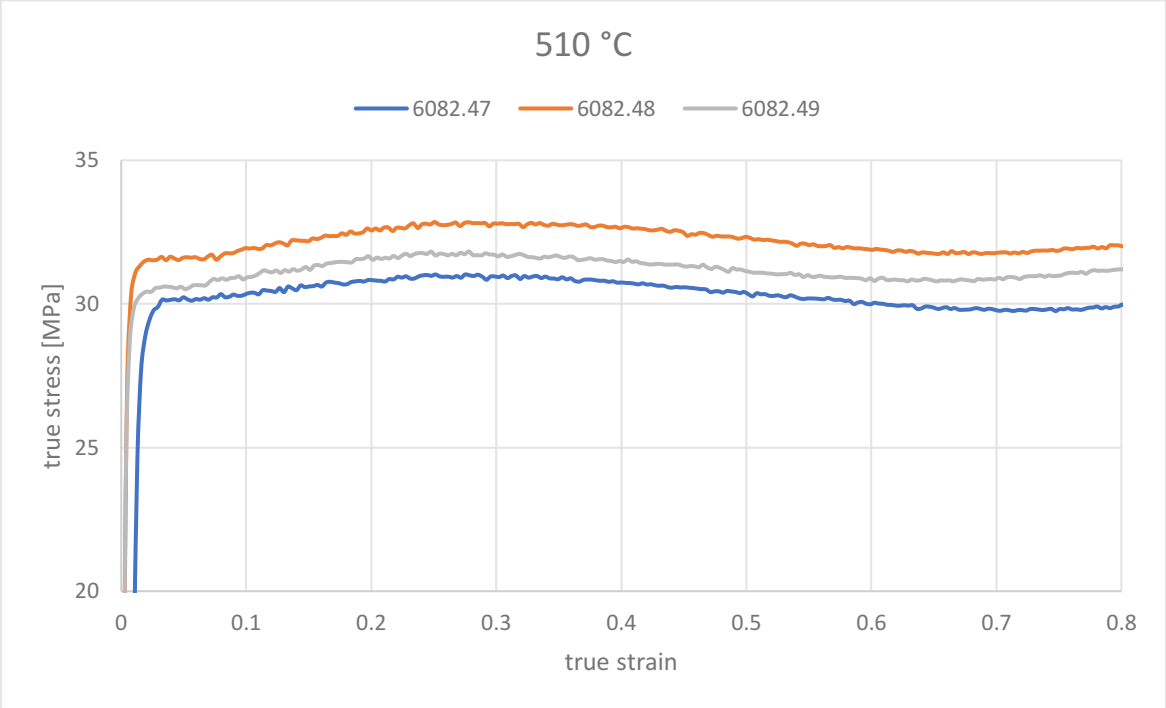

Figure 4.76: Flow-Stress curve for test-temperature 510 °C.

5 Summary and Outlook

This thesis focused on the homogenization of different 6082 Al alloys. For the different homogenization schemes, the heating-up rates, holding temperatures and durations were chosen according to industrially relevant parameters.

Since alloys 6082.47 to 6082.49 contain dispersoid forming elements (Cr or Mn), the formation of dispersoids and their distribution was of major consideration. It is evident that for 580_4_wq of the homogenization schemes for all alloys for which dispersoid-formation was expected, a high number of what appears to be finely dispersed dispersoids was obtained. In contrast, the SEM micrographs of specimens treated with homogenization scheme 530_4_wq showed no visible dispersoid formation in all alloys except 6082.49. Nevertheless, the etched metallographic specimens of 530_4_wq for alloys 6082.47 and 6082.48 showed a significant amount of etching pits, potentially due to dispersoids which were obtained for this lower hold-temperature. It has to be pointed out that during the etch process the dispersoid-phases act a cathode, whereas the surrounding Al-matrix acts as anode an is dissolved significantly during this process. Therefore etching-pits are formed around dispersoids, which are significantly larger than the dispersoids. visible through light-microscope observation. However, this does not give reliable insight into the real size distribution of the formed dispersoids.

Nevertheless, this simple etch method points out that dispersoid formation and growth has likely also occurred for the lower hold temperature of 530 °C. Since the Zener-drag is highly dependent on particle size (Equation (4)), smaller particles lead to a higher Zener-pressure.

It is therefore of high importance to determine if the number density of formed dispersoids is the same for 530_4_wq as it is for 580_4_wq. It could therefore mean that 530_4_wq leads to the same number density of dispersoids and therefore the lower temperature required for this scheme enables shorter homogenization procedures which in addition require less energy consumption.

Since the formula for the Zener-pinning assumes spherical particles which are homogenously spread within the matrix, the formula gives only an estimation. The precise material behavior during extrusion and influence of dispersoids hast to be determined through experimental extrusion trials.

5.1 El. conductivity measurements, metallography and SEM-Observation

For all heat-treatments which have been carried out for the alloys, the expected state of the alloying elements post heat-treatment was assumed (alloying elements in solid-solution or in precipitated form). The same assumptions were made for the as-cast state of the alloys.

For the as-cast state as well as for the post heat-treatment state el. conductivity measurements were carried out. Those measured values were compared to the calculated values for each heat-treatment. This simple method should give insight, how close the real state of the alloying elements of the specimen (which is given by measuring the el. conductivity) is, compared to the assumed state of the alloying elements. It was revealed, that for heat-treatments 580_0_f and 580_4_f for most of the alloys no complete precipitation of Mg-Si phases occurred, but that rather at least half of the available Mg and Si atoms remain in solid solution. Even though for alloys 6082.47, 6082.48 and 6082.49 heat-treatment 580_0_f shows minor differences for $\Delta\sigma$ between calculated and measured values, it is assumed, that Mg-Si precipitation still only occurs partially, but that the alloying elements Cr and Mn precipitate in form of dispersoids, which causes the effect of partial Mg-Si precipitation on el. conductivity to be leveled out. In comparison, the other heat-treatments (580_0_wq, 530_4_wq and 580_4_wq) showed less significant differences between the measured and calculated values.

The comparison of calculated and measured values for the as-cast state also revealed, that the alloying elements remain rather in super-saturated solid solution (with exception of Fe, which was expected to precipitate in form of Al-Fe-Si phases during casting) than in precipitated form during casting.

This simple comparison between calculated and measured values therefore allows a rough estimation, how much the assumed state of the alloying elements differs from their real state in the specimen.

The measured values for el. conductivity post heat-treatment were also referred to the measured values for the as-cast state. Those comparisons of the different alloys treated with the five different heat-treatments showed in general the expected changes in conductivity. The expected precipitation of phases could be detected by this method. In order to further clarify whether the expected phases precipitated, metallographic methods were applied to the according specimens. For alloys and heat-treatments for which precipitation of dispersoids was expected, the specimens were etched with H_2SO_4 in order to make dispersoids visible. For alloys 6082.30, 6082.47, 6082.48 and 6082.49 etched specimens of specimens post heat-treatment 530_4_wq and 580_4_wq indicated formation of dispersoids containing according alloying-elements. The number density and size of apparent dispersoids was higher for 580_4_wq than for 530_4_wq.

For alloy 6082.48 it was assumed, that once the solvus-temperature of the Q-phase was exceeded during heat-treatments, that the dissolved Cu-atoms inhibit precipitation of Mg-Si phases. It is assumed, that the high diffusion-rate for Cu causes Cu-atoms to collide frequently with Mg and Si atoms, reducing their frequency of collisions with each other. This assumed process could inhibit Mg-Si precipitation.

Etched specimens of 6082.29 post heat-treatment 530_4_wq and 580_4_wq showed no visible formation of Fe-dispersoids. Formation of Fe-dispersoids may have occurred for those heat-treatments, however, since the Fe content of alloy 6082.29 is rather low (0.06 mass-%), the size of formed Fe-dispersoids might be too small to be detected by light-microscope observation of etched-specimens.

The changes in morphology for the Al-Fe-Si phases have been noticed for all alloys. Metallographic observation of the as-cast state showed long grey structures at the grain-boundaries, which are most likely ß-Al-Fe-Si phases. For all alloys and for all heat-treatments applied, the specimens showed post heat-treatment, that the grey Al-Fe-Si phases split up into shorter pieces and that the edges changed their morphology towards round-shaped forms.

SEM-observation of unetched specimens post heat-treatment of 530_4_wq for alloys 6082.30 (Fe+), 6082.47 (Cr+) and 6082.48 (Cr+, Cu+) showed no clear indication for dispersoid-formation. SEM-observation for the same alloys (unetched) post heat-treatment 580_4_wq showed visible formation of what is assumed to be dispersoids.

Alloy 6082.49 showed post heat-treatments 530_4_wq and 580_4_wq significant formation of dispersoid-phases.

5.2 DSC-measurements

For all alloys two DSC-measurements were carried out. For the temperature-interval of 225 °C – 260 °C the formation of ß'' and ß' phases was detected. Alloy 6082.29 clearly showed two separate peaks for ß'' and ß' formation. 6082.30 also showed a two-peak trend, however the separation of those two-peaks was not as clearly as for alloy 6082.30. Alloys 6082.47, 6082.48 and 6082-49 showed only a slight peak for ß'' formation. Alloys 6082.29, 6082.47 and 6082.49 showed almost the same peak-temperature for ß'-formation, whereas alloys 6082.30 and 6082.48 showed a shift towards higher temperatures. For alloy 6082.30 the formation of Fe-dispersoids in the same temperature-region is assumed, which causes a "competition" for necessary atoms for Fe-dispersoid and ß'' and ß' formation. This "competition" event could cause the observed shift for ß'' and ß' formation towards higher temperatures. For 6082.29 the lower Fe-content compared to 6082.30 might have only caused minor Fe-dispersoid formation to occur, which shows no effect on ß''/ß'-formation. For 6082.47 and 6082.49 significant formation of dispersoids is not expected, since diffusion-rates of the necessary atoms (Cr and Mn, respectively) are too low for this temperature-region.

For 6082.48 the formation of the Q-phase is assumed to occur in the mentioned temperature-range. The mentioned "competition " for alloy 6082.30 is also assumed to be the reason for the shift of ß'' and ß' formation towards higher temperatures for alloy 6082.48, with the difference, that necessary atoms "compete" for either Q-phase formation or ß''/ß' formation.

Formation of the ß-phase occurred within the temperature interval temperature-range of 380 °C – 430 °C. For alloy 6082.30 it was observed, that ß-formation occurs at lower-temperatures. It was assumed, that Fe-dispersoids which might have formed during-heating up act as nucleation-sites for ß-formation, causing the necessary temperature for precipitation to be lower. Alloy 6082.48 showed no peak for ß-formation but rather a plateau in the mentioned temperature-range. It is assumed, that dissolved Cu-atoms inhibit formation of ß-phases. The high diffusion rate of Cu might cause Cu-atoms to impair diffusion of Mg and Si atoms (by effectively reducing the number of necessary Mg-Si collisions in order to form precipitates). The mentioned effects could cause the plateau-like trend for alloy 6082.48.

The dissolution of the ß-phase occurs within a temperature-range of 460 °C – 560 °C. Alloys 6082.29, 6082.47 and 6082.48 showed a two-peak trend for ß-dissolution. Langkruis et. al showed in their work,

that for phases of same type and for the same heating-rate, the dissolution of smaller-sized phases can be shifted towards lower-temperatures [75]. It is therefore assumed, that the peak for lower temperatures can be attributed to the dissolution of smaller-sized secondary ß-phases (which are formed during heating-up from supersaturated solid-solution) whereas the peak at higher-temperatures is attributed to the dissolution of larger-sized primary ß-phases (which are existent in the as-cast state). Alloy 6082.48 shows a shift for both peaks towards higher temperatures. It is assumed, that Cu-atoms in dissolved-state also inhibit dissolution of Mg-Si phases (for the same reasons which were already mentioned in this chapter).

Alloys 6082.30 and 6082.49 showed rather a plateau-like behavior for ß-dissolution. It is assumed, that for alloy 6082.30 primary and secondary ß-phases may be of similar dimension (causing the shift in temperature for both peaks to be smaller compared to the other alloys) and of similar quantity. The same size and quantity of both phases may be caused by the formation of Fe-dispersoids during heating-up, which act as nucleation sites for secondary ß-phases. This could cause secondary ß-phases to reach larger dimensions compared to alloys 6082.29, 6082.47 and 6082.48 (for which dispersoid formation is not assumed due to low-diffusion rates of the dispersoid-forming elements or content of dispersoid-forming elements might be too low as to cause significant dispersoid-formation). In addition, for alloy 6082.49 minor formation of Mn-containing dispersoids might occur in the same temperature range, causing the heat-flow of ß-dissolution to be partially outweighed, which could result in a rather plateau-like in the mentioned temperature-range.

5.3 High temperature compression tests

The flow curves showed that the Cu-containing alloy 6082.48 showed the highest flow stresses except for test-temperature 480 °C, for which alloy 6082.49 showed the highest flow-stress. It is assumed, that the Mn-dispersoids cause a higher increase in strength than Cu and Cr-dispersoids in alloy 6082.48 for test-temperature 480 °C. For higher test-temperatures it may be easier for dislocations to bypass Mn-dispersoids which could explain the lower flow-stress for test-temperature 510 °C for alloy 6082.49 compared to alloy 6082.48. The Mn-containing alloy 6082.49 showed a higher flow stress compared to the Cr-containing alloy 6082.47 for every test-temperature. This could mean that the dispersoids formed for Mn-containing alloys cause a higher increase in flow stress than Cr-containing dispersoids and that their Zener-drag is higher for the same homogenization scheme. However, the higher flow stress for 580_4_f of alloy 6082.49 obtained in the dilatometer measurement would mean a disadvantage upon extrusion since higher pressures would have to be applied. The expected decrease of the maximum flow stress for higher test temperatures which was reported by Österreicher et. al. (for an AA6082 specimen which contained 0.44 % Mn) was also observed for the dilatometer tests (Figure 5.1)[31]. In their work, they also discovered that specimens which underwent higher homogenization temperatures showed a lower flow-stress. This lower flow-stress indicates that dispersoids underwent coarsening because of Ostwald-ripening for higher temperatures and therefore decreasing the high-temperature strength of the material and probably the exhibited Zener-drag.

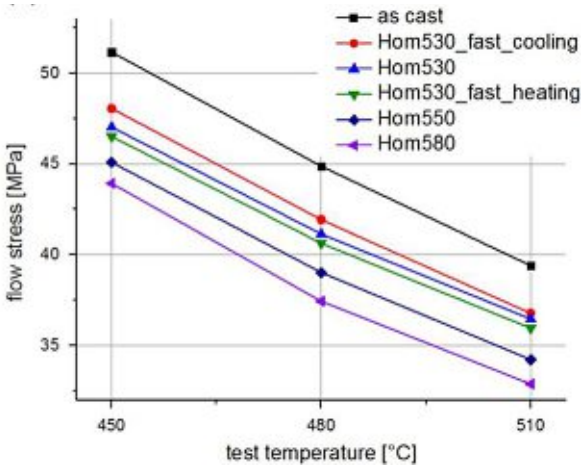

Figure 5.1: maximum flow stress of AA6082 specimens for different homogenization schemes [31].

5.4 Error-Sources

For the homogenization-processes (and temperature- and el. conductivity measurements during the applied heat-treatments), an estimation of the most significant source for errors during the trials should be made.

For all trials and specimens it is assumed, that the as-cast state of the alloy could cause the highest negative impact on representativeness of the trials. For this thesis only a part of approximately 30 cm of the casted bolts was cut out and used for trials, whereas the full length of the bolts was 5m. It is known from LKR's casting-experience, that the alloying elements in the melt can cause significant segregation during casting (the different alloying elements have different mobilities in the melt and their different behavior for turbulent-flow and laminar-flow during casting could explain these observations). Since only a minor part of the whole bolt was used during this thesis, the results obtained during this thesis may show low standard-deviations for the el. conductivity of the measurements, however, it has to be kept in mind that a different part of the bolt could have delivered significantly different results.

The temperature-deviation of the used thermoelements is +/- 2 K. For the el. conductivity measurements standard-deviations of 0.06 – 0.1 MS/m were obtained. The standard deviation for chemical – composition measurements showed a value of +/- 0.01 wt-%. Although for the segregation within the casted bolts no measured values are available it is assumed, that the segregation of the bolts could represent the highest source for errors. Differences in chemical composition along the length of the as-cast bolt would cause the results obtained within this thesis to differ for each part of the bolt (since alloying elements are not distributed homogenously in the as-cast state). Since no measurements of the composition-gradient along the bolt-length is available, for further trials more segments of the bolts should be heat-treated and the results should be compared. At this stage, it is assumed that errors in results (different amount of precipitated or precipitated phases) caused by segregation in the as-cast state outweigh the uncertainty within temperature- and el. conductivity measurement by far.

5.5 Outlook

This thesis showed that possible dispersoid formation for Cr and Mn containing alloys occurred for industrially relevant homogenization schemes. Specimens which were quenched in water at the end of the homogenization scheme were prevented from the formation of Mg-Si phases, whereas specimens which were furnace cooled showed expected Mg-Si-phase formation. The difference between these two procedures lead to a simple method to detect different amounts Mg-Si precipitates through el. conductivity measurements. In addition, metallographic specimens were prepared to give further insights on the different patterns of phases which were formed for the different schemes. In most cases, the results obtained from metallographic observation of specimens were in good accordance with the observed trends in el. conductivity measurements.

Simple etching methods of metallographic specimens made formed dispersoids detectable through light microscope investigations. Alloy 6082.30 showed a high number of what is expected to be Fe-containing dispersoids (without significant amounts of Mn or Cr) which was so far only reported by Reiso to the best of our knowledge [9]. Their role as nucleation site for Mg-Si precipitation was confirmed by applying 580_0_f and 580_4_f to alloy 6082.30. 580_0_f produced a significant number of large Mg-Si plates/needles whereas this pattern completely changed for 580_4_f, which resulted in short and finely dispersed Mg-Si plates/needles. This indicates, that Fe-dispersoids could act as nucleation site for Mg-Si precipitation.

In contrast to studying the etched specimens using light microscopy, dispersoids couldn't be found in all specimens using SEM. The etched specimens showed the formation of dispersoids for 530_4_wq for all alloys except alloy 6082.29. By SEM, dispersoid formation after 530_4_wq was only observed for alloy 6082.49, possibly due to the limited resolution in backscattered SEM. The resolution limit has been estimated to around 35nm (diameter) for Al-Fe-Si-type dispersoids in Al at 20keV [79]. However, etching water-quenched specimens with sulfuric acid causes dispersoids to act as cathode during the reaction, whereas the surrounding Al-matrix acts as anode and is dissolved during the etching process [73]. This process creates etching pits around dispersoids, which are significantly larger (up to several µm in diameter) than the dispersoids (which have a diameters in the range of 50 nm)[73]. Therefore, the etched specimens should only give an answer if dispersoid formation has occurred and at most give a rough estimation of the spread of dispersoids within a grain. Further research using TEM would be needed to clarify the discrepancies observed between the two methods.

Since the etched specimens of heat-treatment 530_4_wq showed for most of the specimens significant dispersoid-formation, observation of recrystallization during/after extrusion would also give an insight on the Zener-Drag of those specimens. Österreicher et. al. reported the higher number density and smaller size of dispersoids for lower homogenization temperatures, and dilatometer tests of those specimens showed a higher flow stress [31]. This could indicate that the lower homogenization temperature causes dispersoids to nucleate and remain small in dimension, causing a higher Zener-Drag. The disadvantage of this could be, that the high temperature strength of the material is increased and therefore higher breakthrough pressures are necessary. If the homogenization temperature is too low, Mg-Si particles will remain in the specimens and might cause eutectic melting reactions during extrusion. Therefore, a temperature range has to be found in order to at least reach the solvus temperature of Mg-Si precipitates, but to be also low enough as to prevent significant coarsening of dispersoids.

Compression tests for three different temperatures were carried out for alloys 6082.47, 6082.48 and 6082.49 which underwent 580_4_f before the compression tests. Alloy 6082.48 showed the highest flow stress (which was expected due to the higher Cu-content) except for test-temperature 480 °C, for which alloy 6082.49 showed the highest flow-stress. It is assumed, that for test-temperature 480 °C Mn-dispersoids of alloy 6082.49 cause a stronger resistance for dislocation movement than Cr-dispersoids and Cu-containing phases in alloy 6082.48. The Mn-containing alloy 6082.49 showed higher flow stresses for every temperature than the Cr-containing alloy 6082.47. The differences however are rather minor and decrease upon temperature increase.

It is of interest to note that the Cu containing specimen showed slightly lower Mg-Si precipitation for the furnace-cooled specimens. This means that the quench-sensitivity is decreased upon Cu-addition if Mg-Si precipitation is of major concern (Chapter 2.1.2.1). Additionally, if the number and sizes of formed dispersoids are the same as for alloy 6082.47 and cause the same Zener-Drag, the addition of Cu might have the beneficial effect of making it easier to achieve desired surface quality of the extrudate [9]. However, it has to be pointed out that a small number of Mg-Si precipitates or their complete non-existence prior extrusion makes it easier to achieve a desired surface quality – since eutectic melting reactions are inhibited. On the other hand, if the major part of Mg and Si atoms is in solid solution, the strength of the material is increased and higher breakthrough pressure has to be applied. The perfect stage of the material for processing would be, if the specimen contains small amounts of Mg-Si precipitates – which lower the stiffness of the material – which are dissolved during the heat generation of extrusion but cause no eutectic melting during this process.

Further steps for the alloys investigated in this thesis would be lab-scale extrusion trials and subsequently evaluation of recrystallization and the determination of dispersoid size distribution through image analysis. Additionally, the lab-scale extrusion process would give an insight on the mechanical properties and surface quality of the specimens.

Österreicher et. al. used electropolishing with Nital (30% (v/v) of concentrated nitric acid in methanol) to drastically improve the contrast of Mg-Si for SEM investigation [80]. Therefore, specimens prepared with Nital can be used to investigate the structure of the Mg-Si precipitates and by using specimens which underwent different homogenization schemes their precipitation behavior and kinetics of those could be studied.

For all post heat-treatments and the as-cast state assumptions were made of the state of alloying elements (in solid-solution or in precipitated form) and Table 4 was used to calculate the value of el. conductivity of those states. Comparison of those calculated results with the measured results gave an option to make a rough assumption on how much the el. conductivity differs from the expected value.

If the el. conductivity of a specimen in a certain state (post heat-treatment or as-cast state) is measured, computer algorithms could be created, which deliver possible states of the alloying elements which could lead to the obtained measured value. An algorithm of this form would deliver all possible combinations of the alloying elements which could lead to the value obtained by measurement. In this stage, an algorithm would lead to a high number of unreasonable results. However, if such algorithms are combined with possible phase-compositions of the alloys and the diffusion-rates of the alloying elements, the possible results could be narrowed down to a significantly lower number of possible results. Those results would have to be considered applying metallurgical knowledge. Algorithms designed this way could allow to make assumptions of the state of a specimen by applying measurements of el. conductivity.

For the DSC-measurements of this thesis only one heating-rate (3 K/min) was applied. Kissinger plots could be carried out, when several heating rates are applied and the peak-temperatures of phase formations/precipitations are determined for each heat-rate [74, 81]. Kissinger plots allow to determine the activation-energy for a precipitation or dissolution event. Those activation energies could allow to make assumptions about the kinetics of precipitation or dissolution events.

The kinetics for dispersoid-formation could be investigated by water-quenching specimens after different homogenization-periods and carrying out SEM-observation of those specimens. If significant inhibition of grain-coarsening during extrusion is of major concern, then the right size-distribution of dispersoids for a certain alloy has to be determined. SEM-observations of specimens which were water quenched at different heating-periods allow to determine the size-distribution of dispersoids. If dispersoids of those specimens cannot be detected by SEM, TEM investigations might give more insight on the size-distribution of dispersoids. Those observations could give insight when dispersoids start to form within an alloy and when they reach the desired size-distribution for significant inhibition of grain-coarsening during extrusion. Metallographic observations of extruded specimens could then reveal which size-distribution of dispersoids delivers the most satisfying results when grain-coarsening is of major concern and what time-periods for homogenization are necessary to obtain those size-distributions.

6 Acknowledgements

I would like to thank my advisors, ao. Univ. Prof. Christian Edtmaier, Dr.-Ing. Andreas Schiffl and Dr. Johannes Österreich for their kind support and for the constructive and fruitful discussions which were led during this thesis. I also want to thank Hammerer Aluminium Industries for allowing me to carry out my thesis within their facilities and special thanks goes to the scientific staff of HAI Braunau for their support and the friendly work environment.

Finally, I want to thank all my colleagues at the LKR for their great scientific support and the great work environment during my thesis.

7 References

[1] *Totten, E. G., & McKenzie, D. S.*: Handbook of Aluminum (Volume 2): Alloy Production and Materials Manufacturing. Marcel Dekker Inc. (2003).
[2] *Ostermann, F.*: Anwendungstechnologie Aluminium (2007).
[3] https://de.wikipedia.org/wiki/B%C3%A9la_Bar%C3%A9nyi (2020).
[4] *Mattheus H.-W.*: Daimler AG, Würzburger Automobilgipfel (2010).
[5] Der neue SL von Mercedes-Benz. ATZ Extra (2012).
[6] *Ellenrieder G.*: Darstellung, Werte Daimler AG (Vortrag) (2005).
[7] https://www.audi-mediacenter.com/de/leichtbau-246 (2020).
[8] *Rinderer, B.*: The Metallurgy of Homogenisation. Materials Science Forum 693, 264–275 (2011).
[9] *Reiso, O.*: Extrusion of Al-Mg-Si Alloys. INTERNATIONAL CONFERENCE ON ALUMINIUM ALLOYS (Times 12) (2004).
[10] *Müller, K.*: Grundlagen des Strangpressens (2003).
[11] *Hornbogen, E., Eggeler, G., & Werner, E.*: Werkstoffe (2012).
[12] *Hatch, J. E.*: Aluminum Properties and Physical Metallurgy (1984).
[13] *Mantina, M., Wang, Y., Chen, L. Q., Liu, Z. K., & Wolverton, C.*: First principles impurity diffusion coefficients. Acta Materialia, 4102–4108 (2009).
[14] *Du, Y., Chang, Y. A., Huang, B., Gong, W., Jin, Z., Xu, H., & Xie, F. Y.*: Diffusion coefficients of some solutes in fcc and liquid Al: critical evaluation and correlation. Materials Science and Engineering, 140–151 (2003).
[15] *Fujikawa, S. I., Hirano, K. I., & Fukushima, Y.*: Diffusion of silicon in aluminum. Metallurgical Transactions, 1811–1815 (1978).
[16] https://en.wikipedia.org/wiki/Boltzmann%E2%80%93Matano_analysis (2020).
[17] *Couper, M. J., Cooksey, M., & Rinderer, B.*: Aluminium Cast House Technology (Seventh Australasian Conference). Effect of Homogenisation Temperature and Time on Billet Microstructure and Extruded Properties of Alloy 6061 (p. 287) (2001).
[18] *Zhang, J., Fan, Z., Wang, Y. Q., & Zhou, B. L.*: Equilibrium pseudobinary Al–Mg2Si phase diagram. Materials Science and Technology, 494–496 (2001).
[19] *Mondolfo, L. F.*: Aluminum alloys: structure and properties (1976).
[20] *Suzuki, H., Kanno, M. & Itoh G.*: A consideration of the two-step aging process in an Al-Mg-Si alloy. Aluminium, 628–629 (1981).
[21] *Edwards, G. A., Stiller, K., Dunlop, G. L., & Couper, M. J.*: The precipitation sequence in Al–Mg–Si alloys. Acta Materialia, 3893–3904 (1998).
[22] *Murayama, M., & Hono, K.*: Pre-precipitate clusters and precipitation processes in Al–Mg–Si alloys. Acta Materialia, 1537–1548 (1999).
[23] *Marioara, C. D., Andersen, S. J., Zandbergen, H. W., & Holmestad, R.*: The influence of alloy composition on precipitates of the Al-Mg-Si system. Metallurgical and Materials Transactions A, 691–702 (2005).
[24] *Takeda, M., Kurumizawa, T., Sumen, S., Fukui, K., & Endo, T.*: Atomic composition of the metastable β ″phase precipitate in an Al–Mg–Si alloy. Zeitschrift für Metallkunde, 93(6), 523-527. Zeitschrift für Metallkunde, 523–527 (2002).
[25] *Hatch, J. E.*: Aluminium: Properties and Physical Metallurgy (1984).

[26] *Marioara, C. D., Andersen, S. J., Stene, T. N., Hasting, H., Walmsley, J., Van Helvoort, A. T. J., & Holmestad, R.*: The effect of Cu on precipitation in Al–Mg–Si alloys. Philosophical Magazine, 3385–3413 (2007).
[27] *Strobel, K., Sweet, E., Easton, M., Nie, J. F., & Couper, M.*: Dispersoid Phases in 6xxx Series Aluminium Alloys. Materials Science Forum 654-656, 926–929 (2010).
[28] *Lodgaard, L., & Ryum, N.*: Precipitation of dispersoids containing Mn and/or Cr in Al-Mg-Si alloys. Materials Science and Engineering: A 283 (2000) 144-152 (1999).
[29] *Yoo, J. E., Shan, A., Moon, I. G., & Maeng, S. J.*: A study on composition and crystal structure of dispersoids in AlMgSi alloys. Journal of materials science, 2679–2683 (1999).
[30] *Lodgaard, L., & Ryum, N.*: Precipitation of chromium containing dispersoids in Al–Mg–Si alloys. Materials Science and Technology 2000, 599–604.
[31] *Österreicher, J. A., Kumar, M., Schiffl, A., Schwarz, S., & Bourret, G. R.*: Secondary precipitation during homogenization of Al-Mg-Si alloys: Influence on high temperature flow stress. Materials Science and Engineering: A 687, 175–180 (2017).
[32] *Rometsch, P. A., Wang, S. C., Harriss, A., Gregson, P. J., & Starink, M. J.*: The effect of homogenizing on the quench sensitivity of 6082. Material Science Forum, 655–660 (2002).
[33] *Hornbogen, E., & Warlimont H.*: Metalle: Struktur und Eigenschaften der Metalle und Legierungen. Springer Verlag (2006).
[34] *Rosefort, M., Baumgart, R., Matthies, C., & Koch, H.*: Light Metals. Influence of microstructure on the folding behaviour of crash relevant aluminum extrusion parts, 201–205 (2014).
[35] *Schiffl, A., Schober, M., & Kühlein, W.*: Hochfeste Crashlegierungen aus dem Haus Hammerer Aluminium Inudstries: Von der Idee zur Umsetzung. Leichtmetall-Tage (2014).
[36] https://en.wikipedia.org/wiki/Zener_pinning (2020).
[37] *Belov, N. A., Eskin, D. G., & Aksenov, A. A.*: Multicomponent Phase Diagrams: Applications for Commercial Aluminum Alloys. Chapter 2: Alloys of the Al-Mg-Si-Fe System (2005).
[38] *Donas, A. L., Pedersen, K., Lohne, O., Pettersen, T., & Bigot, A*: Particle breakup during extrusion. Aluminium 2004, 640–642.
[39] *Sheppard, T.*: Extrusion of Aluminium Alloys (1999).
[40] *Reiso, O., Overlie, H. G., & Ryum, N.*: Dissolution and melting of secondary Al_2Cu phase particles in an AlCu alloys. Metallurgical and Materials Transactions A, 1689–1695 (1990).
[41] *Reiso, O., Ryum, N., & Strid, J.*: Melting of secondary-phase particles in Al-Mg-Si alloys. Metallurgical and Materials Transactions A, 2629-2641 (1993).
[42] *Reiso, O.*: The effect of compositional and homogenisation treatment on extrudability of AlMgSi alloys. Proceedings of the 3rd Interational Aluminium Extrusion Technology Seminar, Atlanta, GA, Aluminum Association, 31–40 (1984).
[43] *Phillips H.W.L.*: Annoted Equilibrium Diagrams of some Aluminium Alloy Systems (1959).
[44] *Castle, A. F. & Lang, G.*: The Influence of Various Alloying Elements and Heat Treatments on the Hot-Workability of Binary Aluminium Alloys During Extrusion. Aluminium 1977, 535–539.
[45] *Andersen, S. J., Marioara, C. D., Frøseth, A., Vissers, R., & Zandbergen, H. W.*: Crystal structure of the orthorhombic U2-Al4Mg4Si4 precipitate in the Al–Mg–Si alloy system and its relation to the β' and β" phases. Materials Science and Engineering: A 390, 127–138 (2005).
[46] *Altenpohl, D.*: Aluminium und Aluminiumlegierungen (1965).
[47] *Zoller, H., & Ried, A.*: Metallkundliche Grundlagen der leicht preßbaren AlMgSi-Legierungen. Aluminium, 626–629 (1965).
[48] *Zoller, H., & Ried, A.*: Metallkundliche Gesichtspunkte bei der Entwicklung wenig abschreckempfindlicher AlMgSi-Legierungen. Zeitschrift für Metallkunde, 351–385 (1971).
[49] *Laue, K. & Stenger, H.*: Extrusion. American Society for Metals, 34–38 (1981).

[50] *Reiso, O.*: Proc. 4th Int. Aluminum Extrusion Technology Seminar, Chigao, IL, Aluminum Association, 287–295 (1988).
[51] *Reiso, O., Tundal, O. & Andersen, S.*: Proc. 6th Int. Alumnium Extrusion Technology Seminar, Chicago, IL, Aluminum Association, 141–147 (1996).
[52] *Milkereit, B., Wanderka, N., Schick, C., & Kessler, O.*: Continuous cooling precipitation diagrams of Al–Mg–Si alloys. Materials Science and Engineering, 87–96 (2012).
[53] *Pogatscher, S., Antrekowitsch, H., Leitner, H., Pöschmann, D., Zhang, Z. L., & Uggowitzer, P. J.*: Influence of interrupted quenching on artificial aging of Al–Mg–Si alloys. Acta Materialia 60, 4496–4505 (2012).
[54] *Gao, R. Q., Stiller, K., Hansen, V., Oskarsson, A., & Danoix, F.*: Influence of aging conditions on the microstructure and tensile strength of aluminium alloy 6063. Materials Science Forum, 1211–1216 (2002).
[55] *Wanderka, N., Lazarev, N., Chang, C. S. T., & Banhart, J.*: Analysis of clustering in Al-Mg-Si alloy by density spectrum analysis of atom probe data. Ultramicroscopy 111, 701–705 (2011).
[56] *Buha, J., Munroe, P. R., Lumley, R. N., Crosky, A. G., & Hill, A. J.*: Positron studies of precipitation in 6061 aluminium alloy. In Materials Forum, 1028–1033 (2004).
[57] *Vissers, R., van Huis, M. V., Jansen, J., Zandbergen, H. W., Marioara, C. D., & Andersen, S. J.*: The crystal structure of the β' phase in Al–Mg–Si alloys. Acta Materialia, 3815–3823 (2007).
[58] *Kammer, C.*: Aluminium-Taschenbuch, Bd. 1: Grundlagen und Werkstoffe. Düsseldorf: Aluminium-Verlag (1998).
[59] *Robinson, A. T., & Dorn, J. E.*: Effect of alloying elements on the electrical resistivity of aluminum alloys. Journal of metals, 457–460 (1951).
[60] *Norbury, A. L.*: The electrical resistivity of dilute metallic solid solutions. Transactions of the Faraday Society, 570–596 (1921).
[61] *Linde, J. O.*: Elektrische Eigenschaften verdünnter Mischkristallegierungen I. Goldlegierungen. Annalen der Physik, 52–70 (1931).
[62] *Linde, J. O.*: Elektrische Eigenschaften verdünnter Mischkristallegierungen III. Widerstand von Kupfer-und Goldlegierungen. Gesetzmäßigkeiten der Widerstandserhöhungen. Annalen der Physik, 219–248 (1932).
[63] *Linde, J. O.*: Elektrische Eigenschaften verdünnter Mischkristallegierungen. II. Widerstand von Silberlegierungen. Annalen der Physik, 353–366 (1932).
[64] *Mott N. F.*: The electrical resistance of dilute solid solutions. Mathematical Proceedings of the Cambridge Philosophical Society, 281–290 (1936).
[65] *Mott, N. F., & Jones, H.*: The Theory of the Properties of Metals and Alloys (1936).
[66] *Zeng, Y., Mu, S., Wu, P., Ong, K. P., & Zhang, J.*: Relative effects of all chemical elements on the electrical conductivity of metal and alloys: An alternative to Norbury–Linde rule. Journal of Alloys and Compounds, 345–354 (2009).
[67] *Cahn, R. W., Haasen, P. & Kramer, E. J.*: Materials Science and Technology: A Comprehensive Treatment. Volume 3A: Electronic and Magnetic Properties of Metals and Ceramics Part 1 (1991).
[68] *Dugdale, J. S.*: The Electrical Properties of Metals and Alloys (1977).
[69] *Stroppe, H. & Schiebold, K.*: Wirbelstrom-Materialprüfung: ein Lehr- und Arbeitsbuch für Ausbildung und Prüfpraxis; mit 29 Tabellen (2011).
[70] https://www.tescan.com/product/sem-for-materials-science-tescan-mira/ (2020).
[71] *Petzow, G.*: Metallographisches, keramographisches und plastographisches Ätzen. (2006).
[72] *Papula, L.*: Mathematik für Ingenieure und Naturwissenschaftler Band 3 (2008).

[73] *Zhu, H., Zhang, X., Couper, M. J., & Dahle, A. K.*: Effect of Initial Microstructure on Surface Appearance of Anodized Aluminum Extrusions. Metallurgical and Materials Transactions A, 3264–3275 (2009).
[74] *Kuijpers, N. C. W.*: Kinetics of the β-AlFeSi to α-Al (FeMn) Si transformation in Al-Mg-Si alloys (2004).
[75] *Van de Langkruis, J., Kuijpers, N. C. W., Kool, W. H., Vermolen, F. J., & Van der Zwaag, S.*: Modeling Mg2Si Dissolution in an AA6063 Alloy During Preheating to the Extrusion Temperature. PROCEEDINGS OF INTERNATIONAL ALUMINUM EXTRUSION TECHNOLOGY SEMINAR, 119–124 (2000).
[76] *Schiffl, A., Schiffl, I., & Österreicher, J.*: Identification of the most influencing parameter for perfect extrudability of high strength 6082. Extrusion Technology, 130–140 (2016).
[77] *Kabliman, E., & Sherstnev, P.*: Integrated Modeling of Strength Evolution in Al-Mg-Si Alloys during Hot Deformation. Materials Science Forum, 429–433 (2013).
[78] *Kabliman, E., Kolody, A. H., Kommenda, M., & Kronberger, G.*: Prediction of Stress-Strain Curves for Aluminium Alloys using Symbolic Regression. AIP Conference Proceedings, 180009–180015 (2019).
[79] *Österreicher, J. A., Grabner, F., Schiffl, A., Schwarz, S., & Bourret, G. R.*: Information depth in backscattered electron microscopy of nanoparticles within a solid matrix. Materials Characterization, 145–153 (2018).
[80] *Österreicher, J. A., Kumar, M., Schiffl, A., Schwarz, S., Bourret, G. R., Schiffl, A., Schwarz, S., Hillebrand, D., & Bourret, G. R.*: Sample preparation methods for scanning electron microscopy of homogenized Al-Mg-Si billets: A comparative study. Materials Characterization, 63–69 (2016).
[81] *Kissinger, H. E.*: Reaction kinetics in differential thermal analysis. Analytical chemistry, 1702–1706 (1957).

8 Illustration Directory

The value of Δσ in Figure 4.21 remains almost the same for the post heat-treatment state as for the as cast state. As already mentioned in the previous section, this heat-treatment should cause all available Mg and Si atoms to form a solid solution with the Al-matrix. However, as Figure 4.26 indicates the formation of Fe-dispersoids, the formation of those dispersoids might consume Mg and Si atoms and therefore reduce the available Mg and Si atoms for the formation of a solid-solution with the Al-matrix. This process might be compensated almost exactly by the addition of Mg and Si atoms through the dissolution of primary Mg-Si phases and therefore cause the value of the el. conductivity to remain almost the same as compared to the as-cast state. However, it remains unclear, why heat-treatment 530_4_wq and 580_4_wq show almost the same result, as it would be expected, that either all Mg-Si atoms are in solid solution for 580_4_wq (due to the higher temperature and therefore stronger diffusion) and therefore the value for Δσ should be higher for 580_4_wq as for 530_4_wq. This could maybe be explained by the fact, that formation of Fe-dispersoids might cause a significant amount of Mg and Si atoms to be consumed for their formation. This missing part of Mg and Si may cause the effect, that the remaining part of Mg and Si atoms is..

The negative value for Δσ in Figure 4.57 reveals, that the measured value was significantly higher than the calculated value. This could be described due to the fact, that probably not all of the Mg-Si phases which precipitate during heating-up are dissolved fully upon exceeding the solvus-temperature of 525°C. In addition although no precipitation of Mn-containing phases was considered precipitation of Mn-containing phases may have occurred. Even if precipitation of Mn-containing phases occurs only to a minor degree, the high influence on el. conductivity of Mn would cause the el. conductivity to significantly increase [Figure 2.21]. Therefore slight precipitation of Mn-

9 Table Directory

10 Attachment

10.1 Grain size ASTM-Norm

TABLE 4 Grain Size Relationships Computed for Uniform, Randomly Oriented, Equiaxed Grains

Grain Size No. G	N_A Grains/Unit Area		$\bar{A}$ Average Grain Area		$\bar{d}$ Average Diameter		$\bar{\ell}$ Mean Intercept		N_L
	No./in.² at 100X	No./mm² at 1X	mm²	µm²	mm	µm	mm	µm	No./mm
00	0.25	3.88	0.2581	258064	0.5080	508.0	0.4525	452.5	2.21
0	0.50	7.75	0.1290	129032	0.3592	359.2	0.3200	320.0	3.12
0.5	0.71	10.96	0.0912	91239	0.3021	302.1	0.2691	269.1	3.72
1.0	1.00	15.50	0.0645	64516	0.2540	254.0	0.2263	226.3	4.42
1.5	1.41	21.92	0.0456	45620	0.2136	213.6	0.1903	190.3	5.26
2.0	2.00	31.00	0.0323	32258	0.1796	179.6	0.1600	160.0	6.25
2.5	2.83	43.84	0.0228	22810	0.1510	151.0	0.1345	134.5	7.43
3.0	4.00	62.00	0.0161	16129	0.1270	127.0	0.1131	113.1	8.84
3.5	5.66	87.68	0.0114	11405	0.1068	106.8	0.0951	95.1	10.51
4.0	8.00	124.00	0.00806	8065	0.0898	89.8	0.0800	80.0	12.50
4.5	11.31	175.36	0.00570	5703	0.0755	75.5	0.0673	67.3	14.87
5.0	16.00	248.00	0.00403	4032	0.0635	63.5	0.0566	56.6	17.68
5.5	22.63	350.73	0.00285	2851	0.0534	53.4	0.0476	47.6	21.02
6.0	32.00	496.00	0.00202	2016	0.0449	44.9	0.0400	40.0	25.00
6.5	45.25	701.45	0.00143	1426	0.0378	37.8	0.0336	33.6	29.73
7.0	64.00	992.00	0.00101	1009	0.0318	31.8	0.0283	28.3	35.36
7.5	90.51	1402.9	0.00071	713	0.0267	26.7	0.0238	23.8	42.04
8.0	128.00	1984.0	0.00050	504	0.0225	22.5	0.0200	20.0	50.00
8.5	181.02	2805.8	0.00036	356	0.0189	18.9	0.0168	16.8	59.46
9.0	256.00	3968.0	0.00025	252	0.0159	15.9	0.0141	14.1	70.71
9.5	362.04	5611.6	0.00018	178	0.0133	13.3	0.0119	11.9	84.09
10.0	512.00	7936.0	0.00013	126	0.0112	11.2	0.0100	10.0	100.0
10.5	724.08	11223.2	0.000089	89.1	0.0094	9.4	0.0084	8.4	118.9
11.0	1024.00	15872.0	0.000063	63.0	0.0079	7.9	0.0071	7.1	141.4
11.5	1448.15	22446.4	0.000045	44.6	0.0067	6.7	0.0060	5.9	168.2
12.0	2048.00	31744.1	0.000032	31.5	0.0056	5.6	0.0050	5.0	200.0
12.5	2896.31	44892.9	0.000022	22.3	0.0047	4.7	0.0042	4.2	237.8
13.0	4096.00	63488.1	0.000016	15.8	0.0040	4.0	0.0035	3.5	282.8
13.5	5792.62	89785.8	0.000011	11.1	0.0033	3.3	0.0030	3.0	336.4
14.0	8192.00	126976.3	0.000008	7.9	0.0028	2.8	0.0025	2.5	400.0